creative commons
COMMONS DEED

저작자표시-비영리-변경금지 2.0 대한민국

이용자는 아래의 조건을 따르는 경우에 한하여 자유롭게

- 이 저작물을 복제, 배포, 전송, 전시, 공연 및 방송할 수 있습니다.

다음과 같은 조건을 따라야 합니다:

저작자표시. 귀하는 원저작자를 표시하여야 합니다.

비영리. 귀하는 이 저작물을 영리 목적으로 이용할 수 없습니다.

변경금지. 귀하는 이 저작물을 개작, 변형 또는 가공할 수 없습니다.

- 귀하는, 이 저작물의 재이용이나 배포의 경우, 이 저작물에 적용된 이용허락조건을 명확하게 나타내어야 합니다.
- 저작권자로부터 별도의 허가를 받으면 이러한 조건들은 적용되지 않습니다.

저작권법에 따른 이용자의 권리는 위의 내용에 의하여 영향을 받지 않습니다.

이것은 이용허락규약(Legal Code)을 이해하기 쉽게 요약한 것입니다.

Disclaimer

dCollection

공학박사 학위논문

Biological and Therapeutic Implications of α-Synuclein Interactive Molecules and Their Application in Sensor Development

알파-시뉴클린 상호작용성 분자들의 생물학적 의의와 질환치료 및 센서 개발 응용 연구

2016년 2월

서울대학교 대학원

화학생물공학부

양 지 은

Abstract

Biological and Therapeutic Implications of α-Synuclein Interactive Molecules and Their Application in Sensor Development

Jee Eun Yang

School of Chemical and Biological Engineering

The Graduate School

Seoul National University

α-Synuclein, amyloidogenic protein, is a major component of Lewy bodies which are commonly observed in Parkinson's disease patients. Oligomeric intermediates which are observed during amyloidogenesis of this protein are assembled into various fibrillar structures via specific pathway called unit assembly. These amyloid fibrils have different physicochemical properties corresponding to amyloid polymorphism. Furthermore, unit assembly of α-synuclein oligomers on the surface of liposome induces the formation of radiating amyloid fibrils, resulting disruption of lipid membrane structure.

Therefore, it can be considered that unit assembly of oligomers on the lipid membrane is the cause of α-synuclein-mediated cellular degeneration in a molecular level.

In this study, α-synuclein interactive molecules have been investigated in order to control the oligomer-mediated cytotoxicity. First of all, mutual effect of α-synuclein and protein partners such as firefly luciferase (LUC) and glutathione peroxidase-1 (GPX-1) are investigated to unveil their involvement in the PD pathogenesis in terms of fibrillar polymorphism and cellular antioxidant defense mechanism. First of all, LUC and GPX-1 bind to α-synuclein with Kd of 8.1 μM and 17.3 nM, respectively and they are shown to accelerate the fibrillation and induce amyloid polymorphism of α-synuclein by acting as a novel template. In case of LUC-directed amyloid fibrils, altered morphological characteristics were inherited to next-generations via nucleation-dependent fibrillation process. The seed control, therefore, would be an effective means to modify amyloid fibrils with different biochemical characteristics. In addition, the LUC-directed amyloid fibrillar polymorphism also suggests that other cellular biomolecules are able to diversify amyloid fibrils, which could be self-propagated with diversified biological activities, if any, inside cells. Mutual interactions of α-synuclein and GPX-1 contributed to not only accelerated α-synuclein fibrillation but also enhancement of GPX-1 activity. Furthermore, the entrapped GPX-1 in the fibrillar meshwork of α-synuclein was protected in a latent form and its activity was fully recovered as released from the matrix. Therefore, novel defensive roles of α-synuclein and its amyloid fibrils against oxidative stress

are suggested as the GPX-1 stimulator and the active depot for the enzyme, respectively.

In this study, several phenolic compounds are examined to control the effects of oligomeric species on cellular membrane and cell viability. First of all, specific oligomer which is β-sheet free, can be assembled into curly amyloid fibril (CAF) through repetitive membrane filtration and instantly transform into radiating amyloid fibril (RAF) on phosphatidylcholine liposome is defined as active oligomer. The changes of tyrosine intrinsic fluorescence of α-synuclein have shown that phenolic compounds such as resveratrol (RSV), curcumin (CUR) and (-)-epigallocatechin gallate (EGCG) directly interact with α-synuclein with Kd of 30.4 mM, 133 mM and 100 mM, respectively. According to the Coomassie Brilliant Blue-stained SDS-PAGE and CD spectroscopy, phenolic compounds have significant influences on the fibrillation of α-synuclein by either facilitating the formation of compact oligomers or accelerating the formation of amyloid fibrils with high β-sheet contents. Furthermore, phenolic compounds could effectively control the formation of CAF and RAF and then reduce the cytotoxicity of active oligomer.

Robust polydiacetylene-based colorimetric sensing material has been developed with amyloid fibrils of α-synuclein in the presence of 10,12-pentacosadiynoic acid (PCDA) by taking advantage of specific fatty acid interaction of α-synuclein and structural regularity of the self-assembled product of amyloid fibrils. PCDA facilitated not only self-oligomerization of α-synuclein but also its fibrillation into the fibrils with increased thickness.

Upon UV irradiation, the PCDA-containing amyloid fibrils (AF/PCDA) turned to blue, which then became red following heat treatment. The blue-to-red color transition was also observed with other stimuli of pH and ethanol. AF/PCDA were demonstrated to be mechanically stable since not only the individual colors of blue and red but also their colorimetric transition were not affected by a number of sonications which readily disrupted the polydiacetylene (PDA) vesicles with instant loss of the colors. Therefore, AF/PCDA can be considered as a novel PDA-based colorimetric sensing material with high mechanical strength, which has potential to be employed in various areas involving advanced sensing technologies. Furthermore, litmus-type sensors capable of detecting temperature and organic solvents have been developed with α-synuclein amyloid fibrils and PCDA. The PCDA molecules localized on the amyloid fibrils through either co-incubation with monomeric α-synuclein (AF/PCDA) or simple mixing with the pre-made α-synuclein amyloid fibrils (AF+PCDA) were photopolymerized with UV to exhibit blue color on paper. The paper sensors prepared with AF/PCDA and AF+PCDA showed distinctive sensitivities toward temperature and solvents. The less tight binding of PCDA to amyloid fibrils and thus increased its molecular freedom would be responsible for the discrete sensing property. In addition, the AF+PCDA sensor was demonstrated to successfully follow ascending temperature change, which could allow the litmus-type sensor to monitor thermal history of materials. Taken together, the amyloid fibrils of α-synuclein are shown to be a decent template for PCDA to develop into the litmus-type thermochromic and solvatochromic sensors.

Keywords

α-Synuclein; Active oligomer; Unit-assembly; α-Synuclein interactive molecules; Polydiacetylene; Amyloid-based sensor

Student number: 2010-23333

Contents

List of Tables

List of Figures

Part I. Biological and Therapeutic Implications of α-Synuclein Interactive Molecules

I. Introduction

1. Amyloidogenesis

Amyloidogenesis is the formation of insoluble protein nanofibrils known as amyloid (Figure 1) through misfolding and abnormal assembly of soluble and innocuous proteins under pathological conditions such as oxidative stress and genetic mutation [1]. Amyloids are typically long and fibrous structure, 5-15 nm in width and several micrometers in length [2, 3] and characterized by a cross β-sheet structure with the hydrogen bonded amino acids aligned perpendicular to the fibrillar axis. When the structure of amyloids is investigated by X-ray diffraction, there are simple patterns with longitudinal diffraction line at 4.7 Å and transverse diffraction line at 10 Å. They are characteristic of a cross-β structure [4-6].

Abnormal aggregation into amyloid fibrils has significant implication in the pathogenesis of neurodegenerative diseases even though the cause-and-effect relationship between amyloidogenesis and onset of diseases remain largely unknown [7]. Amyloid plaques caused by abnormal accumulation of insoluble protein fibrils have been observed in various neurodegenerative diseases such as Alzheimer's disease, Parkinson's disease,

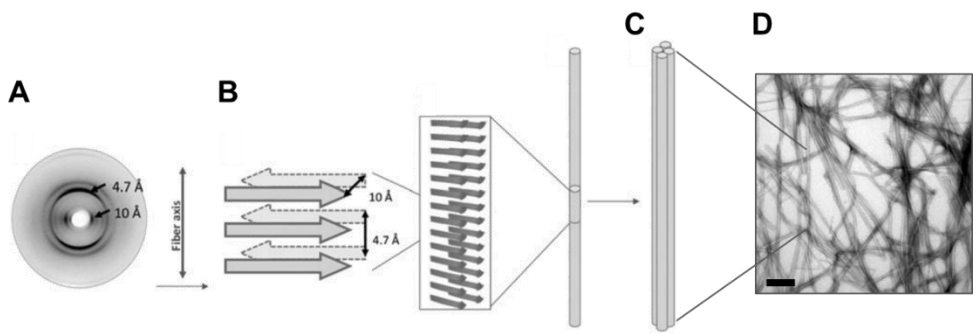

Figure 1. The structure of amyloid. (A) X-ray diffraction of amyloid protofilament. (B) The cross-β structural core of amyloid protofilament. (C) The protofilaments self-associated to from the mature amyloid fibril. [Serpell. *Essays Biochem.* **56** (2014) 1-10] (D) Transmission electron spectroscopy image of amyloid fibril. Scale bar represents 200 nm.

Dementia with Lewy bodies, Creutzfeldt-Jakob disease, Huntington's disease and Amyotrophic lateral sclerosis. (Table 1).

2. Parkinson's disease and α-synuclein

Parkinson's disease, the second most common neurodegenerative disease, is characterized by neuronal loss and neuronal Lewy bodies in the substantia nigra. The most obvious symptoms are related with movement including tremor, rigidity, slowness of movement and difficulty with walking. Previous studies have shown that α-synuclein may be closely connected with PD because this protein is the major component of Lewy bodies in histopathological sections of PD patients (Figure 2) [8].

In particular, it has been investigated that several environmental risk factors contribute to the development of sporadic PD [9-11] and affect abnormal assembly of α-synuclein molecules. For example, exposure to lipophilic pesticide, rotenone, causes the degeneration of dopamine neurons that is associated with movement trouble such as rigidity [12]. Furthermore, high blood levels of heavy metals such as manganese, copper and iron are commonly observed in PD patients [13, 14]. The conformational change and significant acceleration of α-synuclein fibrillation are observed *in vitro* in the presence of pesticides such as rotenone, dieldrin and paraquat [15] and di- and trivalent metal ions, especially copper (II), iron, cobalt, and manganese [16]. Therefore, it can be considered that these environmental toxins are related with the development of late-onset PD and affect α-synuclein

Table 1. Some human brain diseases characterized by progressive misfolding and aggregation of proteins.

Neurodegenerative disease	Pathological features	Major components of the deposits	Injured tissues	Symptoms
Alzheimer's disease (AD)	Senile plaques and neurofibrillary tangles (NFT)	Aβ peptide and hyperphosphorylated tau	Cortex, hippocampus, basal forebrain, brain stem	Impairment of memory, judgement, attention span, and problem solving skills
Parkinson's diseases (PD)	Abnormal proteinaceous cytoplasmic inclusion (Lewy bodies)	α-Synuclein	Substantia nigra	Tremor, rigidity, stooped posture, slowness of voluntary movements, and masklike facial expression
Dementia with Lewy bodies (DLB)	Lewy bodies	α-Synuclein and ubiquitin	Cholinergic and dopaminergic neuron	Dementia and movement problems
Creuzfeldt-Jakob disease	Prominent cerebellar and cerebral cortical spongiform degeneration	Prion	Cerebral cortex, thalamus, putamen, caudate nucleus, and cerebellar cortex	Sleep disturbances, personality changes, progressive dementia, ataxia, muscle atrophy, and myoclonus
Huntington's disease	Intranuclear inclusions and cytoplasmic aggregates	Huntingtin with polyQ expansion	Striatum, other basal ganglia, cortex	Uncoordinated movement, unsteady gait, and psychiatric problems
Amyotrophic lateral sclerosis (ALS)	Bunina bodies in degenerating neurons and surrounding reactive astrocytes	TAR DNA binding protein	Cerebral cortex, brainstem and spinal cord	Stiff muscles, muscle twitching and difficulty with speaking, swallowing and breathing

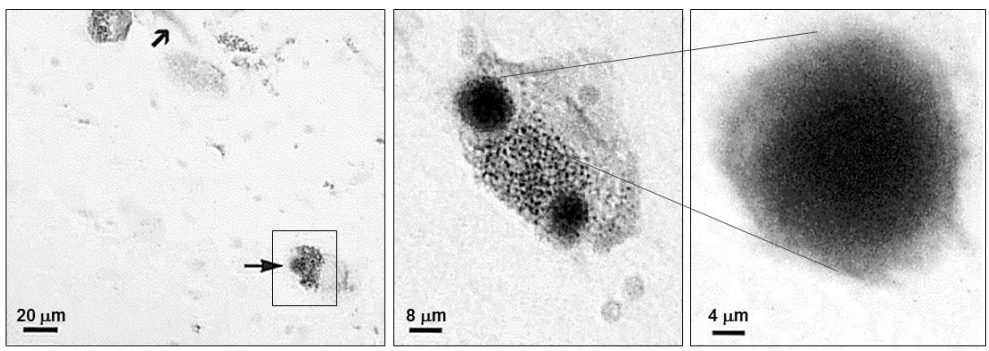

Figure 2. α-Synuclein in Lewy bodies. [Spillantini et al. *Nature* **388** (1997) 839-840].

molecules, inducing α-synuclein dysfuction that is toxic to the dopaminergic neurons [17]. On the other hand, the familial PD is rarely developed due to mutation in specific genes such as *SNCA*, *LRRK2*, and *PINK1*. Especially, three missense mutations in SNCA, which are A30P, E46K and A53T, have been observed in Lewy bodies of PD patients [18–20] and overexpression of wild type α-synuclein due to gene triplication have also reported to lead to the development of PD [21, 22].

3. Mechanism of amyloidogenesis

According to the previous studies, multiple assembly pathways lead to various types of amyloid fibrils with distinct morphologies [23-25]. For example, β_2-microglobulin of amyloidogenic protein are assembled into worm-like fibrils or rod-like fibrils according to experimental conditions such as pH and the concentration of salts [26]. From these studies, it can be considered that amyloidogenesis occurs via multiple mechanisms.

Mechanisms of amyloidogenesis are classified into template-dependent and template-independent fibrillation according to whether the protein assembly depends on pre-existing template [27]. First of all, in template-dependent fibrillation, the conformation of unfolded monomeric proteins may be converted to the amyloidogenic form in the presence of pre-existing template (Figure 3) [28, 29]. The nucleation-dependent fibrillation model reflecting template-dependent fibrillation has been widely accepted as an amyloid fibril formation mechanism [30, 31]. In nucleation-dependent

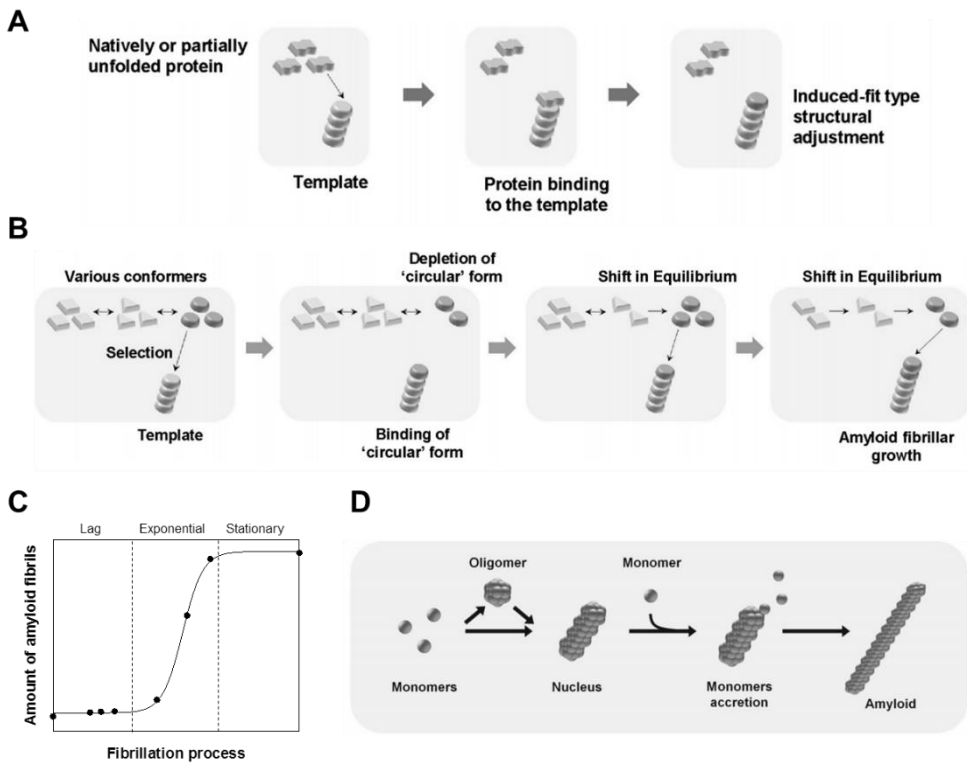

Figure 3. Template-dependent fibrillation. (A) Monomers acting as active growing unit are converted to the amyloidogenic form upon binding to pre-existing template. (B) Monomers acting as passive growing unit selectively binds to pre-existing template, inducing equilibrium shift of conformer. (C) Kinetics of amyloidogenesis. (D) Nucleation-dependent fibrillation. [Bhak et al. *BMB Rep.* **42** (2009) 541-551].

fibrillation, monomeric proteins are assembled into amyloid fibrils through three stages including lag, exponential, and stationary phase (Figure 3C). Once nucleus forms during the lag phase, the monomers adhere to the nucleus, experience the conformational transition into amyloidogenic form and then grow into the fibrillar structures (Figure 3D) [32]. On the other hand, in template-independent fibrillation, the amyloidogenic conformations may be induced in the absence of template prior to the molecular assembly process. A specific conformer among the various conformers in a state of equilibrium is amyloidogenic and self-associative and then turn into final fibrils by shifting equilibrium (Figure 4) [27]. Occasionally, the formation of the self-associative conformer is facilitated by a specific ligand such as a cyclic tetrapyrrole compound [33] and metal irons [34, 35], and then fibrillation can be further accelerated. Recently, a novel amyloidogenesis model of α-synuclein named unit-assembly has been reported and this model reflects the template-independent fibrillation. Based on this unit-assembly model, oligomeric species generated through association of α-synuclein monomers act as a growing unit for the fibril formation in the absence of template (Figure 5). Also, since oligomeric species are thermodynamically pseudo-stable, their conformations are prone to be distorted in the presence of chemical and physical influences, resulting amyloid polymorphisms [36, 37].

4. α-Synuclein, an intrinsically unstructured protein (IUP)

α-Synuclein which is primarily found at pre-synaptic terminals is an

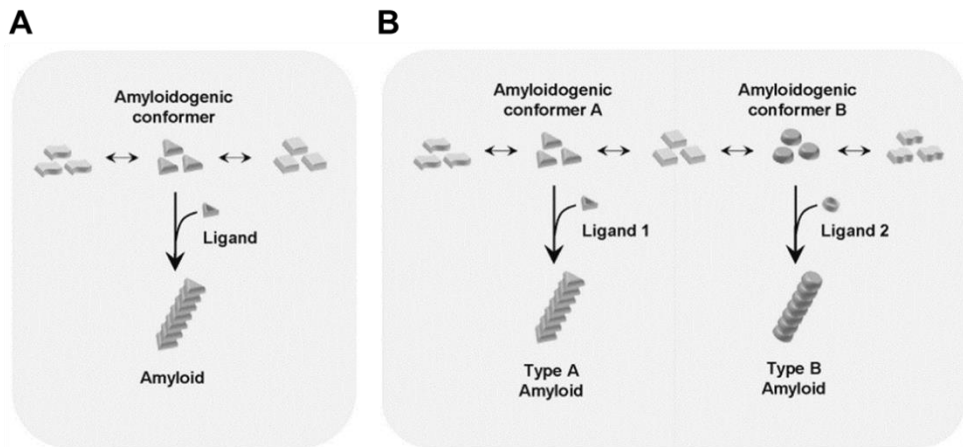

Figure 4. Template-independent fibrillation. (A) Ligand-induced fibrillation. (B) Fibrillar polymorphisms. [Bhak et al. *BMB Rep.* **42** (2009) 541-551].

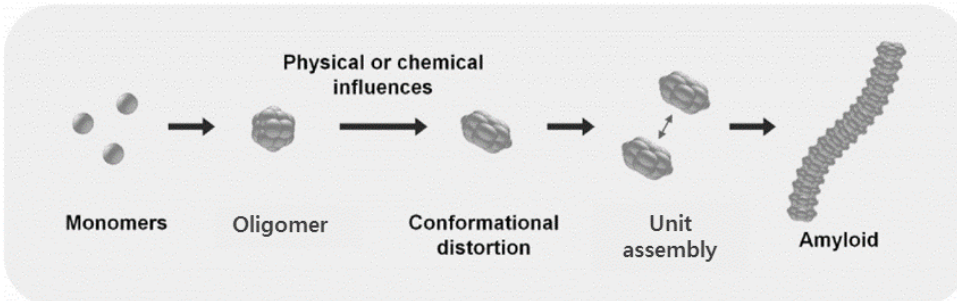

Figure 5. Unit assembly of oligomers. [Bhak et al. *BMB Rep.* **42** (2009) 541-551].

intrinsically unstructured and acidic protein with molecular weight of 14 kDa. The protein has three distinctive domains in its primary structure including amphipathic N-terminal region (residues 1-60), central hydrophobic region (residues 61-95), and highly acidic C-terminal region (residues 96-140) (Figure 6). The N-terminus which consists of four 11-amino acid imperfect repeats (KTKEGV) is related with α-helical structure formation in vitro and membrane binding by interacting with acidic phospholipids [38, 39]. The central hydrophobic region which includes amyloidogenic NAC (non-amyloid-β component) region is essential for protein aggregation by forming a core region of the fibrils of α-synuclein [40]. The C-terminus with abundant acidic amino acids and proline residues contains several sites of ligand binding such as dopamine and its derivatives [41] and metal ions binding such as Ca(II) [42] and Cu(II) [43, 44] ions.

Although it is generally accepted that folded protein structure is necessary for biological function, not all functional proteins are intrinsically structured and folded into stable globular structure. Unstructured regions of significant size have been commonly observed in functional proteins under native conditions by using X-ray crystallography, NMR spectroscopy, CD spectroscopy and protease sensitivity. The flexible structures of proteins containing unstructured regions are involved in molecular recognition. Therefore, intrinsic disorder of proteins plays numerous roles in binding to their substrate, ligand, other proteins, nucleic acid polymers, lipid, heme and metal ions [45-47]. Interestingly, protein disorder databases, DisProt [48] and IDEAL [49], show that 80% of unstructured human proteins in databases

A

1 50
MDVFMKGLSK AKEGVVAAAE KTKQGVAEAA GKTKEGVLYV GSKTKEGVVH
51 100
GVATVAEKTK EQVTNVGGAV VTGVTAVAQK TVEGAGSIAA ATGFVKKDQL
101 140
GKNEEGAPQE GILEDMPVDP DNEAYEMPSE EGYQDYEPEA

B

Figure 6. α-Synuclein. (A) Amino acids sequence of α-synuclein. (B) The three distinctive domains of α-synuclein.

contain one or more of amyloidogenic region. Also, decrease of unstructured region is correlated with decrease of amyloidogenic region content in protein sequence [50]. According to the protein disorder database, a typical amyloidogenic protein, α-synuclein, is a highly intrinsically unstructured protein and its functions include protein binding [51], polymerization and metal binding [52]. In fact, it has been reported that α-synuclein interacts with various chemicals and biomolecules including Cu(II) [43, 44], Coomassie Brilliant Blue [53], oxidized glutathione [54], lipid [55], phthalocyanine tetrasulfonates [56], dequalinium [57], eosin [58], luciferase [59, 60], and glutathione peroxidase [61]. Taken together, it can be considered that there are a lot of unknown α-synuclein interactive molecules and they may affect biological and pathological functions of α-synuclein.

5. Neurotoxicity of α-synuclein oligomers

Many researchers have demonstrated that oligomeric intermediates are the most neurotoxic species [62, 63]. It has been demonstrated that α-synuclein oligomers can disrupt synthetic lipid vesicles [64, 65] and lead to cell death in vitro [66, 67] and in animal models [68, 69]. These effects of α-synuclein oligomers on membrane disruption and permeability have been explained by two mechanisms. First of all, annular oligomers may integrate into membrane and form pores or channel-like structures leading to membrane permeability [70-72]. Otherwise, α-synuclein oligomers may facilitate the movement of ions across the membrane bilayer without the formation of pores [73].

Intermediates which are observed in the early stage of fibrillation are called oligomers and structure and property of these species are highly diverse. For example, it has been reported that β-sheet rich oligomers of α-synuclein are spherical and show the polydispersed size distribution from 10 nm to 60 nm [74]. Also, smaller spheroidal oligomers with 1.5 - 3.2 nm in height were characterized by primarily α-helical structure [75]. The wreath-shaped α-synuclein oligomers with diameter of 18 nm was identified by using small angle X-ray scattering [76]. Furthermore, oligomeric species can recognize environmental changes resulting conformational change and acceleration of fibrillation. For example, subtle conformational distortions were caused by exposure to temperature varying from 37℃ to 43℃, which consequently led to fibrillar polymorphism [77]. Also, when α-synuclein oligomers were incubated with small amount of organic solvent, nanofibrils were instantly generated through unit assembly [78]. Taken together, it can be considered that thermodynamically unstable oligomeric species are attractive therapeutic targets because oligomers may be easily altered into stable and less toxic structure.

6. α-Synuclein interactive molecules

As mentioned previously, α-synuclein has potential for interacting with multiple ligands such as lipids, metal ions, proteins and small chemicals because it is intrinsically unfolded protein. In this study, self-assembly of α-synuclein is modulated by interacting with other protein molecules such as

firefly luciferase and glutathione peroxidase-1 and small molecules from natural phenolic compounds.

6-1. Firefly luciferase

Firefly luciferase (LUC) has been widely used in molecular and cell biology for the detection of ATP and as a reporter to study gene expression [79, 80]. Firefly luciferase (LUC) is an oxidative enzyme that catalyzes generation of yellow-green light from chemicals of luciferin and ATP (Figure 7A). Furthermore, firefly luciferase which is a bifunctional enzyme also has catalytic function of fatty acyl-CoA synthesis (Figure 7B).

6-2. Glutathione peroxidase

Selenium-containing glutathione peroxidases (GPXs) are important antioxidant enzymes protecting the organism from oxidative damages by removing hydrogen peroxide and various organic peroxides. GPX primarily catalyzes the reaction of converting hydrogen peroxide to water by oxidizing reduced glutathione (GSH) to glutathione disulfide (GSSG) in cytoplasm. Glutathione reductase then reduces the oxidized glutathione to complete the cycle (Figure 8A) [81]. GPX-1 of several isozymes is the most abundant enzyme found in the cytoplasm of nearly all mammalian tissues. Because of its crucial role resistant to oxidative stress, GPX-1 has been implicated in development and prevention of many diseases including cancer, neurodegenerative diseases, and cardiovascular disease [82, 83]. According to recent observation, it was revealed that GPX-1 was co-localized with α-

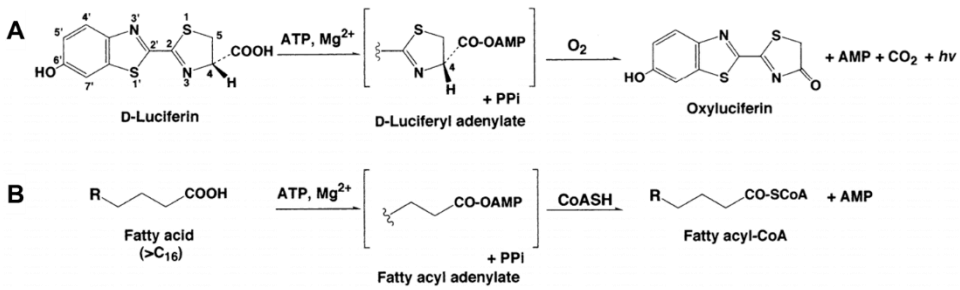

Figure 7. Reactions catalyzed by firefly luciferase. (A) Bioluminescence reaction. (B) Fatty acyl-CoA synthetic reaction.

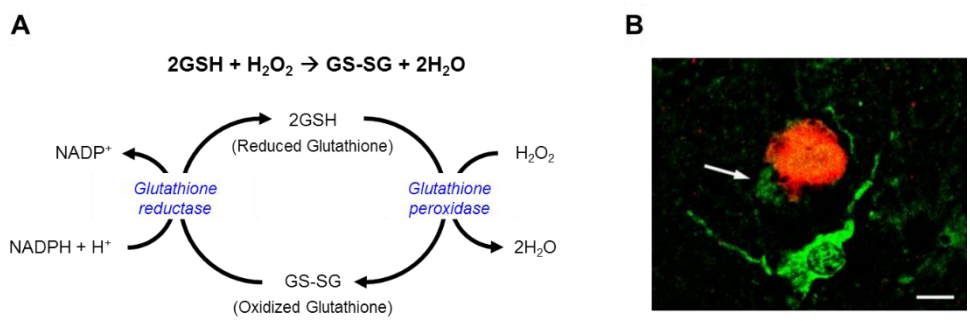

Figure 8. Antioxidant enzyme system and α-synuclein. (A) Glutathione peroxidase reaction. (B) Confocal localization of α-synuclein (red) and glutathione peroxidase (green) in Lewy bodies. Scale bar represents 5 μm. [John et al. *Acta. Beuropathol.* **117** (2009) 63-73].

synuclein in Lewy bodies in the brain tissues of PD patients, suggesting a neuroprotective role of GPX-1 toward the disease (Figure 8B) [84]. Since molecular-level inter-relationship between the two co-localized proteins is basically unknown, their mutual effects have been investigated in this study by assessing the accelerated fibrillation of α-synuclein by GPX-1 and the stimulated GPX-1 activity by α-synuclein.

6-3. Natural phenolic compounds

Natural phenolic compounds are abundant in fruits, vegetable and herbal beverage such as berries, tumeric, soybeans, green tea and red wine. [85] They constitute a large number of phytochemicals with more than 8000 compounds (Figure 9). According to previous studies, phenolic compounds have various physiological properties such as anti-oxidant [86, 87], anti-microbial [88], anti-inflammatory [89] and cardioprotective [90] effects. In particular, protection of plants against reactive oxygen species (ROS) is the most attractive function of phenolic compounds and have been primarily studied. Furthermore, it has been reported that several phenolic compounds such as resveratrol [91] and (-)-epigallocatechin gallate (EGCG) [92, 93] show effects of protection against aging and related neurodegenerative disease [94]. First of all, resveratrol can protect cells against oxidative stresses by reducing generation of ROS [95], scavenging free radicals [96] and preventing accumulation of ROS [97]. Also, studies on neuroprotective effects of curcumin have been showed that curcumin treatment reduces superoxide anion level and lipid peroxidation [98] and increases glutathione

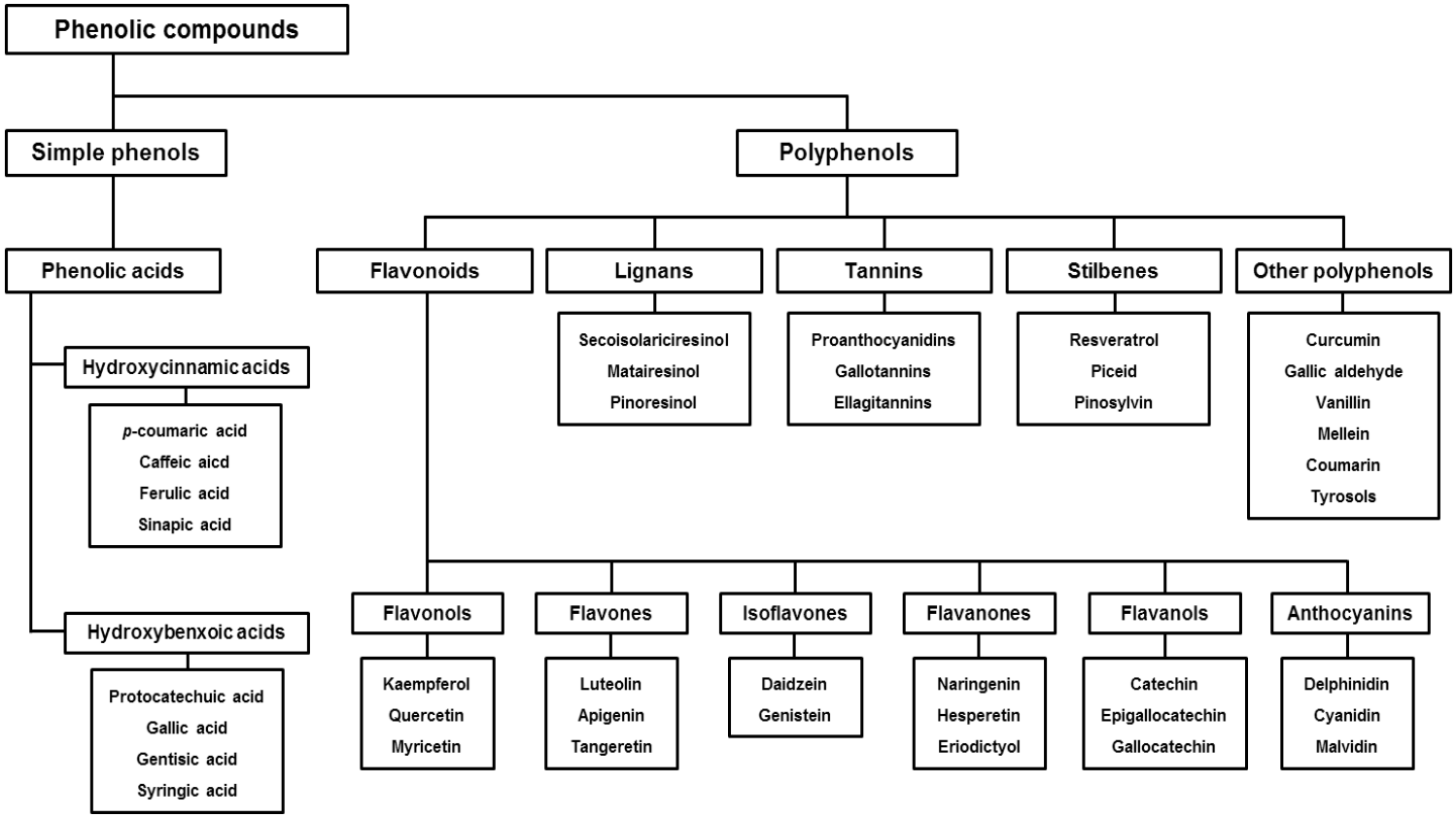

Figure 9. Classification of phenolic compounds.

(GSH) level [99]. It has been revealed that EGCG among different polyphenols is the most effective radical scavenger [100, 101] and long-term treatment with EGCG resulted increase in lifespan and movement improvement in a *Drosophila melanogaster* model of Parkinson's disease [93]. To summarize various studies, neuroprotective effects of phenolic compounds may be resulted from anti-oxidant and anti-amyloidogenic properties, modulation of neural mediators and enzymes, interaction with signaling pathways, and inhibition of NMDA neurotoxicity [102].

II. Experimental Section

1. Purification of α-synuclein

Human recombinant α-synuclein cloned in pRK172 was expressed in *Escherichia coli* BL21 (DE3) and purified according to the procedure described previously [103]. In order to make starter culture for protein expression, a colony of cells transformed with human recombinant α-synuclein plasmid was picked up from LB agar plate and put in 100 mL of LB medium containing 0.1 mg/mL ampicillin. The cells in LB medium were incubated for about 7 hours at 37℃ in orbital shaker at 200 rpm. 1 mL of starter culture was added into 1 L of LB medium with ampicillin and cultured at 37℃ in orbital shaker until the optical density at 600 nm was about 0.6. Then the culture was induced by adding 0.5 mM of isopropylthiogalactoside (IPTG) and further incubated at 37℃ for 4 hours. The cells were harvested

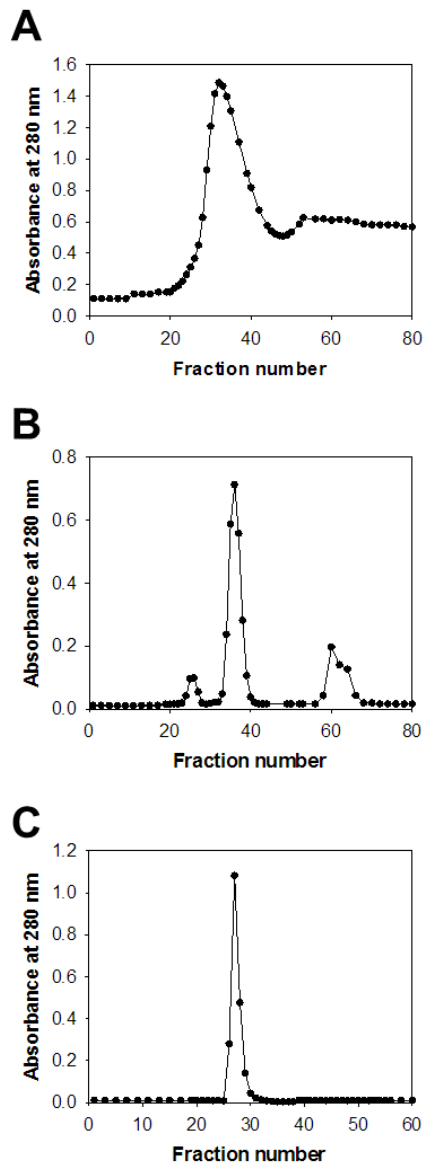

Figure 10. Purification of α-synuclein. (A) DEAE-sephacel anion exchange chromatography. (B) S-sephacryl S-200 size exclusion chromatography. (C) S-sepharose cation exchange chromatography.

by centrifugation and the cell pellet was lysed with freezing-thawing method and lysis buffer containing 0.1 M NaCl, 0.1 mM PMSF, 1 μg/mL Leupeptin, 2 mM EDTA, 0.1 mg/mL lysozyme, and 10 units/mL DNase in 20 mM Tris-HCl (pH 7.5). After cell lysis, the cell debris was removed by centrifugation and the supernatant was boiled at 100℃ for 20 min and cooled down in ice. After the cell lysate was filtered through a syringe-driven filter with a pore size of 0.21 μm, the lysate was purified with three chromatography steps including anion exchange (DEAE Sephacel), size-exclusion (S-200), and cation exchange (S-Sepharose) chromatography (Figure 10). Following dialysis against 6 L of 20 mM Mes (pH 6.5), the completely purified α-synuclein was stored in aliquots at −80℃.

2. Firefly luciferase assay

Assay mixture was made up with 1 mM ATP, 2 mM $MgSO_4$, and 188 μM luciferin in 25 mM Tricine (pH 7.8). Bioluminescence of the Luciferase activity was monitored with chemiluminescence spectrophotometer (LS-55B, Perkin-Elmer). Light emission was measured at 550 nm with an integration time of 0.02 sec.

3. Thioflavin-T binding fluorescence assay

α-Synuclein (0.5 mg/mL) was incubated in 20 mM Mes (2-(N-morpholino)

ethanesulfonic acid, pH 6.5) at 37℃ under a shaking condition at 200 rpm. During the incubation, α-synuclein was mixed with 2.5 mM Th-T in 50 mM glycine (pH 8.5) at room temperature. The fluorescence was monitored with chemiluminescence spectrophotometer (LS-55B, Perkin-Elmer). The resulting fibrillar formation of α-synuclein was estimated with Th-T binding Th-T binding fluorescence at 485 nm with an excitation at 450 nm.

4. JC-1 binding fluorescence assay

α-Synuclein and its amyloid fibrils were incubated with 1.2 μM JC-1 in 20 mM Mes (pH 6.5) containing 5% DMSO. The 5,5',6,6'-Tetrachloro-1,1,3,3'-tetraethylbenzimidazolyl carbocyanineiodide (JC-1) binding fluorescence spectra were obtained between 500 and 600 nm with an excitation at 490 nm. The JC-1 fluorescence was measured with chemiluminescence spectrophotometer (LS-55B, Perkin-Elmer).

5. Quantification of the remaining monomers after fibrillation

After the fibrillation reached a stationary phase, the α-synuclein amyloids were precipitated with centrifugation at 13200 rpm for 30 min. The amount of soluble α-synuclein monomers remaining in the supernatant was measured with bicinchoninic acid (BCA) protein assay (Thermo Fisher Scientific Inc.).

6. Transmission electron microscopy

An aliquot (20 μL) of sample was adsorbed onto a carbon-coated copper grid (200-mesh, Electron Microscopy Sciences) and dried in the air for 3 min. Following negative staining of the air-dried sample with 2% uranyl acetate (Electron Microscopy sciences) for 5 min, the grids containing the amyloid fibrils were visualized with TEM (JEM1010, JEOL).

7. Attenuated total reflectance-Fourier transformation-infrared (ATR – FTIR) spectrophotometer

The collected pellets of amyloid fibrils were placed on ZnSe ATR crystal. ATR spectra of amyloid fibrils were measured with Nicolet 6700 FTIR spectrometer equipped with DTGS detector (Thermo Fisher Scientific Inc.). Data fitting and curve deconvolution for the ATR-FTIR spectra were performed using OriginPro 8.0 software (OriginLab, Northampton, MA).

8. 8-anilino-1-naphthalenesulfonic acid (ANS) binding fluorescence assay

Protein was incubated with 20 μM ANS in 20 mM Mes (pH 6.5) at room temperature. The ANS binding fluorescence spectra were obtained between 400 and 600 nm with an excitation at 350 nm. The fluorescence was measured with chemiluminescence spectrophotometer (LS-55B, Perkin-Elmer).

9. Self-propagation experiment

Amyloid seeds were prepared with ultrasonication of the mature amyloid fibrils using a micro-tip-type ultrasonic processor (VCX 750, Sonics & Materials Inc.). Sonication was performed repeatedly for total of 10 cycles with the fibrils located on ice. Each cycle consisted of an on/off cycle for 15 sec each. After each cycle of sonication, the sample was quiescently placed on ice for 60 sec. The resulting amyloid fragments were examined with TEM and used as the seeds. Daughter fibrils were developed by seeding monomeric α-synuclein with the amyloid fragments at 5% (w/w).

10. Glutathione peroxidase-1 (GPX-1) assay

GPX-1 activity was measured by a coupling system employing cumene hydroperoxide and GSH in the presence of glutathione reductase and NADPH. Oxidized glutathione formed by GPX-1 reaction ($H_2O_2 + 2GSH \rightarrow GSSG + 2H_2O$) was continuously reduced by glutathione reductase activity ($GSSG + NADPH + H^+ \rightarrow 2GSH + NADP^+$). GPX-1 activity was calculated from the decrease in NADPH absorbance at 340 nm. The assay mixture included 0.1 mM each of cumene hydroperoxide, GSH, and NADPH and 0.1 unit glutathione reductase in 50 mM Tris/Cl (pH 7.6) containing 5 mM EDTA. Protein samples were lastly added into the assay mixture and the measurement was performed immediately. Dissociation constant (Kd)

between α-synuclein and GPX-1 was evaluated with a double reciprocal plot of the hyperbolic enhancement curve. The reciprocals of α-synuclein concentrations and initial activities of GPX-1 were plotted on the x- and y-axes, respectively, to obtain Kd from x-intercept.

11. Immunochemical analysis

For immunocytochemistry, neuroblastoma SH-SY5Y cells cultured on the coverslips were fixed in ice-cold methanol/acetone solution (1:1) at −20℃ for 10 min, washed and blocked with a blocking buffer (1% bovine serum albumin in phosphate buffered saline) for 30 min at 37℃. The fixed cells were incubated in the blocking buffer containing mouse anti-α-synuclein antibody and goat anti-GPX-1 antibody for 2 h, and then incubated with the fluorescent secondary antibodies of anti-mouse Alexa Fluor 488 (Thermo Fisher Scientific) and rabbit anti-goat Alexa Fluor 633 (Thermo Fisher Scientific) for 1 h in the dark. After washing with the blocking buffer, the cells were mounted with a mounting medium and examined using a confocal microscope (LSM510, Carl Zeiss). For immunogold labeling of the entrapped GPX-1 within amyloid fibrils, the sample was adsorbed onto a carbon-coated copper grid for 15 min at room temperature. After removing excess liquid with a filter paper, the adsorbed sample was incubated successively with goat anti-GPX-1 antibody and gold-conjugated anti-goat antibody for 1 h each. After washing with 20 mM MES (pH 6.5), the adsorbed sample was negatively stained with 2% uranyl acetate and analyzed using a transmission

electron microscope.

12. Intrinsic fluorescence of α-synuclein

α-Synuclein (35 μM) was preincubated in the absence and presence of various concentrations of phenolic compound for 30 min at 37℃, and the intrinsic tyrosine fluorescence of α-synuclein was monitored between 300 nm and 400 nm with excitation at 274 nm by using a chemiluminescence spectrophotometer (LS-55B, PerkinElmer). A saturation curve was obtained by plotting the difference in the intrinsic fluorescence obtained in the absence (I_0) and presence (I_i) of phenolic compounds as a function of phenolic compounds concentration. Dissociation constant Kd was obtained from the x-intercept of a double-reciprocal plot of the hyperbolic saturation curve between 1/[phenolic compounds] and $1/(I_0 - I_i)$ on the x and y axes, respectively.

13. Liposome synthesis

1,2-di-(9Z-octadecenoyl)-sn-glycero-3-phosphocholine (DOPC, Avanti Polar Lipids Inc.) in a test tube was dissolved with chloroform at 1 mg/mL, and followed by blowing N_2 gas until chloroform evaporated. Furthermore, the tube was stored in desiccator overnight to remove chloroform completely and then stored at −20℃. In order to peel the lipid film readily, the tube was

heated in a water bath of 80℃ for 1 min. And then this film was incubated with 1 mL of 20 mM Mes (pH 6.5) at 60℃ for 1 hr in orbital shaker (300 rpm) to rehydrate lipid film. The suspension was extruded at 60℃ using an extruder set (Avanti Polar Lipids Inc.) and polycarbonate membrane with a pore size of 200 nm. The homogeneous suspension of unilamellar vesicles was examined with TEM.

14. Cytotoxicity assay

Human dopaminergic neuroblastoma cells (SH-SY5Y) were incubated in Dulbecco's modified eagle medium (DMEM, GE Healthcare) with 10 % fetal bovine serum and 50 unit/mL penicillin/streptomycin in 5% CO_2 at 37℃. The cells were inoculated in a 96-well plate at ~1.0 x 10^6 cells/well. After the cell confluency reached about 90%, the mixtures of α-synuclein oligomers and small molecules were added to the cells, and further incubated for 24 hours in 5% CO_2 at 37℃. The cell proliferation was measured with MTS assay which is a colorimetric method for determining the number of viable cells via the reduction reaction of MTS tetrazolium compounds into colored formazan by active cells (Figure 11) [104]. 20 μL of MTS solution was added to culture wells and incubated for 4 hours in 5% CO_2 at 37℃. In order to stop reaction, 25 μL of 10% SDS was added to each well and then absorbance at 490 nm was measured with a 96-well plate reader.

15. Dynamic light scattering (DLS)

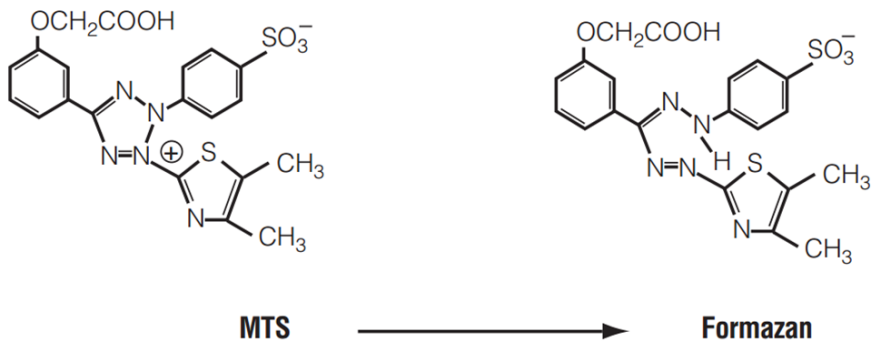

Figure 11. Conversion of MTS tetrazolium to formazan product.

The size distribution of α-synuclein amyloid fibrils incubated with and without EGCG was measured using DLS (Zetasizer Nano ZS, Malvern) at 25℃. Amyloid fibrils isolated with centrifugation were further incubated for 1 hr at 37℃ in orbital shaker with 0 mM, 0.1 mM and 0.3 mM EGCG. After incubation, the mixture of amyloid fibrils and EGCG was collected via centrifugation at 16100 × g for 30 min and then the collected pellets were resuspended with 1 mL of distilled water.

16. Circular dichroism (CD) spectroscopy

Secondary structure of α-synuclein aggregates prepared with phenolic compounds were evaluated with CD spectroscopy (Chirascan-plus, Applied Photophysics). The spectra were obtained between 195 and 260 nm with a step resolution of 0.1 nm and scan speed of 10 nm/min by using a 10 mm path length quartz cell. In order to estimate the secondary structure, CD spectra were analyzed by using the convex constraint algorithm (CCA).

III. Results and Discussion

1. Molecular interaction of α-synuclein and firefly luciferase contributes to the amyloid polymorphism of α-synuclein

α-Synuclein which is abundant in the brain has reported to be involved in brain lipid metabolism by modulating the activity of acyl-CoA synthetase

[105, 106]. Intriguingly, firefly luciferase which is a bifunctional enzyme also has catalytic function of acyl-CoA synthesis [Figure 7B] with a genetic similarity to acyl-CoA synthetase [107, 108]. It can be expected that activity of firefly luciferase is affected by α-synuclein, and therefore this study is deal with interaction between α-synuclein and firefly luciferase.

1-1. α-Synuclein enhances the activity of firefly luciferase

According to the previous study [59], α-synuclein enhanced the bioluminescent activity of firefly luciferase (LUC), which led to suggest α-synuclein as a novel protein regulator for LUC. The initial bioluminescence of LUC increased sharply from 69 to 95 AU in the presence of 7 μM α-synuclein (Figure 12A). When activity of LUC was evaluated with α-synuclein, β-synuclein, bovine albumin serum and lysozyme, the enhancement of bioluminescence was observed only with α-synuclein (Figure 12B). The enhanced bioluminescence of LUC exhibited a hyperbolic relationship with α-synuclein (Figure 12C) and then their dissociation constant was estimated as 8.1 μM from the x-intercept of a double-reciprocal plot of the hyperbolic saturation curve between 1/[α-synuclein] and 1/[bioluminescence] (Figure 12C, *inset*). Therefore, this study has suggested the specific interaction between α-synuclein and LUC and enhancement of LUC activity. Alternatively, LUC can be expected to have influences on the fibrillation kinetics of α-synuclein and the final fibrillar morphology.

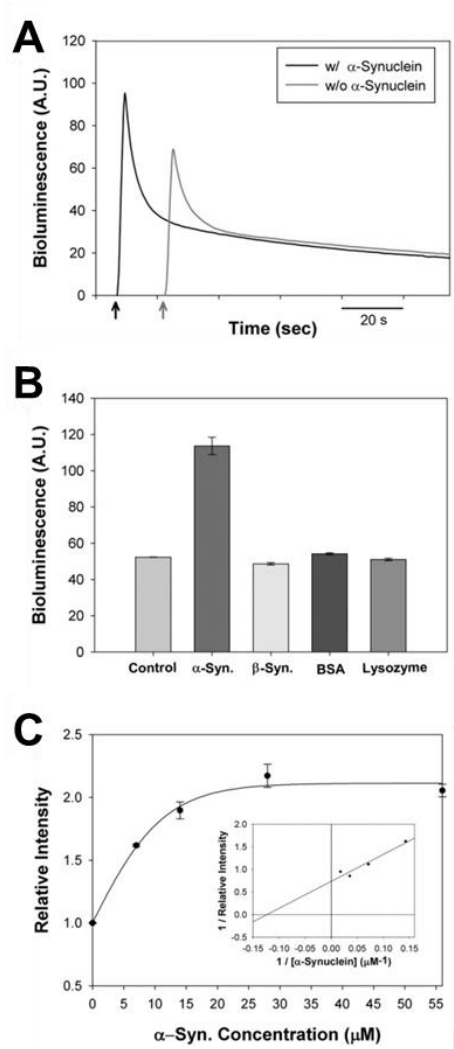

Figure 12. α-Synuclein effects the bioluminescence of firefly luciferase. (A) Enhancement of bioluminescence by α-synuclein. (B) Bioluminescence assay of firefly luciferase in the presence of α-synuclein, β-synuclein, BSA and lysozyme. (C) Relative intensities of the bioluminescence in the presence of α-synuclein at various concentration. The inset shows a double-reciprocal plot of the hyperbolic effect of α-synuclein on bioluminescence. [Kim et al. *Biochim. Biophys. Acta.* **1794** (2009) 309-314.].

1-2. Firefly luciferase accelerates the fibrillation of α-synuclein and induces the morphologically distinctive fibrils

In order to investigate the effect of firefly luciferase (LUC) on the fibrillation of α-synuclein, kinetics of fibrillation was monitored by thioflavin-T (Th-T) binding fluorescence of amyloid fibrils at first. Kinetics study showed that the fibrillation of α-synuclein was considerably accelerated by LUC (Figure 13A). The lag phase reduced from 20 hours to 6 hours and the final intensity of Th-T binding fluorescence increased by one and a half-fold in the presence of LUC at 0.1 μM. According to a previous study, JC-1 (5,5',6,6'-tetrachloro-1,1,3,3'-tetraethylbenzimidazolyl carbocyanine iodide) can also be used as a fluorescent probe to classify α-synuclein according to its assembled states between the intermediate oligomers and the final fibrils [109]. In the absence and presence of LUC, the JC-1 binding fluorescence spectra of amyloid fibrils were monitored between 500 nm and 600 nm with an excitation at 490 nm (Figure 13B). The JC-1 binding fluorescence of the α-synuclein amyloid fibrils prepared in the absence of LUC exhibited the maximum at 539 nm, which was dramatically increased by 4-fold for the fibrils obtained with LUC. In addition, the JC-1 binding fluorescence for the LUC-induced fibrils showed another significant shoulder peak at 561 nm, indicating a distinctive feature of the fibrils derived with LUC.

In order to clarify whether the increases in the final Th-T and JC-1 binding fluorescence intensities were caused by an increase in the actual

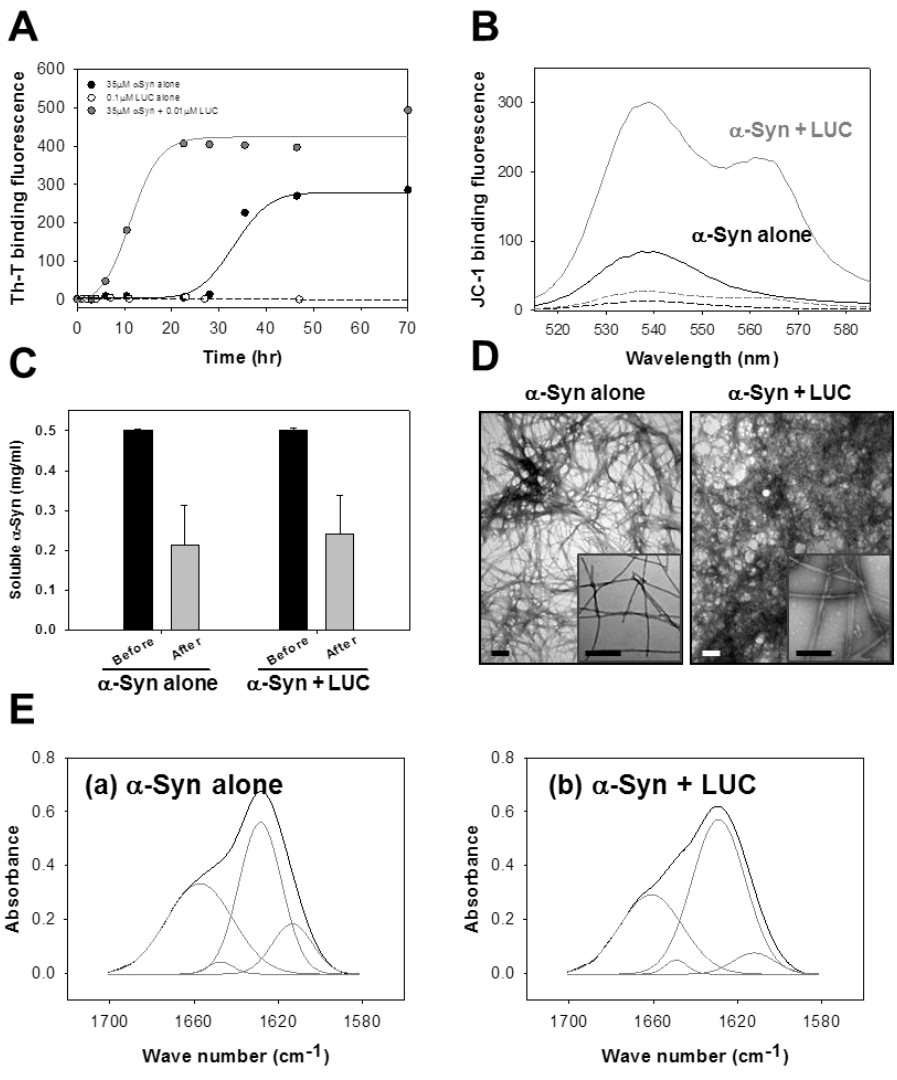
A
35μM αSyn alone
0.1μM LUC alone
35μM αSyn + 0.01μM LUC
Th-T binding fluorescence
Time (hr)
B
α-Syn + LUC
α-Syn alone
JC-1 binding fluorescence
Wavelength (nm)
C
Soluble α-Syn (mg/ml)
Before
After
α-Syn alone
α-Syn + LUC
D
α-Syn alone
α-Syn + LUC
E
(a) α-Syn alone
(b) α-Syn + LUC
Absorbance
Wave number (cm-1)

Figure 13. Enhanced amyloid fibril formation with LUC and the fibrillar polymorphism of α-synuclein in the presence and absence of LUC. (A) Fibrillation kinetics of α-synuclein (35 μM) in the presence (gray) of LUC (0.1 μM). α-Synuclein (black) and LUC (dotted lines) were separately incubated as controls. (B) JC-1 binding fluorescence of the α-synuclein amyloid fibrils prepared without (black) and with LUC (gray). Dotted lines indicate the respective spectra prior to the incubation without (black) and with LUC (gray). (C) Amounts of soluble α-synuclein left in the supernatant before (black) and after (gray) the fibrillation for 70 hours at 37°C. (D) TEM images of amyloid fibrils obtained in the absence (left) and presence (right) of LUC. Magnified (x 4) images are also presented in the insets. Scale bars represent 200 nm. (E) FT-IR spectra of the fibrils prepared in the absence (a) and presence (b) of LUC at amide I region (1600-1700 cm^{-1}). The gray lines obtained via the spectral deconvolution represent protein secondary structures constituting the amyloid fibrils (see Table 2).

amount of fibrils, the monomer levels left behind following 70 hours of the extensive fibrillation in the presence and absence of LUC were monitored with bicinchoninic acid (BCA) protein assay (Figure 13C). The data show that the remaining monomer levels are little different under both conditions with and without LUC, suggesting that LUC presumably yielded a different type of amyloid fibrils. Examination with transmission electron microscopy (TEM) confirmed the distinctive fibrillar structures between the final fibrils obtained in the absence and presence of LUC (Figure 13D). In the presence of LUC, the fibrils were thicker than the fibrils prepared with α-synuclein alone and formed densely populated fibrillar meshwork reflecting more associative nature of the LUC-induced fibrils. The fibrils with LUC showed an average width of 16 nm while the fibrils without LUC was 8 nm.

To elaborate the fibrillar polymorphism, FT-IR spectrophotometer was employed to assess the secondary structures of the fibrils (Figure 13E). In particular, amide I band (1600-1700 cm^{-1}) has been employed to evaluate structural and conformational characteristics of proteins [110-112]. Spectra of the α-synuclein fibrils produced without (Figure 13E-a) and with (Figure 13E-b) LUC were deconvoluted at 1619, 1630, 1650, and 1668 cm^{-1} using OriginPro 8.0 program, which represent anti-parallel β-sheets, parallel β-sheets, α-helices/random coils, and β-turns, respectively [113-115]. The fibrils obtained in the absence of LUC exhibit two major peaks at 1630 cm^{-1} and 1668 cm^{-1} with relative contributions of 50.2% and 29.8% and two minor peaks at 1619 cm^{-1} and 1650 cm^{-1} with 16.3% and 3.7%, respectively (Table 2). The fibrils with LUC, on the other hand, gave rise to the two major peaks

at 1630 cm^{-1} and 1668 cm^{-1} with 58.0% and 29.7% and the two minor peaks at 1619 cm^{-1} and 1650 cm^{-1} with 7.6% and 4.7%, respectively. The results explain that the fibrils with LUC contain higher level of parallel β-sheets with decreased anti-parallel β-sheet content.

1-3. Active conformation of luciferase plays a critical role on the acceleration of α-synuclein fibrillation

In order to confirm whether the enzymatic activity of LUC was essential for the acceleration of α-synuclein fibrillation, the fibrillation kinetics were monitored with and without the inactivated LUC via pre-incubation at 37℃. As the pre-incubation proceeded, LUC was gradually inactivated to 30% of the original activity after 4 hours (Figure 14A). The decrease in LUC activity was accompanied with its structural change as assessed with 8-anilino-1-naphthalenesulfonic acid (ANS) binding fluorescence [116] (Figure 14B). As the enzymatic activity diminished, the fluorescence maximum at 460 nm increased, indicating an exposure of hydrophobic regions of LUC during the pre-incubation. In the presence of the 4 hour pre-incubated LUC, the enhancement of fibrillation was significantly suppressed in comparison with the fibrillation in the presence of fully active LUC even though the suppressed fibrillation was apparently faster than the kinetics observed with α-synuclein alone. Therefore, these data were demonstrated that the accelerated fibrillation by LUC was dependent upon the biological activity and/or active conformation of the enzyme (Figure 14C).

The LUC activity-dependent accelerated fibrillation was further

Table 2. Relative contribution of protein secondary structures to the FT-IR spectra.

Secondary structure	Amide I wavenumber (cm^{-1})	Relative contribution (%)	
		α-Syn alone	α-Syn + LUC
β-Turns	1668	29.8	29.7
α-Helices and/or random coils	1650	3.7	4.7
Parallel β-sheets	1630	50.2	58.0
Antiparallel β-sheets	1619	16.3	7.6

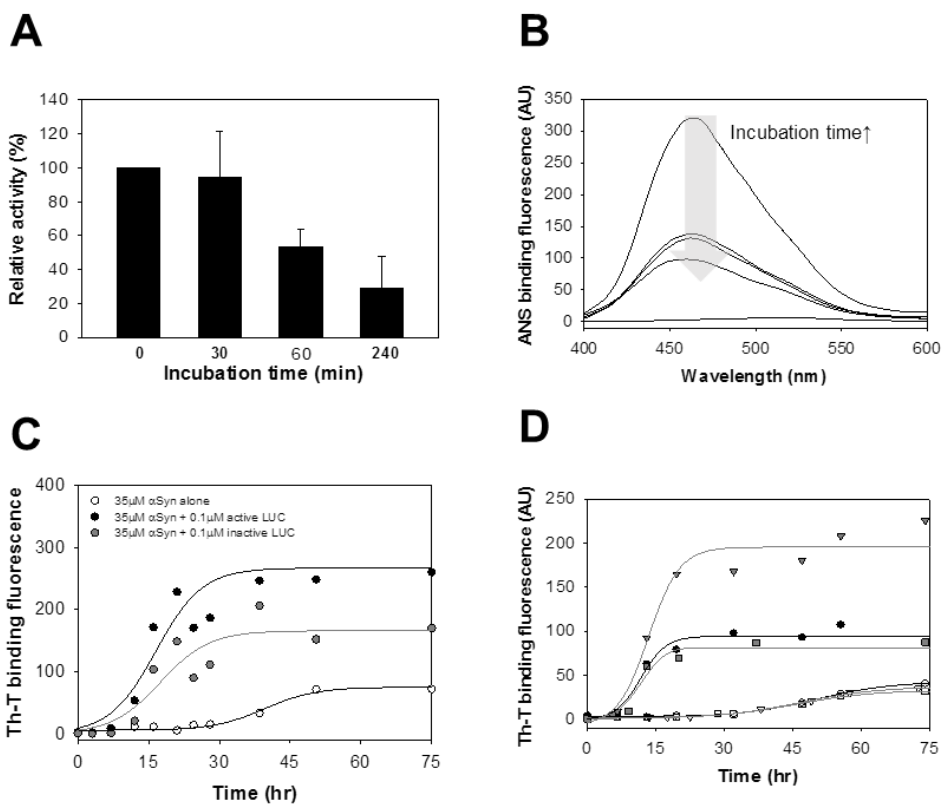
A
Relative activity (%)
140
120
100
80
60
40
20
0
0
30
60
240
Incubation time (min)
B
ANS binding fluorescence (AU)
350
300
250
200
150
100
50
0
Incubation time↑
400
450
500
550
600
Wavelength (nm)
C
Th-T binding fluorescence
400
300
200
100
0
35μM αSyn alone
35μM αSyn + 0.1μM active LUC
35μM αSyn + 0.1μM inactive LUC
0
15
30
45
60
75
Time (hr)
D
Th-T binding fluorescence (AU)
250
200
150
100
50
0
0
15
30
45
60
75
Time (hr)

Figure 14. Requirement of LUC activity for the accelerated α-synuclein fibrillation. (A) LUC activity remaining after incubations at 37°C for 0, 30, 60, and 240 min was examined with an emitted light at 550 nm. (B) ANS binding fluorescence of LUC after incubations at 37°C for 0, 30, 60, and 240 min. Fluorescence spectra of ANS was monitored between 400 and 600 nm with an excitation at 350 nm. (C) Fibrillation kinetics of α-synuclein in the presence of active (black) and inactive (gray) LUC. α-Synuclein (black) was separately incubated at 35 μM as a control. (D) Fibrillation kinetics of α-synuclein with LUC and substrates (luciferin and ATP-Mg^{2+}). In the absence of LUC, α-synuclein (35 μM) was fibrillated without (○) and with the substrate of either 0.5 μM luciferin (□) or 0.5 μM ATP-Mg^{2+} (▽). The fibrillation kinetics of α-synuclein was also monitored in the presence of LUC (0.1 μM) without the substrates (●) and with either 0.5 μM luciferin (■) or 0.5 μM ATP-Mg^{2+} (▼).

investigated in the presence of LUC's substrates such as luciferin and ATP-Mg^{2+}. In the absence of LUC, neither luciferin nor ATP-Mg^{2+} at 0.5 μM affected the fibrillation kinetics of α-synuclein. With LUC at 0.1 μM, however, luciferin increased the Th-T binding fluorescence at the stationary phase twice as much as the fluorescence obtained without the luciferin (Figure 14D). ATP-Mg^{2+}, on the other hand, decreased the Th-T binding fluorescence by 0.8-fold from its absence. From these results, the active conformation of LUC which could be influenced by the substrates during the initial period of fibrillation appears to be crucial for the enhanced amyloidogenesis.

1-4. Self-propagation of the altered morphology of α-synuclein fibrils prepared with luciferase

To clarify whether the newly developed morphology of the LUC-induced amyloid fibrils of α-synuclein was transient or inherent to the fibrils, the self-propagation experiment of amyloid fibrils was carried out. Previous studies demonstrated that the properties of amyloid fibrils can be transferred to subsequent daughter fibrils by introducing a small amount of amyloid fragments derived from their parent strands to a fibrillation process of amyloidogenic protein [117-119]. α-Synuclein fibrillation was seeded at 5% (w/w) with the amyloid fragments obtained from the parent fibrils prepared in the presence and absence of LUC with sonication (Figure 15). In the presence of the seeds derived from the fibrils prepared without LUC, the lag period completely disappeared while the final Th-T binding fluorescence

reached to the same level as the fibrillation obtained without the seeds. In the presence of the LUC-induced seeds at 5% (w/w), on the other hand, the final Th-T binding fluorescence increased drastically by more than 4-folds, which was reminiscent of the accelerated LUC-induced α-synuclein fibrillation as observed in Figure 13A. The lag phase, however, was also shortened significantly from the unseeded fibrillation, but it was definitely longer than the kinetics obtained with the seeds prepared in the absence of LUC. To confirm whether the increase in the final Th-T binding fluorescence was due to the altered morphology of amyloid fibrils instead of their actual quantity, the fluorescence intensity was divided by the mass of fibrils [120]. The result indicated that the fibrils derived with LUC-induced seeds yielded higher Th-T binding fluorescence per mass of fibrils by two-fold than that of the fibrils obtained with the seeds prepared with α-synuclein alone (Figure 15B). The data suggest that the increased Th-T binding fluorescence was not due to the actual amount of the fibrils but their altered properties reflected in the fibrillar morphology.

As morphologies of the final amyloid fibrils were examined with transmission electron microscope, structural characteristics of the paraental strands were transferred to their respective daughter fibrils. While rather straight and untangled fibrils were obtained for the daughter fibrils with the seeds prepared with α-synuclein alone, the LUC-induced seeds produced the associative daughter fibrils which resembled the fibrils of α-synuclein prepared in the presence of LUC (Figure 15D). This self-propagation property of the LUC-induced fibrils would suggest that the unique morphology of α-

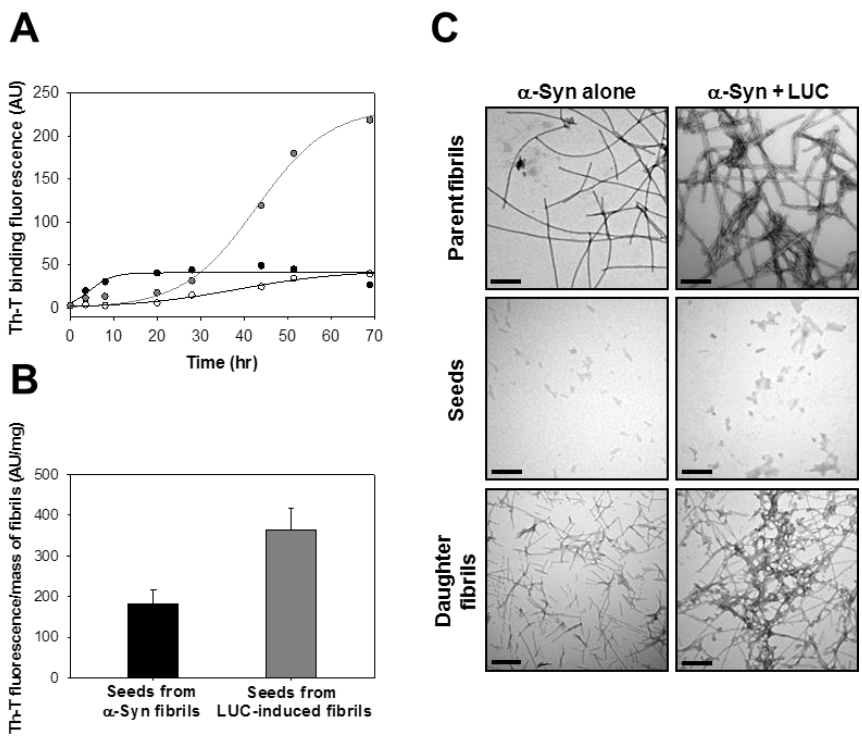

Figure 15. Self-propagation of the two amyloid polymorphs. (A) Fibrillation kinetics of α-synuclein with the seeds at 5% (w/w). α-Synuclein at 35 μM was incubated in the absence (black open dot) and presence of the seeds prepared from either the α-synuclein fibrils (black closed dot) or the LUC-induced fibrils (gray closed dot). (B) The Th-T binding fluorescence per mass of fibrils self-propagated in the presence of the seeds derived from either the α-synuclein fibrils (black) or the LUC-induced fibrils (gray). (C) TEM images of the α-synuclein amyloid fibrils (top row) and the LUC-induced fibrils (bottom row) from the parent amyloid fibrils to their daughter fibrils. Scale bars, 200 nm.

synuclein fibrils derived with LUC became inherent to the fibrils.

This study has shown that a single amyloidogenic protein turns into two different fibrils with distinctive morphologies. This difference of protein assembly has been achieved with a biologically active enzyme of luciferase. The process can be hypothesized that α-synuclein exists in a kinetically trapped state from which the protein escapes by demolishing certain part(s) of the surrounding energy barrier. Once the protein surpasses the surrounding energy barrier, the protein might be stabilized into thermodynamically stable states via one or more pathways by yielding various forms of amyloid fibrils (Scheme 1). Both LUC and a transformed aggregative α-synuclein might be able to lower the activation barrier by acting as a template for the pristine α-synuclein. The resulting two distinctive fibrils could directly work as the seeds in the fibrillation process, amplifying the amyloid fibrils.

In fact, all the data shown in this study illustrate that the fibrillar polymorphism has been directed by the seed generated by specific mutual interaction between α-synuclein and the biologically active LUC. The observations including the drastically reduced lag phase of α-synuclein fibrillation in the presence of LUC, the altered dye binding properties of the LUC-induced amyloid fibrils with thioflavin-T and JC-1, and the biochemical and morphological analysis of the fibrils with FT-IR and TEM support the seed-dependent alternative amyloid fibril formation. This phenomenon, therefore, emphasizes the significance of nucleation centers for amyloid fibril formation in terms of not only facilitating the fibrillation process but also

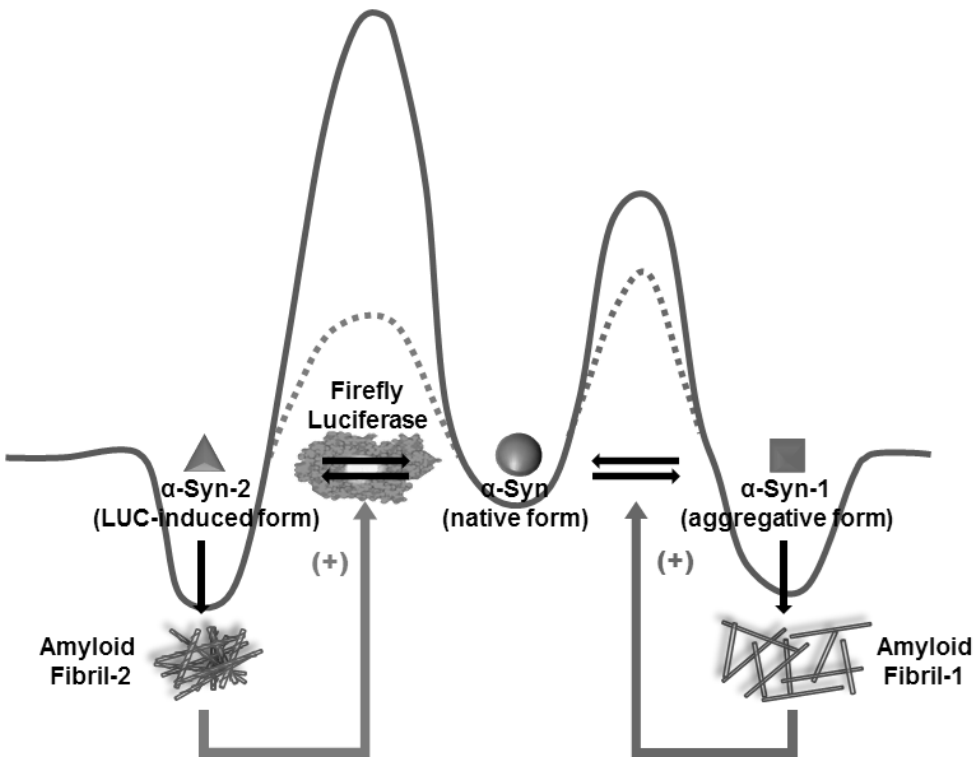

Scheme 1. Amyloid polymorphism of α-synuclein with and without LUC.

endowing those fibrils with certain biochemical properties. Those fibrils with unique properties, then, could be further amplified via the self-propagation procedure since the morphological characteristics become inherent to the newly developed fibrils.

This study, therefore, opens up a possibility that enzymes or even other biomolecules could have potentials to act as templates for amyloidogenic proteins like α-synuclein, exhibiting the fibrillar polymorphism. By assuming that the cellular toxicity of amyloidogenic proteins could be associated the morphological and thus biochemical characteristics of amyloid fibrils in addition to the fact that those fibrils could be self-propagated, the diversified fibrils produced by a lot of biological partners could be considered as independent toxic causes.

2. Mutual influences of α-synuclein and glutathione peroxidase

2-1. α-Synuclein enhances antioxidant activity of glutathione peroxidase-1

To investigate mutual interactions between α-synuclein and GPX-1, an effect of α-synuclein on the antioxidant activity of GPX-1 was first examined. The GPX-1 activity was monitored with a coupling system employing cumene hydroxide and GSH in the presence of glutathione reductase/NADPH [121]. The enzyme was pre-incubated with α-synuclein at 4˚C for 20 min before assessed by observing the decrease in NADPH absorbance at 340 nm due to the reduction of GSSG back to GSH by glutathione reductase. Significant

enhancement of GPX-1 activity was observed with α-synuclein (Figure 16). As shown the increased negative slopes reflecting enhanced NADPH consumption in Figure 16A, GPX-1 activity became continuously increased as α-synuclein level increased. Neither glutathione reductase activity nor oxidation of NADPH was affected by α-synuclein. Direct molecular interaction between α-synuclein and GPX-1 was evaluated by plotting the initial activities of GPX-1 obtained as changes of moles of NADPH per min per mg protein as a function of α-synuclein in molarity (Figure 16B). The enhanced GPX-1 activities exhibited a hyperbolic relationship with α-synuclein, indicating a possible specific binding between the two proteins. By performing a double reciprocal plot, their dissociation constant was estimated as 17.3 nM (Figure 16B, inset). The α-synuclein-mediated enhancement of GPX-1 activity and the exceptionally high molecular affinity would suggest a novel physiological role of α-synuclein in cellular anti-oxidative processes. In fact, a direct and tight interaction between the two proteins under physiological condition was demonstrated with immunocytochemical analysis of neuroblastoma cell-line, SH-SY5Y. Confocal microscopic images of immunofluorescence-stained cells with anti-α-synuclein and anti-GPX-1 antibodies showed that both intrinsic proteins were found to be co-localized in SH-SY5Y cells (Figure 16C). Taken together, these results suggest a physiological function of α-synuclein as a GPX's natural partner in cellular environment working as a GPX-1 activator and thus acting as an anti-oxidative agent.

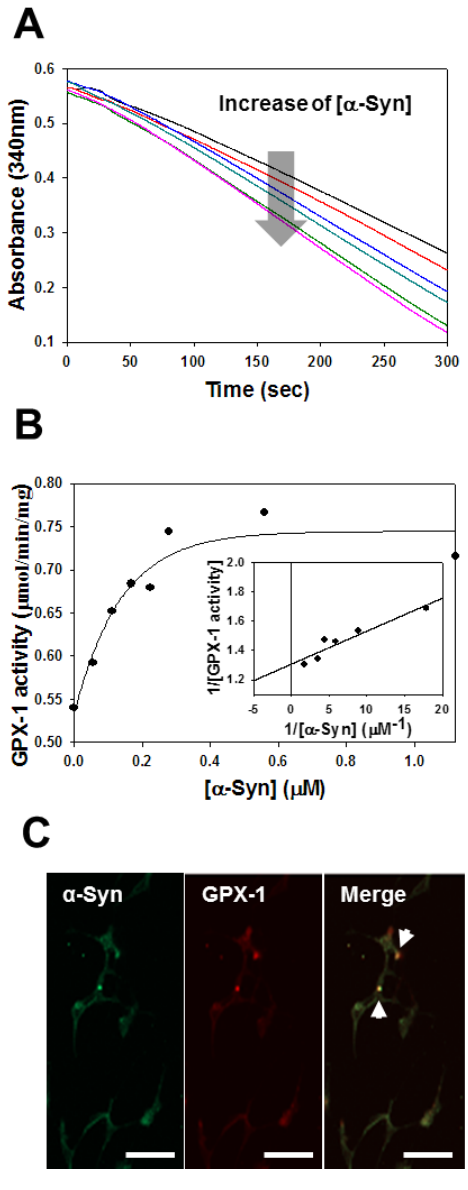
A
Increase of [α-Syn]
Absorbance (340nm)
Time (sec)
B
GPX-1 activity (μmol/min/mg)
[α-Syn] (μM)
1/[GPX-1 activity]
1/[α-Syn] (μM-1)
C
α-Syn
GPX-1
Merge

Figure 16. α-Synuclein-mediated enhancement of GPX-1 activity. (A) GPX-1 activities with increased α-synuclein concentrations. GPX-1 (5 nM) was pre-incubated with 0 (black), 56 (red), 112 (blue), 224 (cyan), 280 (green), and 560 nM (pink) of α-synuclein at 4°C for 20 min, and the enzyme activity was monitored by observing the decrease in NADPH absorbance at 340nm. (B) Initial activities of GPX-1 are plotted as a function of α-synuclein in molarity. Double reciprocal plot was performed to obtain the dissociation constant between GPX-1 and α-synuclein (inset). (C) Immunocytochemical analysis of SH-SY5Y neuroblastoma cell-line. Co-localization of GPX-1 and α-synuclein was visualized by staining cells with anti-α-synuclein and anti-GPX-1 antibodies. Scale bar, 50 μm.

2-2. Glutathione peroxidase-1 accelerates amyloid fibrillation of α-synuclein

Since GPX-1 was found to exist in α-synuclein-enriched Lewy bodies [84], GPX-1 effect on the amyloidogenesis of α-synuclein has been examined. By using typical kinetics study using thioflavin-T (Th-T) fluorescence assay, it was demonstrated that *in vitro* fibrillation of α-synuclein was remarkably accelerated by GPX-1 in a dose-dependent manner (Figure 17A). Addition of GPX-1 at 0.05 μM was sufficient to show the facilitated fibrillation of α-synuclein at 20 μM by shortening the lag period and increasing the final Th-T binding fluorescence. As the GPX-1 level increased twice, the lag further decreased from 40 hours to 20 hours. Moreover, the final Th-T binding fluorescence also increased by almost two-fold from that of the kinetics obtained with α-synuclein alone. Based on the high affinity with Kd at nM range, the tight α-synuclein-GPX-1 complex would provide a nucleation center for the accelerated and enhanced amyloidogenesis.

To demonstrate whether the activity of GPX-1 is crucial for the GPX-1-mediated acceleration of α-synuclein fibrillation, the fibrillation kinetics was carried out with GPX-1 in varying activities after pre-incubating the enzyme at 37℃ by itself (Figure 17C). In the presence of the enzyme at 100%, 50% and 25% of its activity, the shortened lag period was 13.1 hr, 15.6 hr and 25.5 hr, respectively, whereas α-synuclein required about 40 hr to be fibrillated in the absence of the enzyme (Figure 17B). In addition, the enhanced final fluorescence obtained with the enzyme at its full activity

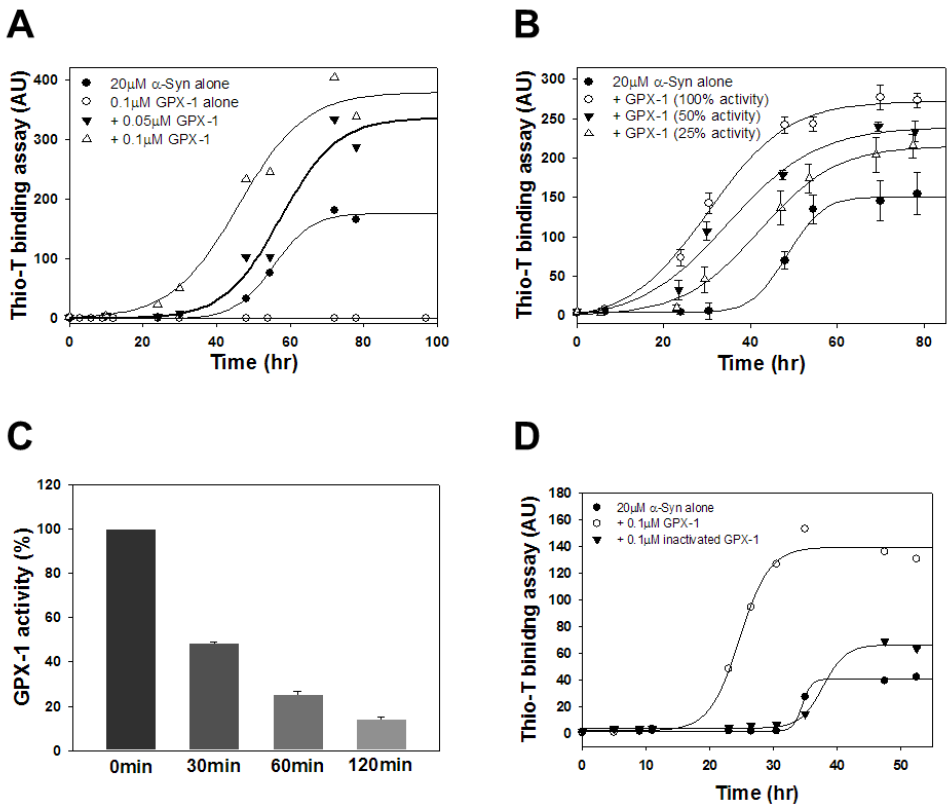
A
Thio-T binding assay (AU)
Time (hr)
20μM α-Syn alone
0.1μM GPX-1 alone
+ 0.05μM GPX-1
+ 0.1μM GPX-1
B
Thio-T binding assay (AU)
Time (hr)
20μM α-Syn alone
+ GPX-1 (100% activity)
+ GPX-1 (50% activity)
+ GPX-1 (25% activity)
C
GPX-1 activity (%)
0min
30min
60min
120min
D
Thio-T binidng assay (AU)
Time (hr)
20μM α-Syn alone
+ 0.1μM GPX-1
+ 0.1μM inactivated GPX-1

Figure 17. GPX-1-mediated acceleration of the amyloid fibrillation of α-synuclein. (A) Aggregation kinetics of α-synuclein in the presence of GPX-1. α-Synuclein (20 μM) was incubated with 0.05 (▼) and 0.1 μM GPX-1 (△) at 37°C with vigorous shaking. Amyloid fibrillation was monitored by thioflavin-T binding fluorescence at 482 nm (emission at 450 nm) during incubation. α-Synuclein (●) and GPX-1 (○) were separately incubated as controls. (B) GPX-1 activity-dependency of the amyloid fibrillation of α-synuclein. Partially inactivated GPX-1 was obtained at various time points during pre-incubation of the enzyme alone at 37°C. α-Synuclein (20 μM) was fibrillated with 0.1 μM GPX-1 with decreasing activities from 100 % (○), 50 % (▼), and 25 % (△). (C) The time-dependent decrease of GPX-1 activity. GPX-1 alone was incubated at 37°C for 0 min, 30 min, 60 min, and 120 min under quiescent condition. The enzyme activity was monitored by observing the decrease in NADPH absorbance at 340nm (n=3). (D) Amyloid fibrillation of α-synuclein in the presence of heat-inactivated GPX-1. 20 μM α-synuclein was incubated with active GPX-1 (○) and heat-inactivated GPX-1 (▼) at 37°C with vigorous shaking. Amyloid fibrillation was monitored by thioflavin-T binding fluorescence at 482 nm (emission at 450 nm) during incubation.

proportionally decreased as the enzymatic was inactivated (Figure 17B). These findings clearly indicate that the biochemically active GPX-1 is required for the enzyme-mediated acceleration of α-synuclein fibrillation by both shortening the lag phase and increasing the final fibrillation level. Addition of completely inactivated GPX-1 obtained via heating at 100˚C resulted in a fibrillation kinetics indistinguishable from that of α-synuclein alone (Figure 17D).

2-3. Entangled fibrillar aggregates of α-synuclein acting as a depot for active GPX-1

Morphological comparison of the final fibrillar aggregates of α-synuclein obtained in the absence and presence of GPX-1 revealed that the fibrils resulted from the accelerated fibrillation with the enzyme were densely entangled (Figure 18A). Immunogold labeling was performed with anti-GPX-1 antibody in order to evaluate the GPX-1 distribution within the entanglement. The enzymes were found to be locally clustered into the GPX-1-islets within the fibrillar meshwork (Figure 18B). This entrapment of GPX-1 into the α-synuclein fibrils which has occurred during the *in vitro* fibrillation process is compatible with the previous observation of their co-existence in the Lewy bodies of PD patient's brain [84].

In order to examine the enzymatic activity of the entrapped GPX-1, the GPX-1-containing fibrils were resuspended in the assay mixture and the decrease of NADPH absorbance at 340 nm was monitored. Impressively, the entrapped GPX-1 retained most of their activities during the prolonged

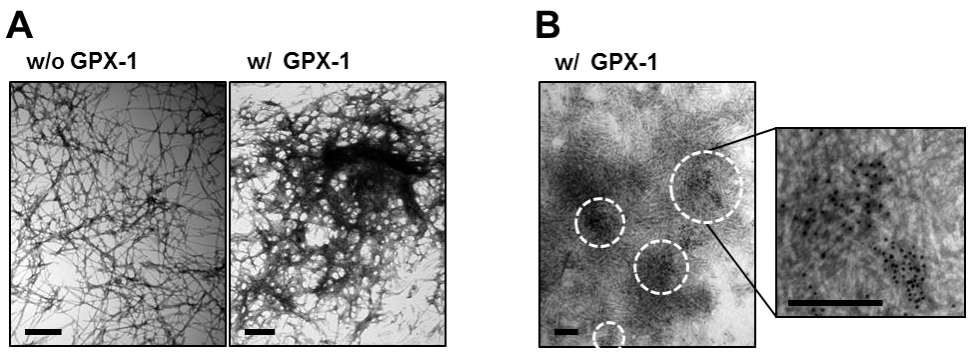

Figure 18. Localization of GPX-1 within entangled α-synuclein fibrils. (A) Morphologies of GPX-1-induced α-synuclein fibrils. Scale bar, 0.5 μm. (B) Distribution of GPX-1 within the entangled fibrils. Immunogold labeling was performed with anti-GPX-1 and gold-conjugated secondary antibodies. Dashed circles indicate GPX-1-islets. All samples for TEM analysis were negatively stained with 2 % uranyl acetate on carbon-coated copper grids. Scale bar, 200 nm.

incubation of the fibrillation for 70 hr while the activity was almost completely vanished following only 2 hr of incubation at 37℃ in the absence of the fibrils (Figure 19A and Figure 17C). The time course of the entrapped GPX-1 activity exhibited hysteresis, indicating that the NADPH consumption gradually increased as a function of time (Figure 19B). By plotting slopes of the tangent lines of the activity trace at various time points, the GPX-1 activity previously entrapped in the matrix was shown to increase linearly to its maximum during the initial 25 min, and then the activity remained unaffected until the substrate was completely consumed (Figure 19B, inset).

To account for the hysteresis in activity, the enzyme-entrapped fibrillar matrix was successively extracted with a fixed amount (100 μL) of 20 mM MES, pH 6.5, and the GPX-1 activity in the extracts was measured. Interestingly, the extracted activity also exhibited the hysteresis when compared with a control of GPX-1 (Figure 19C). As the extraction proceeded, the GPX-1 was continuously released in solution with subsequently diminished activities. In addition, the hysteresis became less apparent as the extracted GPX-1 activity decreased (Figure 19C, *inset*). This result indicates that the GPX-1 would be entrapped within the fibrillar matrix, which can be slowly activated upon its release. Moreover, the gradual increase in the GPX-1 activity observed with the GPX-1 containing matrix (Figure 19B) would be also due to the slow release of the enzyme from the matrix.

Based on findings, antioxidative function of α-synuclein has been suggested in terms of mutual activation between GPX-1 and amyloidogenesis of α-

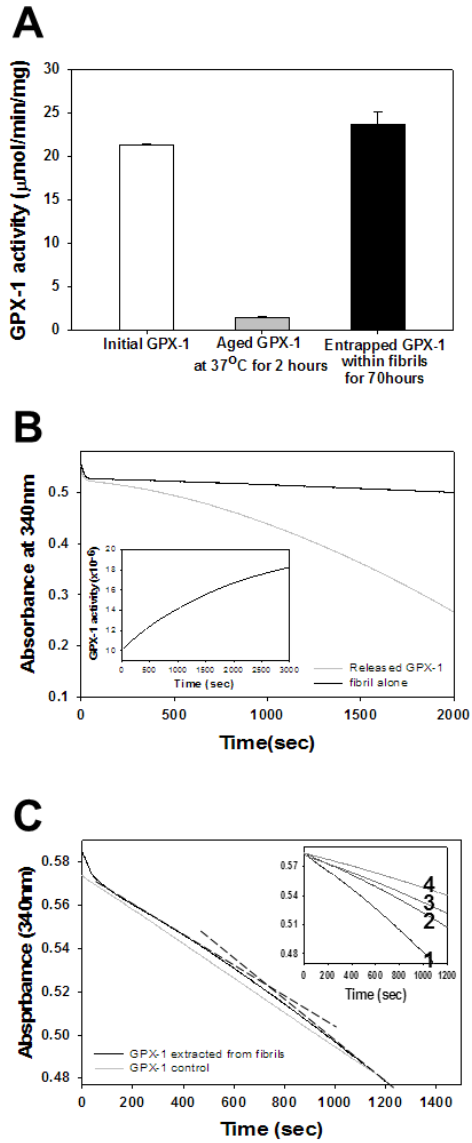
A
GPX-1 activity (μmol/min/mg)
30
25
20
15
10
5
0
Initial GPX-1
Aged GPX-1 at 37°C for 2 hours
Entrapped GPX-1 within fibrils for 70hours
B
Absorbance at 340nm
0.5
0.4
0.3
0.2
0.1
0
500
1000
1500
2000
Time(sec)
GPX-1 activity(x10⁻⁶)
Time (sec)
Released GPX-1
fibril alone
C
Absorbance (340nm)
0.58
0.56
0.54
0.52
0.50
0.48
0
200
400
600
800
1000
1200
1400
Time (sec)
GPX-1 extracted from fibrils
GPX-1 control
4
3
2
1

Figure 19. Enzymatic activity of the entrapped GPX-1. (A) Protection of GPX-1 activity within the fibrillar matrix. GPX-1 activity was monitored after the α-synuclein fibrillation was carried out in the presence of GPX-1 for 3 days at 37°C. Initial and 2 hr-aged activities of GPX-1 at 37°C were shown as controls. (B) Time course of the entrapped GPX-1 activity. The GPX-1-containing fibrils were isolated by centrifugation at 16100 $\times$ g for 30 min, and resuspended in the GPX-1 assay mixture. The slope of the tangent lines of the activity trace was re-plotted at various time points (inset). (C) Reactivation of GPX-1 released from fibrils. Successive extraction of the GPX-1-entrapped fibrillar matrix was carried out with 100 mL of 20 mM MES (pH 6.5) and each extract was subjected to the activity measurement. Black-dashed lines indicate initial and final activities of the released enzyme in the first extract. GPX-1 without the prior entrapment was used as a control (gray). The enzyme activities in the successive extracts were shown (inset); number indicates the extraction order.

synuclein (Scheme 2). The H_2O_2-removing process of GPX-1 is significantly activated by interacting with α-synuclein, and the α-synuclein-GPX-1 complex provides a possible nucleation center for the accelerated amyloid fibril formation of α-synuclein, which results in the entangled filamentous aggregates with the GPX-1 deposited in a locally concentrated fashion. In addition, it has been previously reported that oxidized GSH (GSSG) also enhanced the amyloidogenesis of α-synuclein [54]. Taken together, the physiological function of α-synuclein and its amyloidogenesis can be understood with respect to the anti-oxidative GPX-1 system including glutathione turnover. Therefore, it can be considered that the mutual effects between α-synuclein and GPX-1 would contribute to strengthen the cellular defense against toxic insults; as an activator of cellular GPX-1, α-synuclein improves the enzyme's antioxidant activity by removing toxic H_2O_2 with the formation of GSSG, and the resulting α-synuclein-GPX-1 complex along with GSSG removes the toxic oligomers of α-synuclein by facilitating the innocuous amyloid fibril formation [122]. Under pathological conditions, α-synuclein has been reported to be involved in the oxidative stress via causing mitochondrial dysfunction or direct generation of ROS from its aggregates [123-125]. In this report, however, it has been suggested that α-synuclein might be a novel physiological partner of GPX-1, which improves the enzyme's capability of preventing oxidative damages. Since a considerable amount of oxygen is consumed in brain tissues and the activity of GPX-1 in brain is relatively low compared to other tissues, brain tissues are vulnerable

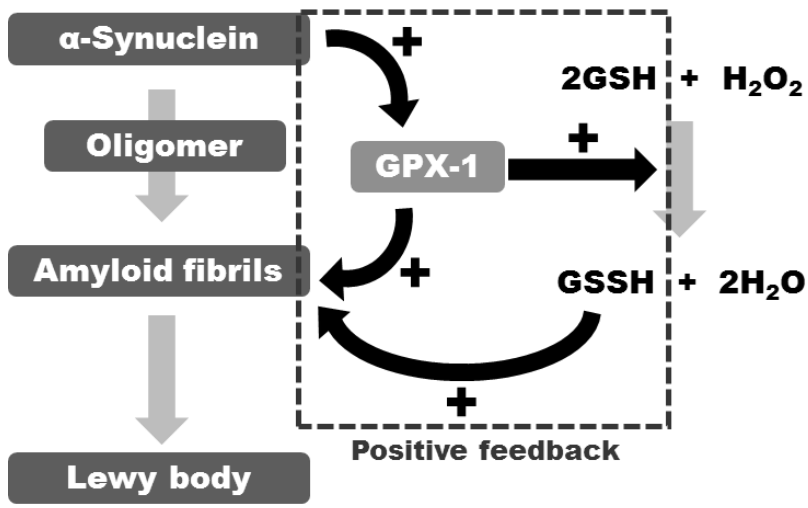

Scheme 2. Mutual relationship between GPX-1 and the amyloidogenesis of α-synuclein.

to oxidative insults and PD may be exacerbated by the substantial decrease of GSH in the affected region of substantia nigra [126-128]. Therefore, it is hypothesized that abundant pre-synaptic α-synuclein may complement the weakened antioxidant defense of nerve tissues by acting as an activator of cellular GPX-1. More surprisingly, it was also found that the GPX-1 entrapped within the entangled fibrils retained most of its activity during the prolonged incubation, which could be slowly released and also partially activated. These facts would suggest that α-synuclein fibrils can act as a biologically meaningful depot to retain GPX-1 in a latent form. Consequently, α-synuclein and its fibrils could be considered to be involved in antioxidative processes within neuronal cells. Although the issue of toxic effects of amyloid fibrils is still controversial, these well-promoted pathological structures now could be conceptually transformed into a physiologically active component of cellular biogenesis.

3. Effects of phenolic compounds on assembly of α-synuclein

3-1. Molecular interaction between α-synuclein and phenolic compounds

In order to examine the influences of phenolic compounds on α-synuclein fibrillation, α-synuclein was treated with three phenolic compounds (Figure 20) which are abundant in daily foods such as red wine, curry and green tea. The molecular interaction between α-synuclein and phenolic compounds were investigated by monitoring tyrosine intrinsic fluorescence of α-

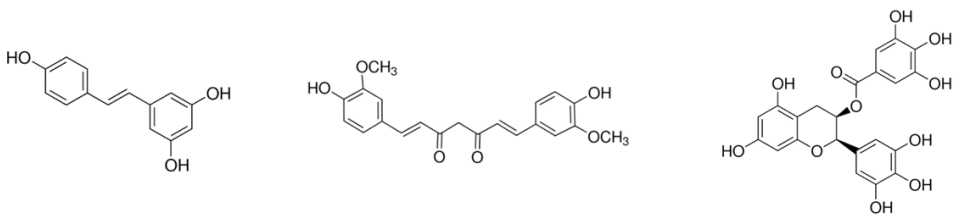

Resveratrol (RSV) | **Curcumin (CUR)** | **(-)-Epigallocatechin gallate (EGCG)**

Figure 20. Phenolic compounds of resveratrol, curcumin and (-)-epigallocatechin gallate from red wine, curry and green tea.

synuclein in the presence of resveratrol (RSV) (Figure 21A-a), curcumin (CUR) (Figure 21B-a) and (-)-epigallocatechin gallate (EGCG) (Figure 21C-a) at various concentrations. Their interactions were verified by plotting the differences in the intrinsic fluorescence at 308 nm as a function of phenolic compounds concentration (Figure 21-b). In Figure 21C-a, emission peaks at around 380 nm indicate the intrinsic fluorescence of EGCG with excitation at 274 nm. The x-intercepts in double-reciprocal plots (Figure 21-b, *inset*) show that RSV, CUR and EGCG bind to monomeric α-synuclein with a dissociation constant (Kd) of 30.4 μM, 133 μM and 100 μM, respectively. Therefore, it has been clearly revealed that these phenolic compounds are α-synuclein interacting molecules.

3-2. Interference of phenolic compounds in detecting amyloid formation with thioflavin-T binding fluorescence method.

As shown in the Figure 21C-a, phenolic compounds exhibit individually intrinsic fluorescence (Table 3) because they are typical conjugated compounds resulting in strong $\pi \rightarrow \pi^*$ electronic transitions. For this reason, the thioflavin-T (Th-T) fluorescence assay is considered unsuitable for amyloid fibril detection in the presence of phenolic compounds [129]. In order to examine the interferences of phenolic compounds in Th-T fluorescence assay, fluorescence spectra from 460 nm to 600 nm were obtained with excitation at 450 nm after pre-made amyloid fibrils (AF) and Th-T were incubated for 5 min in the absence and presence of phenolic compounds (Figure 22A). First of all, Th-T binding to AF was excited at 450

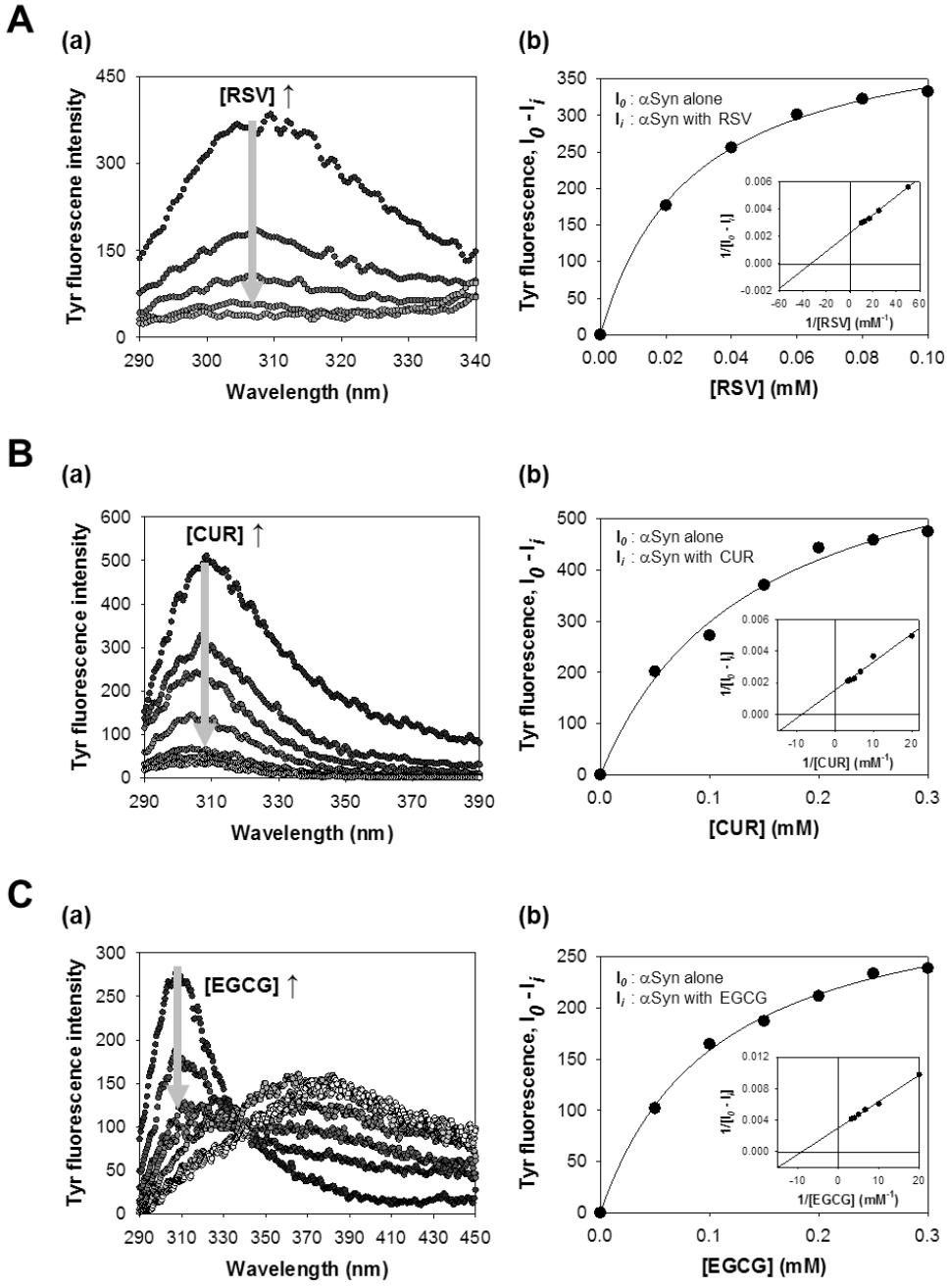
A
(a)
[RSV] ↑
Tyr fluorescene intensity
Wavelength (nm)
(b)
I_0 : αSyn alone
I_i : αSyn with RSV
Tyr fluorescence, $I_0 - I_i$
1/[RSV] (mM^{-1})
[RSV] (mM)
B
(a)
[CUR] ↑
Tyr fluorescence intensity
Wavelength (nm)
(b)
I_0 : αSyn alone
I_i : αSyn with CUR
Tyr fluorescence, $I_0 - I_i$
1/[CUR] (mM^{-1})
[CUR] (mM)
C
(a)
[EGCG] ↑
Tyr fluorescence intensity
Wavelength (nm)
(b)
I_0 : αSyn alone
I_i : αSyn with EGCG
Tyr fluorescence, $I_0 - I_i$
1/[EGCG] (mM^{-1})
[EGCG] (mM)

Figure 21. Molecular interaction between α-synuclein and phenolic compounds. Tyrosine intrinsic fluorescence of α-synuclein was monitored after coincubation with various concentration of resveratrol (RSV) (A-a), curcumin (CUR) (B-a) and (-) epigallocatechin gallate (EGCG) (C-a) for 30 min at 37°C. The differences in the intrinsic fluorescence at 308 nm were plotted as a function of phenolic compounds concentration (b). According to the x-intercepts in double-reciprocal plots (b, *inset*), monomeric α-synuclein binds to RSV, CUR and EGCG with a dissociation constant (Kd) of 30.4 μM, 133 μM and 100 μM, respectively.

Table 3. Intrinsic fluorescence of Thioflavin-T, RSV, CUR, and EGCG.

αSyn interactive molecules	Absorption (Excitation)	Fluorescence emission
Thioflavin T with amyloid fibrils	450 nm	482 nm
Resveratrol (RSV)	320 nm	300-600 nm
Curcumin (CUR)	426 nm	540 nm
(-)-Epigallocatechin gallate (EGCG)	275 nm	350 – 400 nm

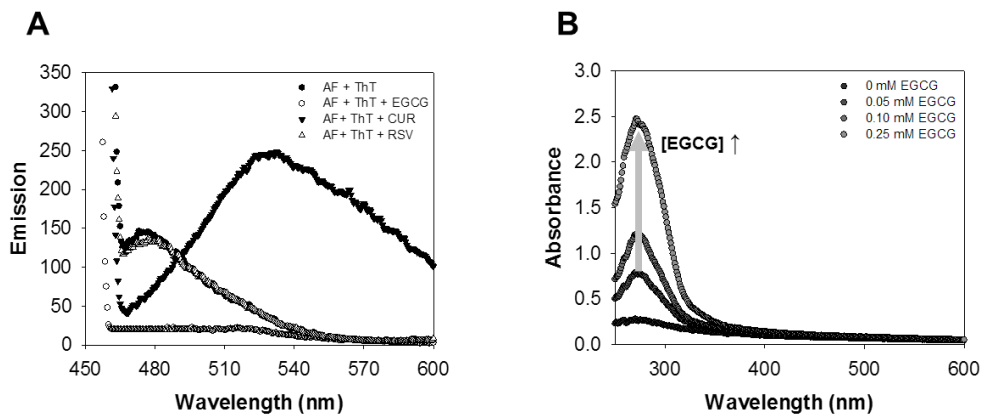

Figure 22. Effects of phenolic compounds on thioflavin-T (Th-T) fluorescence assay for detecting amyloid fibrils. (A) The Th-T fluorescence spectra in the absence (●) and presence of EGCG (○), CUR (▼) and RSV (△). The fluorescence spectra between 460 nm and 600 nm with excitation at 450 nm were obtained after pre-made amyloid fibrils and Th-T were incubated with EGCG, CUR and RSV for 5 min in the dark. (B) Absorption spectra of EGCG at various concentration.

nm and exhibited fluorescence at 480 nm in the absence of phenolic compounds (●) and in the presence of RSV (△), clarifying that RSV did not affect the fluorescence of Th-T. In the presence CUR (▼), however, Th-T fluorescence quenching was occurred because CUR molecules totally absorbed the lights with wavelength both 450 nm and 480 nm (data not shown) and exhibited their fluorescence at 530 nm. Strangely, the Th-T fluorescence disappeared in the presence of EGCG although EGCG did not absorbed lights at 450 nm and 480 nm (Figure 22B). Taken together, it has been verified that Th-T fluorescence assay is not appropriate for monitoring the effects of phenolic compounds on the fibril formation.

In Figure 22, it was observed that EGCG specifically interrupted Th-T binding fluorescence assay for detecting amyloid fibrils. This result showed that Th-T molecule might be hindered in binding to amyloid fibrils rather than its fluorescence was quenched by EGCG because EGCG did not absorb Th-T emission light. In order to examine the effect of EGCG on binding of Th-T to amyloid fibrils, Th-T fluorescence was monitored in the presence of EGCG at various concentration (Figure 23). Pre-made amyloid fibrils at 7 μM were incubated with 2.5 μM of Th-T and various concentration of EGCG for 5 min in the dark and the emission spectra of mixtures were obtained with excitation at 450 nm (Figure 23A). According to the graph of differences of Th-T fluorescence at 482 nm as a function of EGCG concentration (Figure 23B), Th-T fluorescence decreased as EGCG concentration increased with half maximal inhibitory concentration (IC_{50}) of 0.044 mM.

In order to verify whether the decrease of Th-T fluorescence was

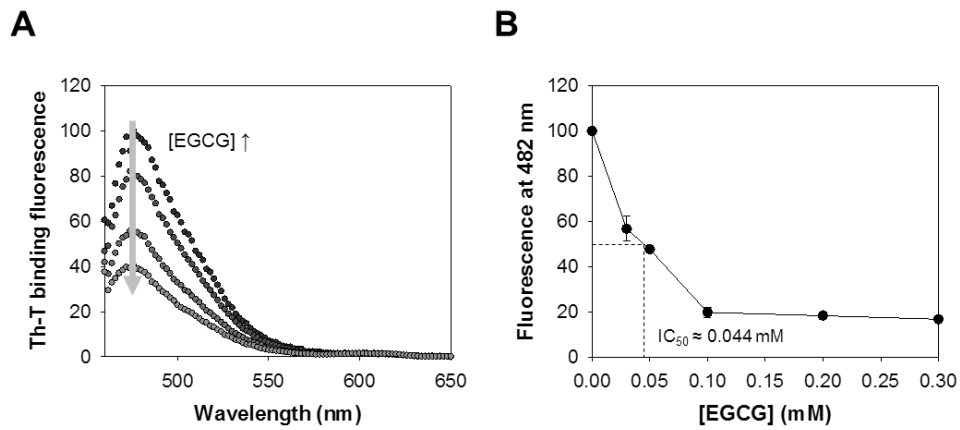

Figure 23. Interference of EGCG in Th-T binding fluorescence assay for detecting amyloid fibrils. (A) Fluorescence spectra were obtained after Th-T and amyloid fibrils interacted with various concentration of EGCG for 5 min in the dark. (B) A graph shows decrease of Th-T fluorescence at 482 nm with increase of EGCG concentration.

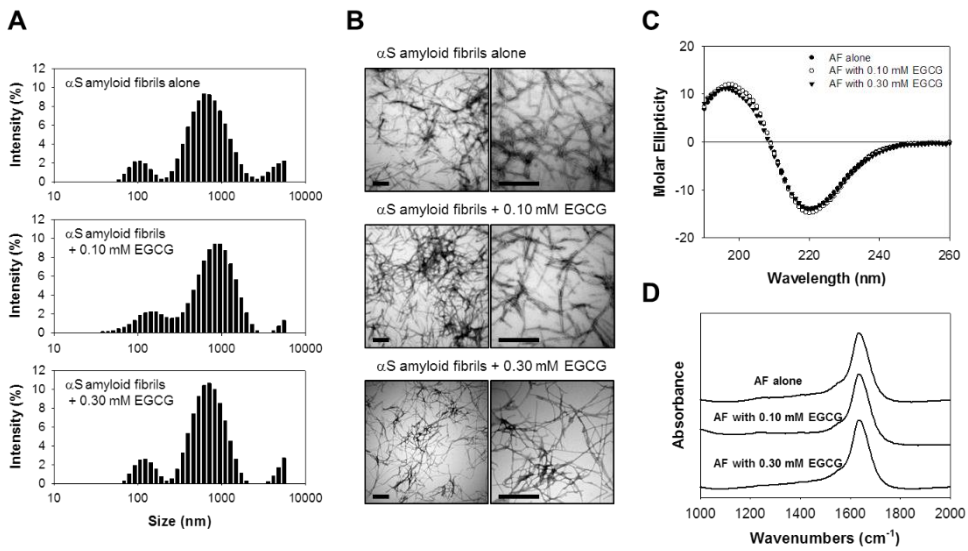

Figure 24. Effects of EGCG on α-synuclein amyloid fibrils. After incubation with EGCG for 1 hr at 37°C, α-synuclein amyloid fibrils were analyzed by dynamic light scattering system (A), TEM (B), CD spectroscopy (C) and FT-IR spectroscopy (D).

caused by EGCG-induced disintegration and structural alteration of amyloid fibrils, α-synuclein fibrils were post-treated with EGCG for 1 hr at 37℃ and analyzed with dynamic light scattering (DLS) system, transmission electron microscopy (TEM), circular dichroism spectroscopy (CD) and Fourier transform-infrared spectroscopy (FT-IR) (Figure 24). First of all, according to the results from DLS (Figure 24A) and TEM (Figure 24B), the size distribution and morphology of amyloid fibrils were not affected by EGCG, clarifying that amyloid fibrils were not fragmented by EGCG. By investigating with CD (Figure 24C) and FT-IR (Figure 24D), it was also observed that post-incubation with EGCG did not induce the structural changes of amyloid fibrils. Taken together, it can be considered that EGCG molecules may interact with amyloid β-sheets in competition with Th-T molecules, resulting the decrease of Th-T fluorescence in the presence of EGCG.

3-3. Phenolic compounds have influences on fibrillation of α-synuclein

In order to verify the phenolic compounds effects on fibrillation of α-synuclein, time-resolved α-synuclein assembly in the absence and presence of phenolic compounds was monitored by using SDS-PAGE and Coomassie Brilliant Blue staining (Figure 25). First of all, the amount of α-synuclein monomers decreased and protein band smearing was observed with time in the absence and presence of phenolic compounds. These results demonstrated that phenolic compounds were not able to inhibit the assembly of α-synuclein

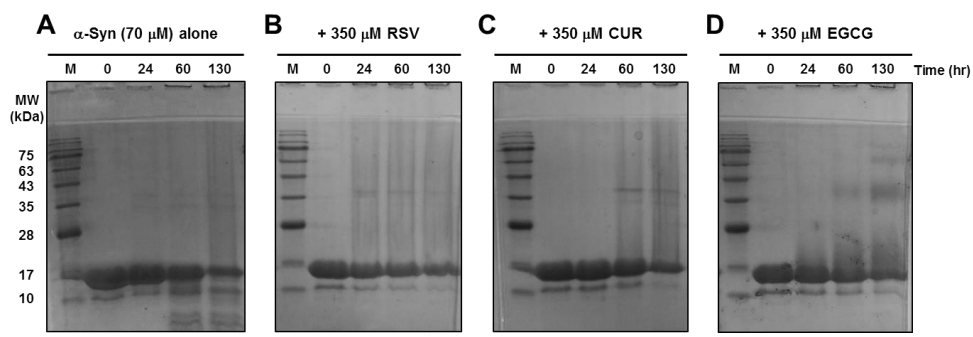

Figure 25. Time-resolved SDS-PAGE analysis of fibrillation of α-synuclein in the absence and presence of phenolic compounds. α-Synuclein monomer (70 μM) was incubated at 37°C for the indicated intervals without (A) and with 350 μM of RSV (B), CUR (C) and EGCG (D). SDS-resistant aggregates of α-synuclein were revealed as protein bands on Coomassie Brilliant Blue-stained 15% SDS-PAGE gel.

whereas several studies have reported the inhibitory effects of phenolic compounds on fibrillation [130, 131]. In other words, RSV (Figure 25B) and CUR (Figure 25C) were shown to accelerate rather than prevent the aggregation of α-synuclein. EGCG, meanwhile, facilitated the formation of SDS-resistant and compact oligomers (Figure 25D) through off-pathway aggregation as previously reported [132]. Moreover, SDS-PAGE analysis shows that degradation of α-synuclein was completely inhibited with phenolic compounds during the prolonged incubation. When α-synuclein was incubated alone, fragments of α-synuclein emerged as protein bands below 14 kDa (Figure 25A), whereas α-synuclein was entirely protected from degradation through co-incubation with phenolic compounds. According to TEM images in Figure 26A, RSV, CUR and EGCG are shown to have little effect on assembly of α-synuclein into amyloid fibril structures and then morphology of amyloid fibrils seems to equal each other. However, the amount of amyloid fibrils and β-sheet contents in end products were affected by phenolic compounds treatment. To compare β-sheet propensity of these end products, analysis of CD spectra was performed by using convex constraint algorithm (CCA) (Table 4). First of all, amyloid fibrils of α-synuclein incubated alone are composed of β-sheet and β-turn (29.1%) and random coil (70.9%). However, aggregates prepared with RSV have considerable contents of β-sheet and β-turn structure (42%) and random coil (58.0%) structures. Furthermore, aggregates of α-synuclein with CUR are comprised of α-helix (2.6%), β-sheet and β-turn structure (38.3%) and

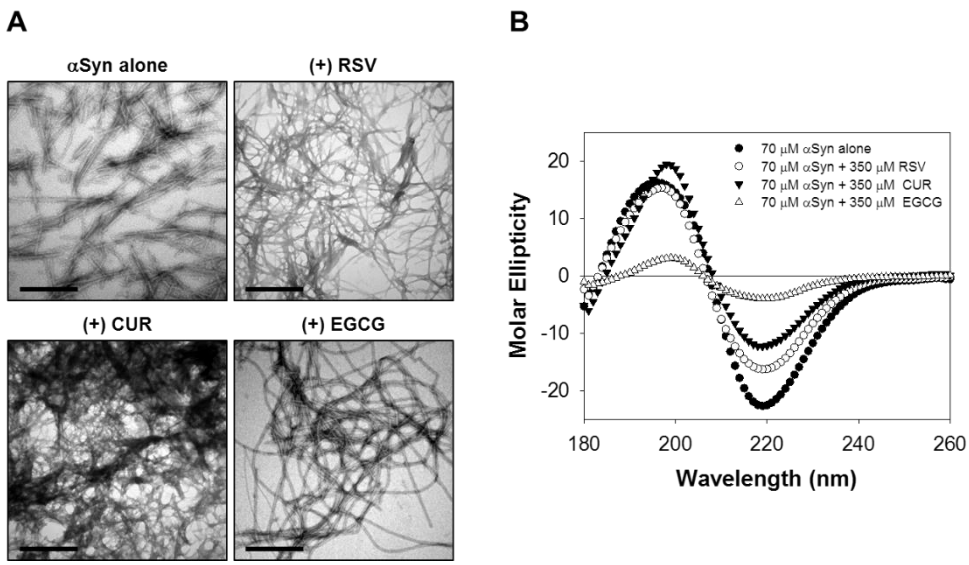

Figure 26. Effects of phenolic compounds on the morphology and structure of α-synuclein amyloid fibrils. (A) TEM images of α-synuclein amyloid fibrils prepared without and with RSV, CUR and EGCG. Scale bars represent 0.5 μm. (B) Circular dichroism spectra of α-synuclein amyloid fibrils prepared without (●) and with RSV (○), CUR (▼) and EGCG (△). α-Synuclein and phenolic compounds were coincubated for 130 hr at 37°C with agitation and the end products were precipitated with centrifugation.

Table 4. Secondary Structure contents of α-synuclein amyloid fibrils prepared without and with phenolic compounds.

Species	α-Helix (%)	β-Sheet (%)	β-Turn (%)	Random Coil (%)
αSyn alone	~ 0	28.2	0.9	70.9
αSyn with RSV	~ 0	23.0	19.0	58.0
αSyn with CUR	2.6	~ 0	38.3	59.2
αSyn with EGCG	16.3	~ 0	57.1	26.5

random coil (59.2%). According to SDS-PAGE analysis and CD spectrum, few precipitates were obtained after incubation of α-synuclein with EGCG because most α-synuclein remained soluble and monomeric proteins. End products from α-synuclein and EGCG have substantial contents of α-helix (16.3%) and β-sheet and β-turn structure (57.1%) with low random coil contents (26.5%). Therefore, CD spectra show that phenolic compounds may promote the formation of β-sheet amyloid fibrils, inducing the fibrillar polymorphism. Taken together, therapeutic effects of phenolic compounds may be displayed by the acceleration of α-synuclein self-assembly and removal of toxic α-synuclein species and then inducing the fibril polymorphism.

This study has suggested that the phenolic compounds can play a role as a partner molecule for α-synuclein and have promising therapeutic potential in Parkinson's disease (PD). For example, resveratrol, curcumin and (-)-epigallocatechin gallate interact with α-synuclein molecules and have significant influences on self-assembly of α-synuclein, inducing the fibril polymorphism (Scheme 3). In other words, the formation of high β-sheet contents amyloid fibrils demonstrates that the phenolic compounds may prevent the formation of toxic on-pathway α-synuclein species and then result in less toxic off-pathway α-synuclein aggregates. These results suggest that the phenolic compounds could be helpful for therapeutic strategy for PD.

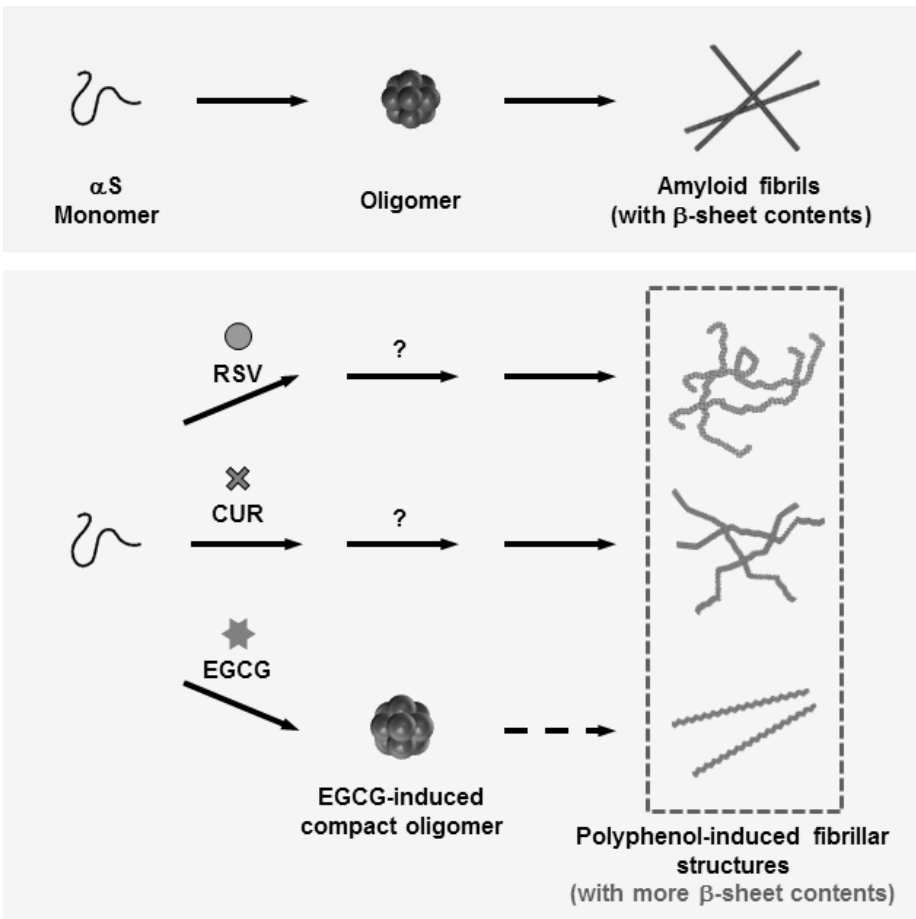

Scheme 3. Polyphenol-induced amyloid polymorphism.

4. Control of the unit assembly of α-synuclein active oligomers

4-1. Definition of α-synuclein active oligomer

4-1-1. Fibrillation of α-synuclein

Intermediates of amyloid fibrillation which are called as oligomer or protofibrils are usually observed in the early phase of fibrillation. In this study, specific oligomer species among intermediates of α-synuclein fibrillation are defined as active oligomer and characterized in detail.

First of all, the kinetics of α-synuclein fibrillation monitored by using Th-T binding fluorescence is characterized by an 'S-shaped' sigmoidal curve (Figure 27A). As shown in TEM images (Figure 27B), monomers (i) are assembled into oligomers (ii), and then grow into amyloid fibrils (iii). According to the fibrillation kinetics and TEM images, most proteins in gray region in Figure 27A may be oligomeric intermediates and specific oligomers among them are prone to be affected by chemical and mechanical effects.

4-1-2. Active oligomers are rapidly assembled into curly amyloid fibril (CAF) via repetitive membrane filtration

To observe the unit assembly of distorted oligomers and the formation of curly amyloid fibrils (CAF), fibrillation intermediates are analyzed with Th-T binding fluorescence (Figure 28A) before and after they were repetitively filtered through centrifugal membrane at 14000 g for 10 min. As a results, fluorescence intensities of intermediates incubated for 6 hr abruptly increased

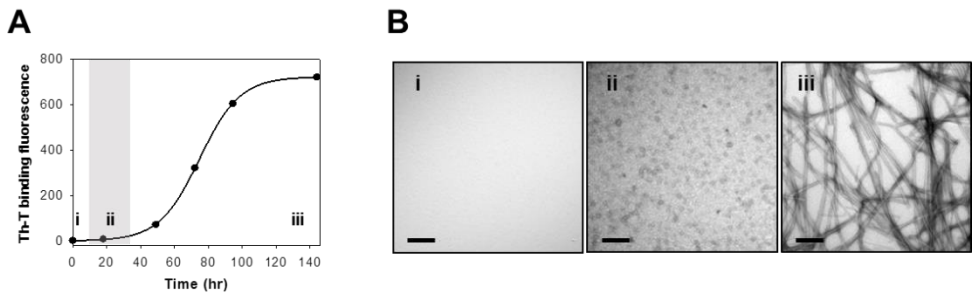

Figure 27. Fibrillation of α-synuclein. (A) Kinetics of α-synuclein fibrillation monitored with Th-T binding fluorescence. α-Synuclein (1 mg/mL) was incubated at 37°C with agitation. (B) TEM images of monomers (i), intermediates (ii) and fibrils (iii) of α-synuclein. Scale bars represent 200 nm.

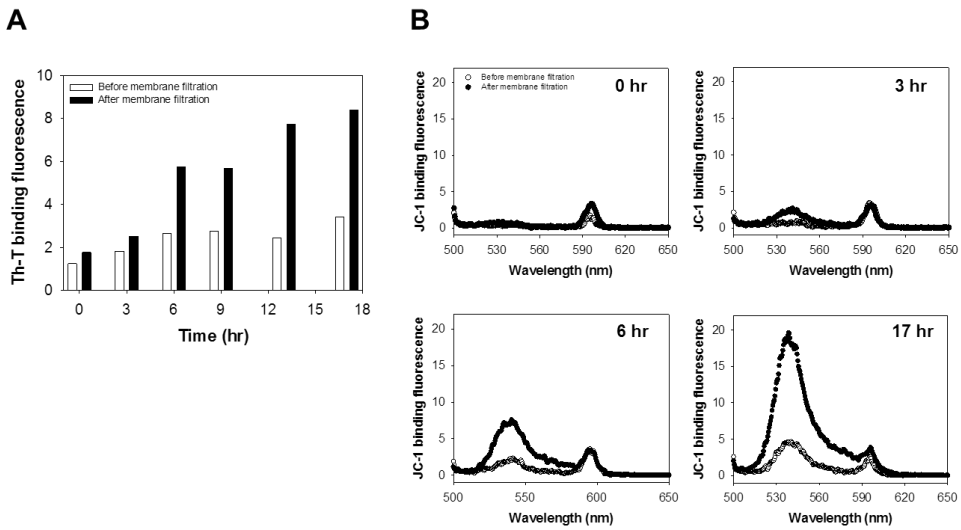

Figure 28. The formation of curly amyloid fibrils was monitored by using dye binding fluorescence. Intermediates on fibrillation were analyzed with Th-T (A) and JC-1 (B) binding fluorescence before (white) and after (black) repetitive membrane filtration with centrifugation at 14000 g for 10 min. When fluorescence dyes interact with β-sheet structures, Th-T emits fluorescence at 482 nm with excitation at 450 nm and JC-1 emits fluorescence at 538 nm with excitation at 490 nm.

3-fold at the first time after membrane filtration. This result means that mechanical effect through repetitive membrane filtration facilitated the unit assembly of oligomers and fibril formation. Rapid fibrillation by membrane filtration was also observed by JC-1 binding fluorescence (Figure 28B). According to the previous study [109], JC-1 could discriminate monomer, oligomeric intermediates and fibrils on fibrillation pathway by emitting the enhanced fluorescence at 590, 560 and 538 nm, respectively with excitation at 490 nm. After the intermediates at 6 hr were repetitively filtered through centrifugal membrane, fluorescence at 538 nm ascended 3-fold, corresponding to unit assembly of oligomers and rapid fibrillation. The unit assembly of oligomers under mechanical stress induced the amyloid polymorphism and developed curly amyloid fibrils (CAF) unlike straight amyloid fibrils (SAF) generally produced via nucleation-dependent fibrillation pathway (Figure 29).

4-1-3. Radiating amyloid fibril formation (RAF) of active oligomer on the surface of lipid membrane

Unit assembly of α-synuclein oligomers on the surface of liposome can lead to radiating amyloid fibril (RAF) formation and membrane disruption. Liposome containing DOPC (Figure 30A) which is a major component of biological membranes and neutral lipid can react with oligomeric intermediates only. When DOPC liposomes were incubated with α-synuclein monomers (Figure 30B) and fibrils (Figure 30D), intact liposomes were observed in TEM images. However, when DOPC liposome and α-synuclein

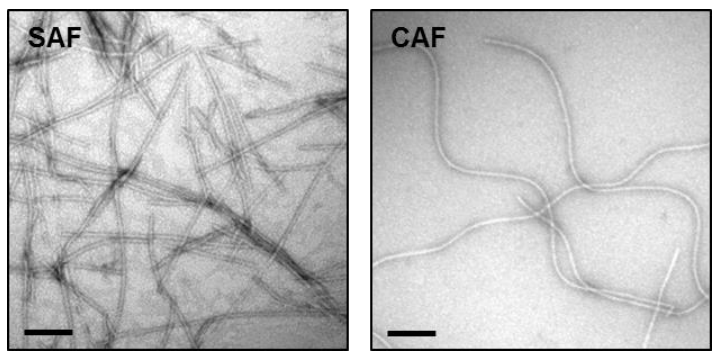

Figure 29. TEM images of straight amyloid fibrils (SAF) and curly amyloid fibrils (CAF). Scale bars represent 200 nm.

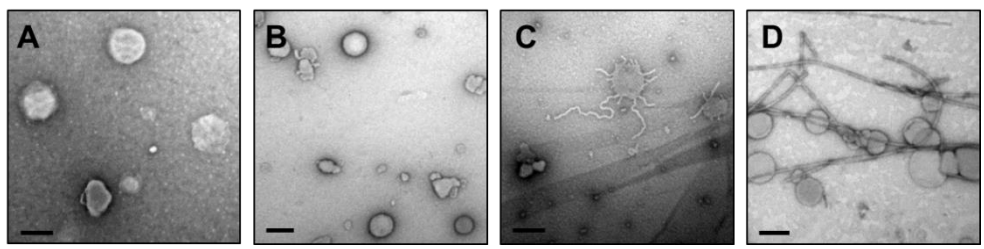

Figure 30. TEM images of radiating amyloid fibril (RAF) formation on the phosphatidylcholine (PC) liposome and lipid membrane disruption through unit assembly of α-synuclein active oligomers. PC liposomes were incubated with MES buffer (A), α-synuclein monomers (B), active oligomers and fibrils (D) for 15 min at 25°C. Scale bars represent 200 nm.

oligomers were incubated for 15 min, RAFs were formed on the surface of DOPC liposomes and the lipid membranes were disrupted (Figure 30C). According to previous studies, it has been demonstrated that unit assembly of oligomers on the liposome surface mechanically pulled lipid molecules out and then destroyed the structure of liposome, corresponding to α-synuclein oligomer toxicity to cell membrane.

Furthermore, lipid membrane disruption by active oligomers is dramatically enhanced under pathological conditions such as high temperature and high cholesterol contents. (Figure 31). First of all, the percentage of disrupted liposomes increased as cholesterol level increased. The 16.4%, 22.3% and 26.4% of liposomes with cholesterol at 0% (w/w), 10% and 20%, respectively are disrupted at 25℃. Furthermore, the RAF formation and liposome disruption remarkably increased from 20.6 % to 57.6%, from 21.4% to 59.7% and from 41.5% to 70.9% with temperature increase from 37℃ to 40℃. Therefore, it can be considered that high fever which is a typical feature of inflammation is closely related to cell membrane disruption by active oligomers of α-synuclein. Also, higher cholesterol level in lipid membrane is associated with increase of membrane disruption induced by active oligomers. This results may be caused by direct binding of α-synuclein to cholesterol in lipid membrane [133]. In fact, brain cholesterol is an essential component of all mammalian cell membranes, and it has a critical role in central nervous system processes such as synaptogenesis [134] and myelin formation [135]. However, the dysregulation of cholesterol homeostasis is a pathological characteristic of neurodegenerative diseases

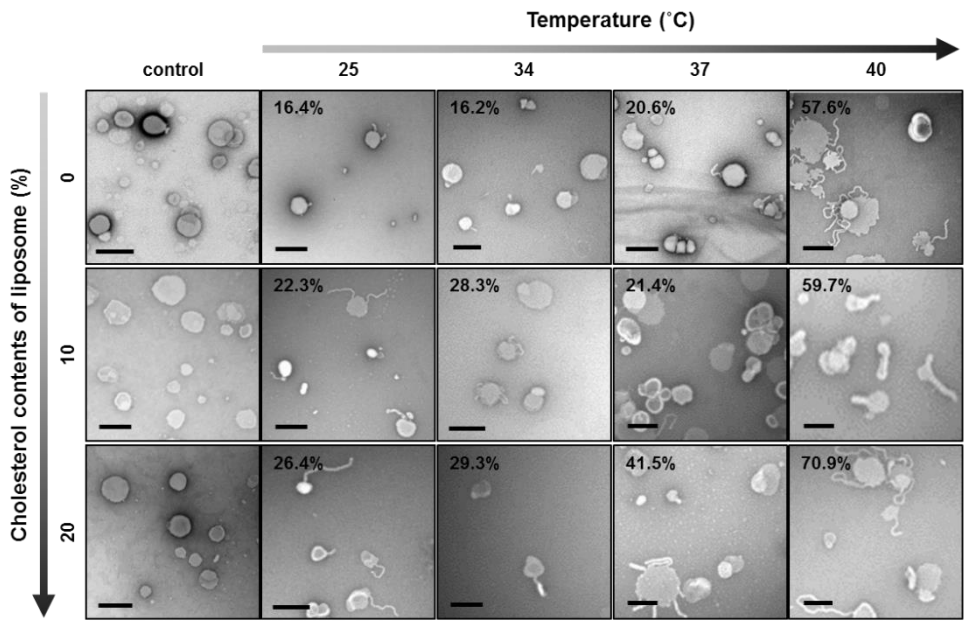

Figure 31. RAF formation and PC lipid membrane disruption by active oligomers under pathological conditions such as high temperature and high cholesterol contents. Scale bars represent 0.5 μm.

[136-138]. Furthermore, several studies about the effect of cholesterol-depleting agent on models of Parkinson's disease have shown that decrease of cholesterol levels can reduce the levels of α-synuclein accumulation in neuronal membranes [139, 140]. Therefore, high cholesterol level in lipid membrane may be a risk factor and a therapeutic target for Parkinson's disease.

Taken together, 'active oligomer' is designated as oligomeric species which meet all of the requirements as follows: (1) Active oligomers should be β-sheet free intermediates formed in early phase of fibrillation; (2) They can be assembled into CAF through repetitive membrane filtration (Scheme 4A); (3) When they are incubated with PC liposome, RAF will be instantly developed on the surface of lipid membranes, resulting in membrane disruption (Scheme 4B).

4-2. Effects of α-synuclein interactive molecules on the unit-assembly of active oligomer

4-2-1. Curly amyloid fibril formation in the presence of α-synuclein interactive molecules

In order to find an effective modulator for unit assembly of α-synuclein active oligomer, curly amyloid fibrils (CAF) were developed via repetitive membrane filtration in the presence of several molecules examined previously (Figure 32). Prior to membrane filtration, 70 μM of α-synuclein

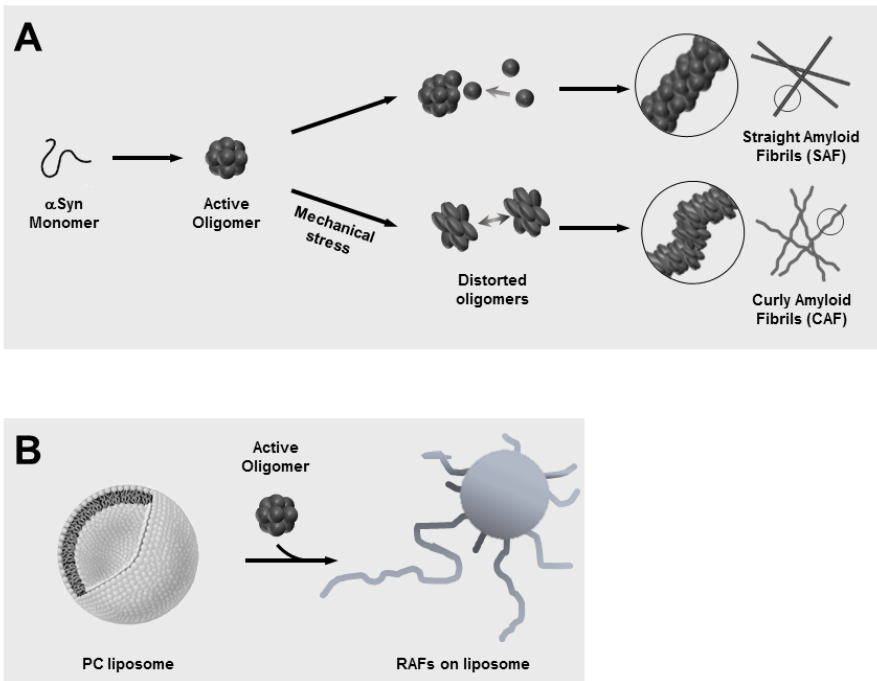

Scheme 4. Unit assembly of α-synuclein active oligomer. (A) The formation of curly amyloid fibril (CAF) via repetitive membrane filtration. (B) The formation of radiating amyloid fibril (RAF) on the surface of PC liposome and disruption of lipid membrane.

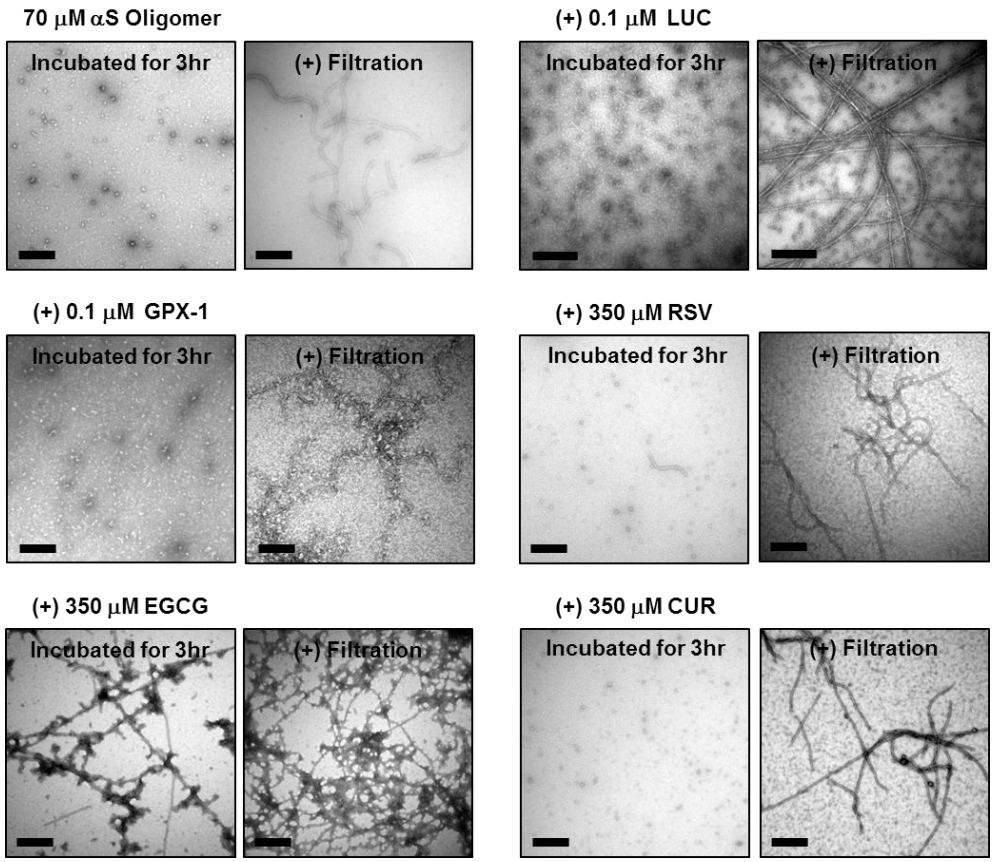

Figure 32. The formation of CAF in the absence and presence of α-synuclein interactive molecules. Prior to repetitive membrane filtration, active oligomers were coincubated with α-synuclein interactive molecules for 3 hr 37°C with agitation. Scale bars represent 0.5 μm.

active oligomers were incubated for 3 hr at 37℃ in orbital shaker with GPX-1 (0.1 μM), LUC (0.1 μM), EGCG (350 μM), CUR (350 μM) and RSV (350 μM). After additional incubation, α-synuclein oligomers remained spherical and amyloid fibrils were not observed in the absence of α-synuclein interactive molecules and in the presence of LUC, GPX-1, CUR and RSV. However, in the presence of EGCG, almost oligomers were assembled into aggregates and amyloid fibrils, resulting the removal of active oligomers.

Furthermore, the TEM images after repetitive membrane filtration show that GPX-1 did not affect the unit assembly of active oligomers and the formation of CAF was clearly observed. On the other hand, LUC and phenolic compounds significantly influenced on unit assembly and CAFs were not observed in TEM images. In particular, EGCG extremely accelerated the unit assembly of active oligomers and did not allow active oligomers to be structurally distorted and develop into CAF through membrane filtration. Active oligomers with CUR and RSV were not completely assembled into CAF and a large portion of active oligomers remained as oligomeric species. Therefore, these data show that EGCG is the most effective molecule to control the unit assembly of active oligomer and have a possibility to reducing neurotoxicity of active oligomers.

4-2-2. Radiating amyloid fibril formation in the presence of EGCG

EGCG can inhibit active oligomer-induced disruption of lipid membrane by facilitating intermolecular interaction between active oligomers (Figure 33). In the absence of EGCG, 86% of lipid membranes containing DOPC are

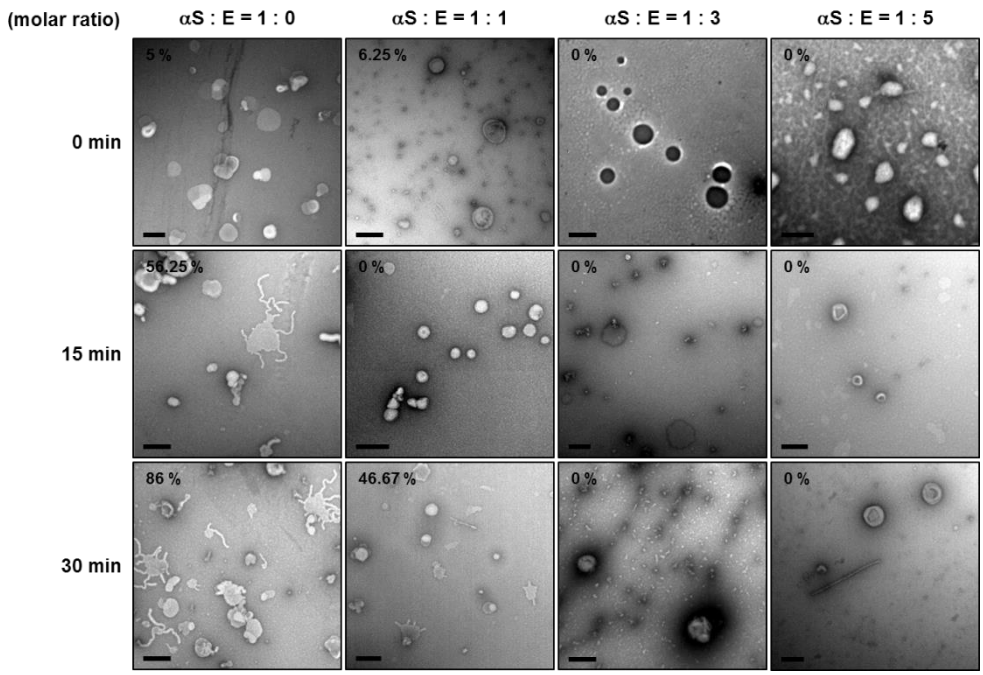

Figure 33. TEM images of PC liposomes after incubation with active oligomers and various concentration of EGCG for 0 min, 15 min and 30 min. Scale bars represent 200 nm.

disrupted by interacting with active oligomer and RAFs are formed on the surface of liposome after incubated for 30 min. In the presence of EGCG, however, intact liposomes are observed after coincubation for 30 min and aggregates and amyloid fibrils of α-synuclein are found around the liposomes instead of RAF on lipid membrane surface.

In order to examine the effect of EGCG on cultured cell, human dopaminergic neuroblastoma cells (SH-SY5Y) were incubated with active oligomers and EGCG for 24 hr (Figure 34). First of all, decrease of cell viability as a function of concentration of active oligomers demonstrates *in vitro* cytotoxicity of α-synuclein active oligomers (Figure 34A). When SH-SY5Y cells were incubated with 7 μM of active oligomers and EGCG at various concentration (Figure 34B), cell viability slightly increased from 62.5% to 74.7% in the presence of 35 μM of EGCG. According to these results, EGCG binds to α-synuclein and facilitates intermolecular interaction between active oligomers, inhibiting that active oligomers mechanically affect cellular compartments such as cell membrane. Taken together, it is confirmed that α-synuclein active oligomers may be neurotoxic and EGCG can work as a therapeutic agent for reducing cytotoxicity of active oligomers.

In this study, it has been verified that unit assembly of α-synuclein active oligomers is controlled by several α-synuclein interactive molecules such as firefly luciferase, glutathione peroxidase, resveratrol, curcumin and (-)-epigallocatechin gallate (EGCG) (Scheme 5). These molecules interact with active oligomers of α-synuclein and then influence on the formation of curly

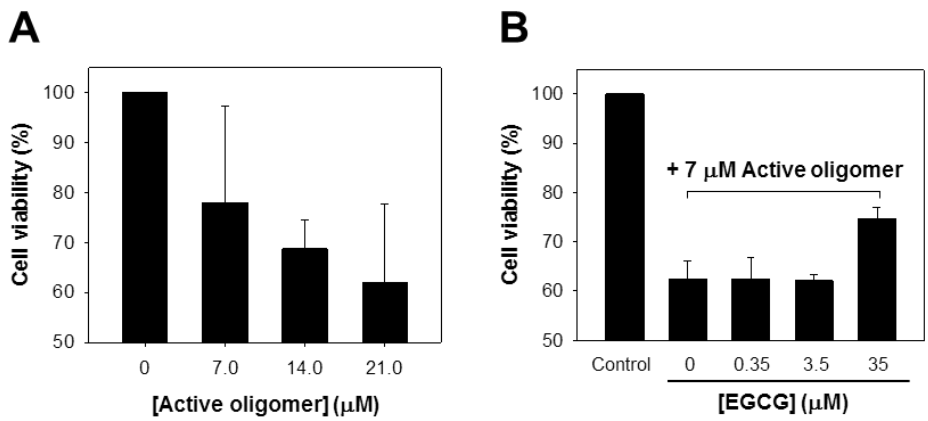

Figure 34. Cytotoxicity of active oligomers and EGCG-induced reduction in cytotoxicity. (A) SH-SY5Y cells (~ 1.0 x 10^6 cells/mL) were treated with various concentration of active oligomers and incubated for 24 hr at 37°C in the CO_2 incubator. (B) SH-SY5Y cells were treated with active oligomers at 7 μM and EGCG at various concentration and incubated for 24 hr at 37°C in the CO_2 incubator. Cell viability was analyzed by using colorimetric MTS assay and absorbance of reduced MTS by viable cells was measured at 490 nm.

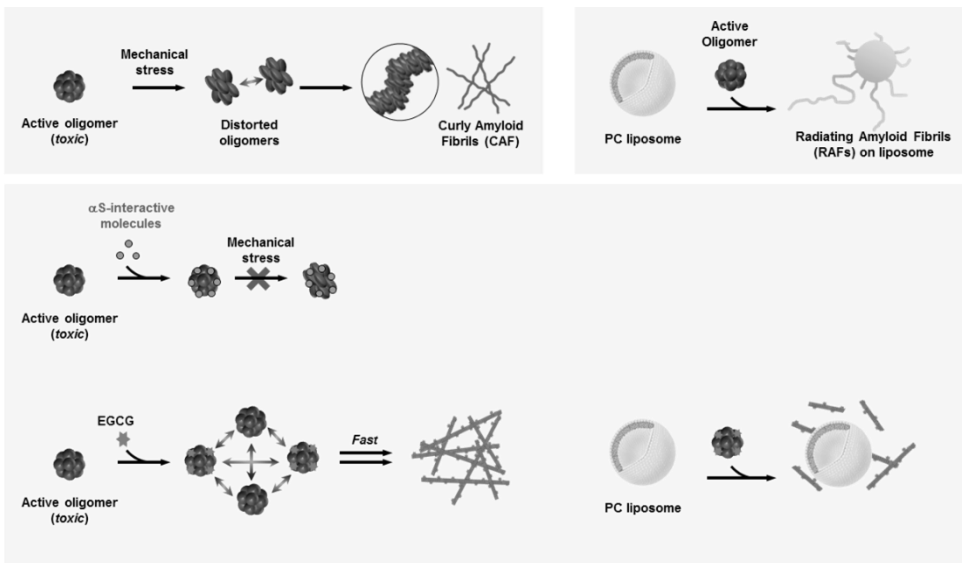

Scheme 5. Effects of α-synuclein interactive molecules on unit assembly of active oligomer.

amyloid fibrils (CAFs) via repetitive membrane filtration. Particularly, EGCG has the most dramatic effects on the unit assembly of active oligomers by facilitating the interaction between α-synuclein active oligomers. This EGCG-induced rapid intermolecular interaction allowed active oligomers to avoid mechanical stress caused by repetitive membrane filtration and the CAF formation. It has been also observed that active oligomers post-treated with EGCG cannot disrupt the lipid membrane through the formation of radiating amyloid fibrils on the surface of liposome. Furthermore, the cell viability test showed that these EGCG effects can reduce the cytotoxicity of α-synuclein active oligomers. Taken together, many α-synuclein interactive biomolecules and natural compounds are expected to influence unit assembly of active oligomers and reduce neurotoxicity of α-synuclein active oligomer.

IV. Conclusions

α-Synuclein, intrinsically unstructured protein, can bind multiple ligands. In this study, several α-synuclein interactive molecules have been studied and their biological and therapeutic implications have been suggested.

(1) Interaction between LUC and α-synuclein (Kd = 8.1 μM) contributes to enhance the bioluminescence activity of LUC and the fibrillation of α-synuclein. Also, complex of LUC and α-synuclein work as a novel nucleation center, inducing amyloid polymorphism.

(2) Interaction between GPX-1 and α-synuclein (Kd = 17.3 nM) contributes

to boost antioxidant activity of GPX-1 and the fibrillation of α-synuclein. Furthermore, the novel function of α-synuclein and entangled α-synuclein fibrils have been suggested as a activator for antioxidative system and depot for active GPX-1, respectively.

(3) Phenolic compounds such as resveratrol, curcumin, EGCG bind to α-synuclein monomers and promote the formation of β-sheet rich amyloid fibril, resulting in the fibril polymorphism. In particular, EGCG induces the formation of compact oligomer of α-synuclein via off-pathway assembly.

(4) Specific oligomer species of α-synuclein defined as active oligomer are affected by several α-synuclein interactive molecules.

(4-1) In the presence of LUC, RSV, CUR and EGCG, the formation of CAF was inhibited.

(4-2) Especially, EGCG dramatically accelerated the unit assembly of active oligomers, showing the enhanced intermolecular assembly of α-synuclein active oligomers.

(4-3) RAF formation and lipid membrane disruption by active oligomer are noticeably reduced by additional treatment of EGCG.

(5) Also, EGCG has a significant effect on reducing the cytotoxicity of active oligomer.

In summary, α-synuclein interactive molecules have biological and therapeutic implications through accelerating the fibrillation, inducing the amyloid polymorphism and reducing the cytotoxicity of active oligomer.

Part II. Colorimetric Sensor Development with α-Synuclein Amyloid Fibrils and Polydiacetylene

I. Introduction

1. Polydiacetylene-based colorimetric sensors

Colorimetric sensing materials have been valued for easy and convenient detection of environmental signals. Polydiacetylene (PDA) has been widely employed to monitor color-transition caused by external stimuli such as temperature, pH, solvents, ions, and ligand-receptor interactions [141-143]. PDA-based sensors are prepared via ordered structures of diacetylene monomers. 10,12-Pentacosadiynoicacid (PCDA) is a diacetylene monomer comprised of a carboxylic group with along aliphatic chain containing two triple bonds, whose structure is reminiscent of fatty acids in nature. Well-ordered PCDA monomers are polymerized via 1,4-addition reaction by UV irradiation at 254 nm (topochemical photopolymerization) and the polymerized PCDA (poly-PCDA) with alternating double and triple bonds (ene-yne) (Figure 35) exhibit blue in color [144-146]. When poly-PCDA is exposed to the external stimuli, the blue-to-red color transition and a related phenomenon of fluorescence enhancement occur via structural relaxation of the strained ene-yne conjugation of the PCDA molecules. It is this unique chromic property of poly-PCDA that allows the system to be utilized for

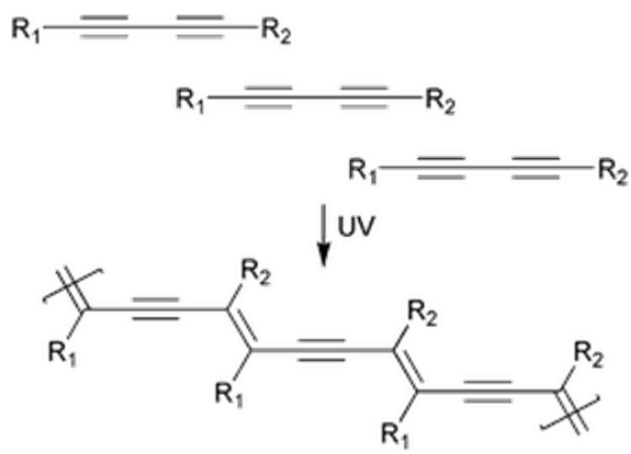

Figure 35. Topochemical photopolymerization of diacetylenes.

various sensing applications including biosensors detecting microorganism [147], membrane interaction of casein oligomers [148], and gas like NH_3 and its derivatives [149, 150]. In order to improve its sensing properties and thus expand the fields of application, the PDA vesicles have been further modified by conjugating with phenolate [151], biotin [152], and KTTKS peptide from collagen [153]. Although the PDA-based colorimetric materials have readily been produced in vesicles, the vesicular structures suffer from vulnerability to mechanical stress and deterioration via aggregation in the presence of water-soluble polymers [154] and cations such as Ca^{2+} and Na^{+} [155-157].

2. Amyloid fibrils in material science

Amyloids, a common pathological phenomenon observed in various neurodegenerative disorders such as Alzheimer's disease, Parkinson's disease, and amyotrophic lateral sclerosis [158, 159], are insoluble fibrous protein aggregates produced via self-assembly of soluble proteins. Amyloid fibrils are produced by forming highly ordered cross β-sheet conformation, which result in straight and long nanofibrils with an average width centered at 10 nm [160-163]. From the perspective of materials, amyloid fibrils become an attractive biomaterial because of not only their mechanical strength shown to be comparable to steel [164], but also they can be readily manipulated to yield amyloid-based nanowire [165], nanostructured protein film [166], and hollow nanotubes [167]. Additionally, other types of amyloid-based biomaterials have been reported to be produced, which include pea-pod

type gold nanoparticle chain with in amyloid fibrils [168], conductive nanowire networks [169], thermo-reversible amyloid fibrils [170], and enzymatically active fibrils [171]. Herein, the amyloid-based colorimetric material was made of α-synuclein and PCDA by simply co-incubating both components.

II. Experimental Section

1. Oligomerization of α-synuclein in the presence of 10,12-pentacosadiynoic acid (PCDA)

The oligomerization of α-synuclein was examined in the presence of various concentrations of PCDA monomer by using an EEDQ cross-linker. The oligomers were revealed as discrete ladders on a silver-stained 10−20% Tricine SDS-PAGE gel. α-Synuclein (35 μM) was preincubated with various concentrations of PCDA in 20 mM MES (pH 6.5) containing 5% DMSO for 30 min at 25℃. Following the addition of 0.3 mM EEDQ, the mixture was further incubated for 1 h at 25℃. Each sample was combined with the tricine sample buffer containing 24% (v/v) glycerol, 8% (w/v) SDS, 0.015% CBBG, and 0.005% phenol red in 0.3 M Tris/HCl at pH 8.45 in a 1:1 (v/v) ratio, boiled for 5 min, and analyzed with the precast 10−20% tricine gel.

2. Dissociation constant (Kd) between α-synuclein and PCDA

α-Synuclein (35 μM) was preincubated in the absence and presence of various concentrations of PCDA for 30 min at 37℃, and the intrinsic tyrosine fluorescence of α-synuclein was monitored at 304 nm with excitation at 274 nm by using a chemiluminescence spectrophotometer (LS-55B, PerkinElmer). A saturation curve was obtained by plotting the difference in the intrinsic fluorescence obtained in the absence (I_0) and presence (I_i) of PCDA as a function of PCDA concentration. Dissociation constant Kd was obtained from the x-intercept of a double-reciprocal plot of the hyperbolic saturation curve between 1/[PCDA] and $1/(I_0 - I_i)$ on the x and y axes, respectively.

3. Fibrillation of α-synuclein in the absence and presence of PCDA

The fibrillation of α-synuclein was monitored by Th-T binding fluorescence and the amount of protein remaining in the supernatant. α-Synuclein (35 μM) was incubated in 20 mM MES (pH 6.5) containing 5% (v/v) DMSO at 37℃ under shaking at 200 rpm. During the incubation, an aliquot (20 μL) of α-synuclein was reacted with 2.5 μM Th-T in 50 mM glycine (pH 8.5) for 5 min at room temperature. Th-T binding fluorescence at 485 nm with excitation at 450 nm was monitored with a chemiluminescence spectrophotometer (LS - 55B, PerkinElmer). To quantify soluble α-synuclein remaining in the incubation mixture, the amyloid fibrils were precipitated with centrifugation at 16,100g for 30 min. The amount of soluble α-synuclein left in the

supernatant was measured with a microbicinchoninic acid (BCA) protein assay kit (Thermo Fisher Scientific Inc.) [172]. Fibrillation of α-synuclein (35 μM) in the presence of PCDA at various concentrations was monitored by measuring the turbidity of the incubation mixture at 405 nm with a UV/visible spectrophotometer (Ultrospec 2100 pro, GE Healthcare). A mixture of α-synuclein and PCDA was incubated in 20 mM MES (pH 6.5) containing 5% (v/v) DMSO at 37℃ under shaking at 200 rpm.

4. Preparation and characterization of AF/PCDA

After the incubation of α-synuclein and PCDA in 20 mM MES (pH 6.5) containing 5% (v/v) DMSO at 37℃ for 100 hr, AF/PCDA was isolated in the precipitates through repetitive centrifugation at 16 100g for 30 min and washing with distilled water. The collected AF/PCDAs were subjected to UV light exposure at 254 nm for 10 min and heat treatment at 80℃ for 10 min. The morphological features and fluorescence property of AF/PCDA were analyzed by transmission electron microscopy (TEM) and confocal laser scattering microscopy (CLSM), respectively. AF/PCDA were absorbed onto a carbon-coated copper grid (200-mesh, Electron Microscopy Sciences) and dried in air for 3 min. Following negative staining with 2% uranyl acetate (Electron Microscopy Sciences) for 5 min, the grids containing AF/PCDA were visualized with TEM (JEM-1010, JEOL). AF/PCDAs on a glass slide were examined with CLSM (LSM 710, Carl Zeiss) to observe the fibrillar fluorescence with excitation at 405 nm. UV/vis absorption spectra of the

colorimetric response of AF/PCDA were obtained by scanning the samples with a UV/visible spectrophotometer from 450 to 750 nm (Ultrospec 2100 pro, GE Healthcare).

5. Preparation of poly-PCDA vesicles

PCDA was dissolved in chloroform to 0.5 mg/mL, and then the solution was blown with inert nitrogen gas while being vortex mixed. After complete removal of the chloroform, a thin film layer of PCDA was formed on the inner surface of a glass tube and the sample was frozen at −20℃. The dried PCDA film was then hydrated simply by dissolving it in distilled water to the same volume as for the chloroform, resulting in a translucent solution. PCDA vesicles were produced by prewarming the solution to 75℃ for 20 min, followed by bath sonication for another 30 min at the same temperature. After sonication, the solution was filtered through a microfilter with a pore size of 0.45 μm, which was subsequently stored at 4℃ overnight. Finally, the PCDA vesicle solution was polymerized with UV exposure at 254 nm for 5 min, and the color transition to blue confirmed that the reaction had taken place. Prepared poly-PCDA vesicles was examined with TEM (Figure 36A) and UV/vis absorptions between 450 nm and 750 nm (Figure 36B).

6. Colorimetric responses of AF/PCDA and poly-PCDA vesicles to temperature, pH, and ethanol

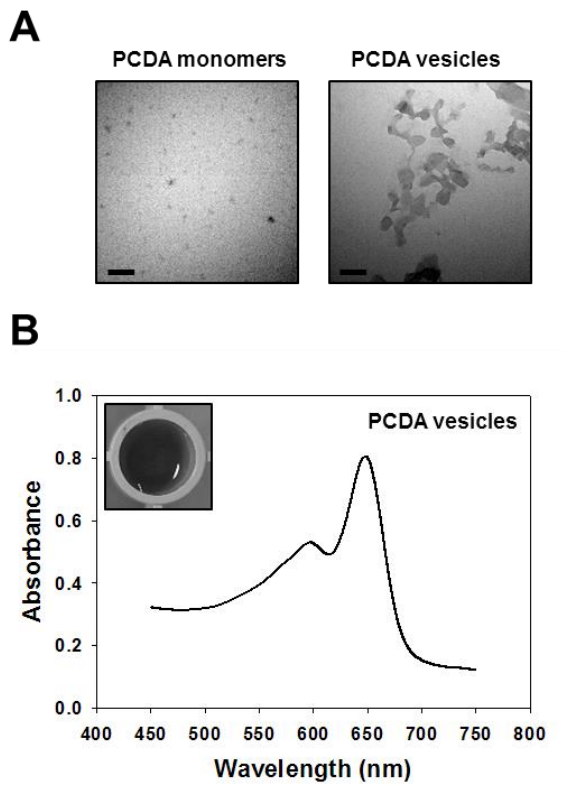

Figure 36. Preparation of the solution of PCDA vesicles. (A) TEM images of PCDA monomers and PCDA vesicles in solution. The scale bars represent 200 nm. (B) Colorimetric response and absorption spectrum of the solution of PCDA.

Aliquots of AF/PCDA and poly-PCDA vesicles were placed into Eppendorf tubes, and they were separately incubated at different temperatures from 25 to 90℃ for 20 min to reach equilibrium. Following incubation, their UV/vis absorptions were monitored from 450 to 750 nm. To verify the colorimetric transitions of AF/PCDA and poly-PCDA vesicles at different pH, the solutions were prepared at different pH values from 2.2 to 12.4 by adding 1 N HCl and 1 N NaOH. For the colorimetric response to ethanol, AF/PCDA and poly-PCDA vesicles were also prepared at different % ethanol concentrations. After 30 min of incubation, UV/vis absorption spectra of AF/PCDA and poly-PCDA vesicles were also obtained for both pH- and ethanol-treated samples. To quantify the blue-to-red color transition, the % colorimetric response (%CR) was calculated according to the equation $\%CR = [(PB_0 - PB)/PB_0] \times 100$ [173]. The PB denoting percent blue is calculated from $A_{650}/(A_{550} + A_{650})$, where A_{550} and A_{650} are the maximum peaks of absorption spectra of red and blue phases, respectively. PB_0 represents the initial percent blue obtained before any exposure to the stimuli.

7. Mechanical stability of AF/PCDA, poly-PCDA vesicles, and AF against sonication

AF/PCDA, poly-PCDA vesicles, and AF were sonicated with a microtip-typeultrasonic processor (VCX 750, Sonics & Materials Inc.) at 20 kHz under 750 W with an on/off cycle of 10 s each. Following every 20 on/off cycle of sonication in ice, the absorption spectra of AF/PCDA and poly-PCDA

vesicles were monitored to a maximum of 80 cycles. Furthermore, the fibrillar states of AF and AF/PCDA were examined with TEM (JEM1010, JEOL) during the sonication.

8. Preparation of litmus-type sensors with amyloid fibrils and PCDA

The amyloid fibril and PCDA composites (AF/PCDA) were prepared by incubating monomeric α-synuclein (70 μM) for 70 hr at 37℃ in the presence of PCDA at 1 mM under agitation at 200 rpm. The resulting AF/PCDA were collected via centrifugation at 16100 × g for 30 min. The mixture between pre-made amyloid fibrils and PCDA (AF+PCDA) was obtained by incubating the pre-made amyloid fibrils of α-synuclein and PCDA (1 mM) for 15 min at ambient temperature. The AF+PCDA were also precipitated with the centrifugation. The collected pellets of AF/PCDA and AF+PCDA were resuspended with 200 μL of 20 mM Mes (pH 6.5). Aliquots (10 μL) of AF/PCDA and AF+PCDA solutions were dropped onto Whatman filter paper and air-dried for 2 hours. The spots of AF/PCDA and AF+PCDA on the filter paper turned to blue in color after UV exposure at 254 nm for 1 min.

9. Colorimetric and fluorescent responses of the litmus-type sensors to temperature and organic solvents

Litmus-type sensors prepared with AF/PCDA and AF+PCDA were either incubated at different temperatures from 25℃ to 90℃ for 5 min or exposed

to various organic solvents in vapor or liquid. The colorimetric change of litmus-type sensors was recorded with digital camera and the fluorescence enhancement was analyzed with confocal laser scattering microscopy (CLSM, LSM 710, Carl Zeiss) with excitation at 405 nm. In order to quantitatively analyze the fluorescence enhancement, the fluorescence intensity of the spots was evaluated with microscope and imaging software provided by Carl Zeiss.

10. Monitoring of heat progress and detection of localized heating

Following UV exposure, the litmus-type AF+PCDA sensor was put on top of a hot plate steadily heated from 25℃ to 60℃ and monitored for its color transition from blue to red. In order to apply a localized heat to the litmus-type sensor, the copper tape was glued on the back of the paper sensors in a musical sharp sign and heated to 120 ˚C with a hot plate.

11. Tightness of the PCDA binding to amyloid fibrils

The collected AF/PCDA and AF+PCDA were resuspended with 200 μL of 20 mM Mes (pH 6.5) and sonicated with micro-tip-type ultrasonic processor (VCX 750, Sonics & Materials Inc.) for 2 sec at 20 kHz under 750 W. Following the removal of free PCDA molecules unleashed from the amyloid fibrils with centrifugation at 16100 x g for 30 min, the precipitated AF/PCDA and AF+PCDA were again resuspended with 20 mM Mes (pH 6.5).

Aliquots(10 μL) of the AF/PCDA and AF+PCDA solutions were dropped onto Whatman filter paper, air-dried for 2 hours, and exposed to UV light at 254 nm for 1 min. The sonication step was repeated until the blue-dots did not appear on the paper upon the UV exposure.

III. Results and Discussion

1. Stimuli-responsive biomaterials from α-synuclein amyloid fibril

1-1. Molecular interaction between α-synuclein and PCDA

To demonstrate specific interaction between α-synuclein and PCDA, self-oligomerization of α-synuclein was evaluated in the presence of various concentrations of PCDA by using a cross-linker of 2-ethoxy-1-ethoxycarbonyl-1,2-dihydroquinoline (EEDQ) [44, 53, 174]. The α-synuclein oligomers induced by PCDA were revealed in a discrete ladder formation on a silver-stained 10-20% Tricine SDS-PAGE gel (Figure 37A). The ladder formation started to appear from 0.1 mM PCDA and became apparent from 0.5 mM, indicating that α-synuclein was specifically influenced by PCDA to be self-assembled into the oligomers. In addition, their specific interaction was reassessed with a saturation binding curve of α-synuclein with various concentrations of PCDA (Figure 37B). Their binding was monitored by obtaining difference of the intrinsic fluorescence of tyrosine residues of α-synuclein in the presence and absence of PCDA. A

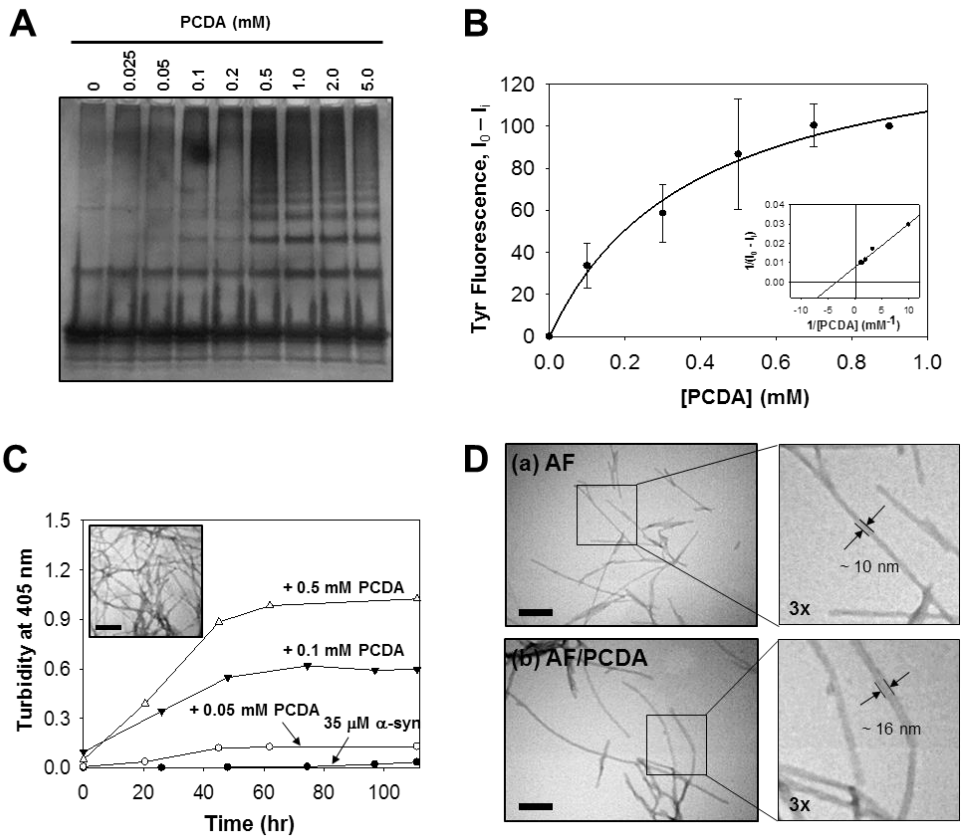
A
PCDA (mM)
0
0.025
0.05
0.1
0.2
0.5
1.0
2.0
5.0
B
Tyr Fluorescence, $I_0 - I_i$
[PCDA] (mM)
1/(I_0 - I_i)
1/[PCDA] (mM^{-1})
C
Turbidity at 405 nm
Time (hr)
+ 0.5 mM PCDA
+ 0.1 mM PCDA
+ 0.05 mM PCDA
35 μM α-syn
D
(a) AF
~ 10 nm
3x
(b) AF/PCDA
~ 16 nm
3x

Figure 37. Specific molecular interaction of 10,12-pentacosadiynoic acid (PCDA) for α-synuclein leading to facilitated amyloid fibril formation. (A) Self-oligomerization of α-synuclein (35 μM) induced by PCDA at various concentrations was revealed as a ladder formation on a silver-stained 10-20% Tricine SDS-PAGE gel following the EEDQ-mediated crosslinking step. (B) Difference in the tyrosine intrinsic fluorescence of α-synuclein obtained in the absence (I_0) and presence (I_i) of various concentrations of PCDA. Double reciprocal plot of the saturation curve between $1/(I_0-I_i)$ and 1/[PCDA] (inset). (C) The fibrillation of α-synuclein (35 μM) in the presence of PCDA at various concentrations was monitored by measuring solution turbidity at 405 nm. The resulting fibrils of α-synuclein obtained with PCDA (0.1 mM) after 100 hours of incubation are shown in TEM image (inset). Scale bar, 200 nm. (D) TEM images of amyloid fibrils (AF) and PCDA-containing amyloid fibrils (AF-PCDA). Scale bars represent 200 nm. These fibrils were collected after incubating α-synuclein (35 μM) in the absence (a) and presence (b) of PCDA (0.1 mM) for 100 hours. Parts of the fibrils were also shown in 3-fold magnification.

double-reciprocal plot of the hyperbolic saturation curve yielded Kd of 0.29 mM from the x-intercept (Figure 37B, inset). This half-saturating PCDA concentration was relevant to the concentration dependence of the ladder formation in Figure 38A. Then, PCDA effect on the α-synuclein fibrillation was examined with protein aggregation kinetics by monitoring solution turbidity at 405 nm after correcting the turbidity with that of PCDA alone (Figure 37C). Thioflavin-T binding fluorescence which has routinely been used to monitor the amyloid fibril formation could not be employed here because PCDA interferes with the light emission. According to results from thioflavin-T binding fluorescence and bicinchoninic acid-based quantitation of the protein remaining in the supernatant following precipitation of the fibrils, α-synuclein alone at 35 μM has been shown to effectively transformed into amyloid fibrils during more than 100 hours of shaking incubation at 37℃ (Figure 38). The fibrillar end-products were observed with transmission electron microscope (TEM) (Figure 38, inset) although the final turbidity was not drastically increased (Figure 37C). In the presence of PCDA, the turbidity started to increase rapidly without a lag period and reached plateau within 60 hours of incubation (Figure 37C), which was also assessed with decrease of the soluble protein remaining in the supernatant (Figure 39). The final turbidities increased as the amount of PCDA increased. The resulting amyloid fibrils were revealed with TEM (Figure 37C, inset). Taken together, the α-synuclein fibrillation was dramatically accelerated by PCDA, which supports the previous report indicating that polyunsaturated fatty acids enhanced the fibrillation [175-178]. When the amyloid fibrils prepared in the absence or

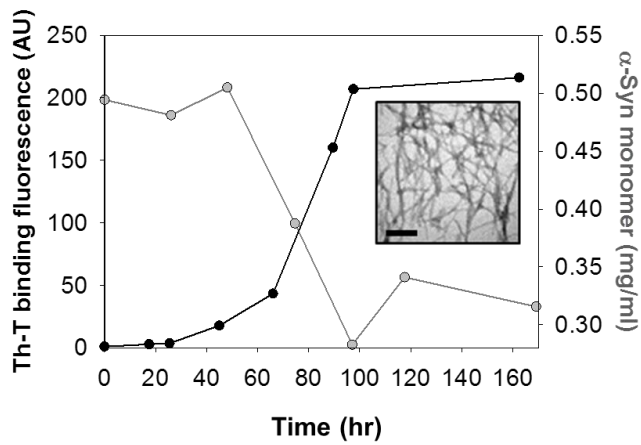

Figure 38. Amyloid fibril formation of α-synuclein in the absence of PCDA. Fibrillation of α-synuclein (35 μM) in the absence of PCDA was monitored by using thioflavin-T binding fluorescence and the quantitation of α-synuclein monomer remaining in the supernatant. The final fibrillar structures of α-synuclein are shown in TEM image. The scale bar represents 200 nm (inset).

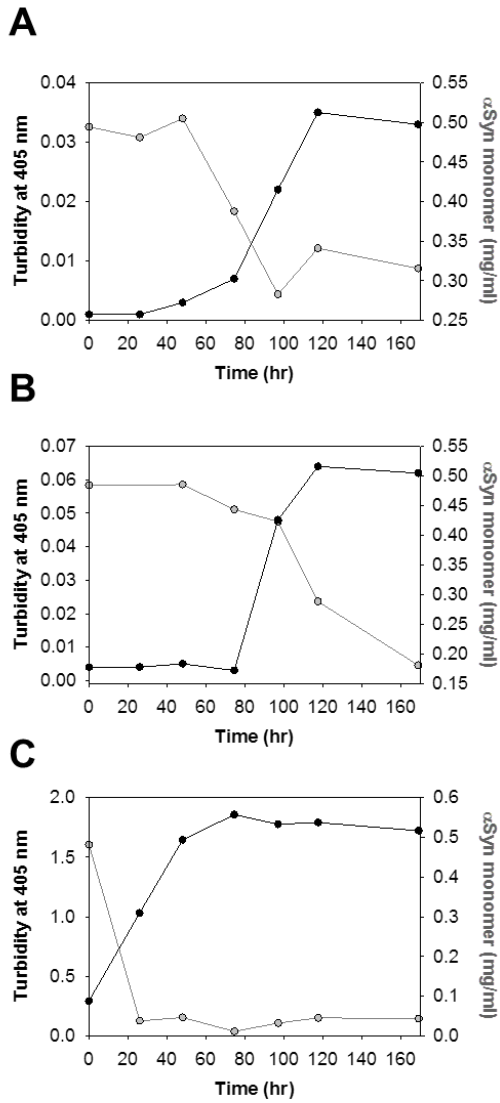

Figure 39. Fibril formations of α-synuclein in the absence and presence of PCDA. Fibril formation was monitored by measuring both increase of solution turbidity at 405 nm and decrease of the amount of α-synuclein in the supernatant during the incubation. α-Synuclein (35 μM) was incubated without (A) and with PCDA at 10 μM (B) and 100 μM (C).

presence of PCDA were compared with each other, the width of α-synuclein fibrils increased from 10 nm to 16 nm as PCDA was added at 0.1 mM (Figure 37D). By considering that molecular dimension of a PCDA molecule was measured at 3.4 nm [179], the thickening may indicate specific molecular association of PCDA into the amyloid fibrils. In order to examine the properties of AF and PCDA in the conjugate material, structural properties were monitored by using FT-IR spectroscopy and Raman spectroscopy. No significant difference was found in the amide I region (1600-1700 cm^{-1}) of FT-IR spectra collected with AF and AF/PCDA (Figure 40A). Therefore, it is considered that the structure of AF has not been affected by the co-assembly with PCDA. On the other hand, however, the 785 nm-laser excited Raman spectra indicate that molecular characteristics of PCDA have been affected by its incorporation into amyloid fibrils in AF/PCDA conjugates (Figure 40B). The spectrum of AF/PCDA shows a slight upshift of the line obtained at 1442 cm^{-1} with PCDA alone to 1469 cm^{-1} and emergence of two new lines at 1531 cm^{-1} and 2131 cm^{-1}.

1-2. Chromic and fluorescent properties of AF/PCDA

In order to examine the chromic and fluorescent properties of AF/PCDA, amyloid composites were subjected to UV and heat treatment (Figure 41). Upon UV exposure at 254 nm for 10 min, AF/PCDA turned to blue while either PCDA alone at 0.1 mM or amyloid fibrils (AF) prepared with 35 μM α-synuclein did not show the color change (Figure 41A). Following heat treatment at 80℃ for 10 min, the blue AF/PCDA changed their color to red

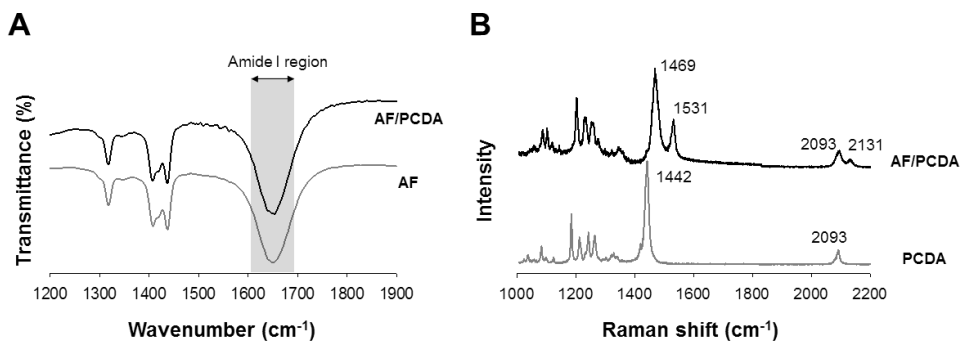

Figure 40. Structural properties of amyloid fibrils (AF) and PCDA in AF/PCDA. (A) FT-IR spectra of AF and AF/PCDA. Grey box represents amide I region. (B) Raman spectra of PCDA and AF/PCDA.

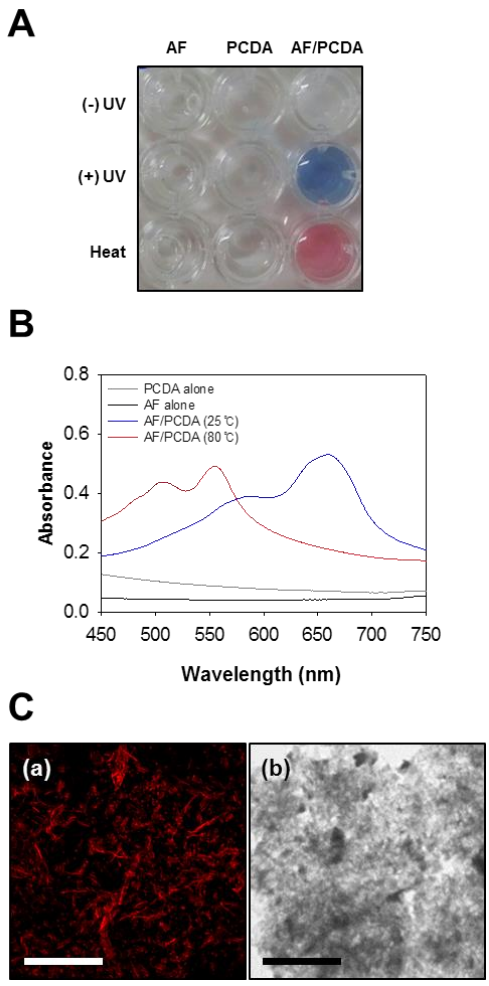

Figure 41. Chromic and fluorescent properties of AF-PCDA. (A and B) Following 100 hours of incubation with and without 0.1 mM PCDA, the blue color development and the blue-to-red color transition of AF, PCDA monomer, and AF-PCDA upon UV exposure at 254 nm for 10 min and subsequent heating for 10 min at 80°C, respectively, were shown with a photographic image (A) and absorption spectra (B). (C) Fibrillar aggregates of the UV- and heat-treated AF-PCDA were revealed in red fluorescence with confocal laser scanning microscope (a) and TEM (b). Scale bars represent 10 μm.

(Figure 41A). UV/Vis absorption spectra of AF/PCDA also indicated the chromic property (Figure 41B). For the blue fibrils, the spectrum exhibited double maxima at 650 nm and 570 nm, which were shifted to 550 nm and 500 nm as AF/PCDA experienced the color transition to red. According to these results, PCDA molecules are expected to be incorporated into the fibril in a well-ordered state and transform into polydiacetylene (PDA), exhibiting the colorimetric response of blue-to-red transition. In order to investigate whether the chromic property was intrinsic to the fibrils, the red AF/PCDA were examined with both confocal laser scanning microscope (CLSM) and TEM at the same scale. The red fluorescence of AF/PCDA in CLSM image (Figure 41C-a) seems to correlate with the fibrillar network in TEM image (Figure 41C-b), indicating that the colorimetric response of PCDA has occurred in association with the amyloid fibrils. All the data therefore suggest that the α-synuclein amyloid fibrils containing PCDA exhibit the chromic and fluorescent properties comparable to those elicited by poly-PCDA vesicles [180-183].

1-3. Stimuli-responsive amyloid fibrils

To assess a potential of AF/PCDA to develop into a robust environment sensing agent, their colorimetric responses were explored to changes of temperature (Figure 42), pH (Figure 43), and ethanol concentrations (Figure 44) in comparison with those of conventional poly-PCDA vesicles. With temperatures raised, the blue AF/PCDA at 25℃ gradually changed their color to purple and red at 60℃ and 80℃, respectively, while the poly-PCDA

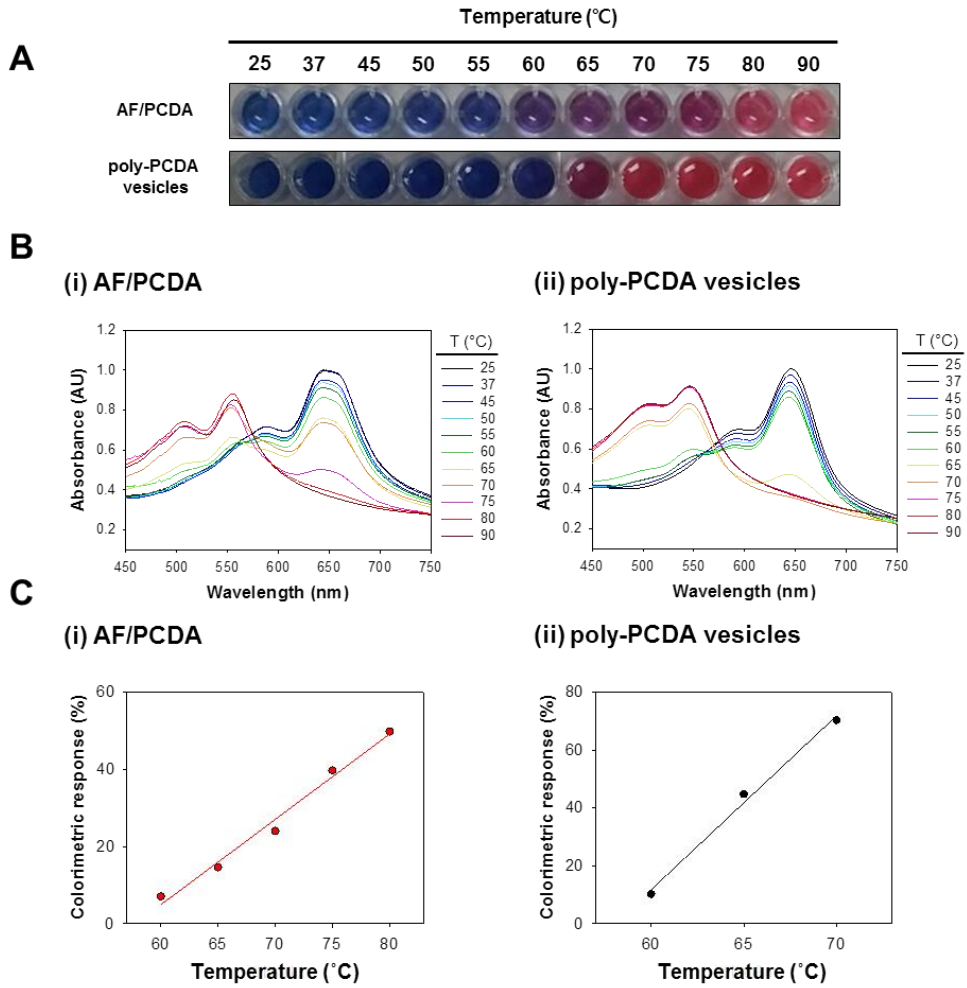

Figure 42. Colorimetric response of AF/PCDA to temperature. (A) The color transition to red from initial blue was visualized for AF/PCDA and poly-PCDA vesicles with variations in temperature. (B) Absorption spectra of AF/PCDA and poly-PCDA vesicles with changes of temperature. (C) The colorimetric responses of AF-PCDA and poly-PCDA vesicles obtained in % CR were plotted as a function of temperature.

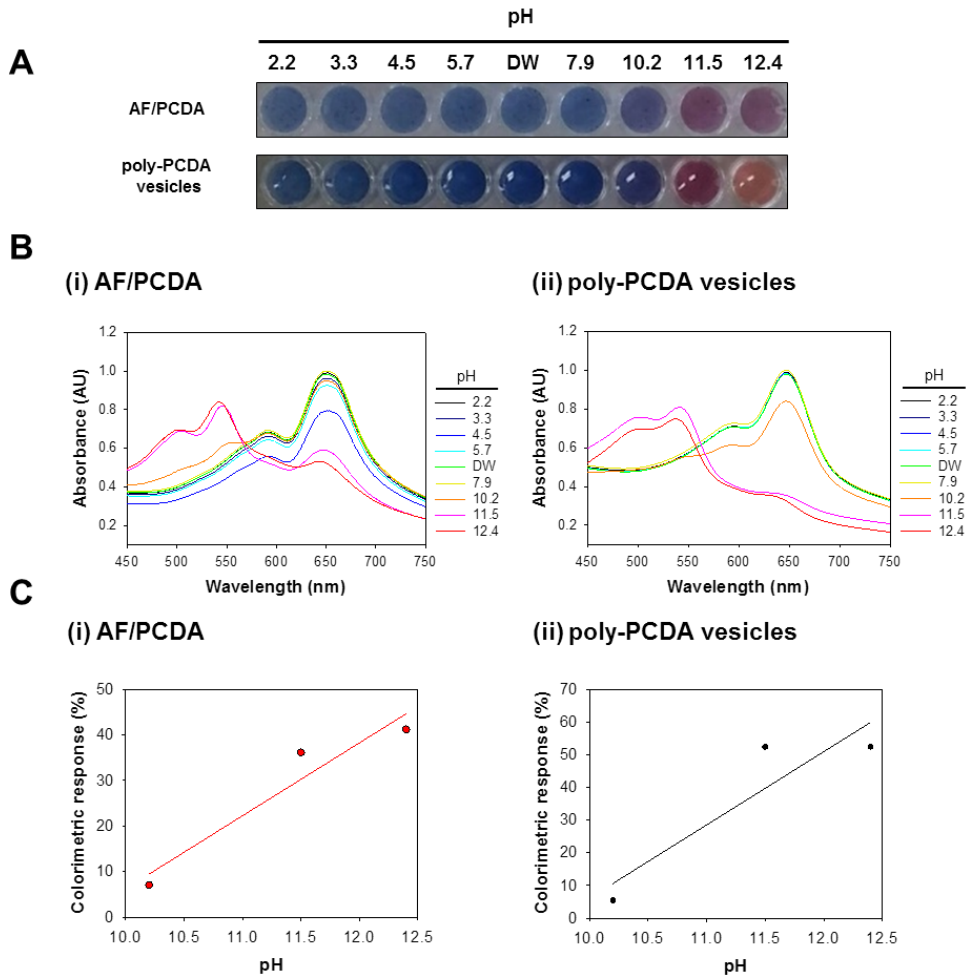

Figure 43. Colorimetric response of AF/PCDA to pH. (A) The color transition to red from initial blue was visualized for AF/PCDA and poly-PCDA vesicles with variations in pH. (B) Absorption spectra of AF/PCDA and poly-PCDA vesicles with changes of pH. (C) The colorimetric responses of AF-PCDA and poly-PCDA vesicles obtained in % CR were plotted as a function of pH.

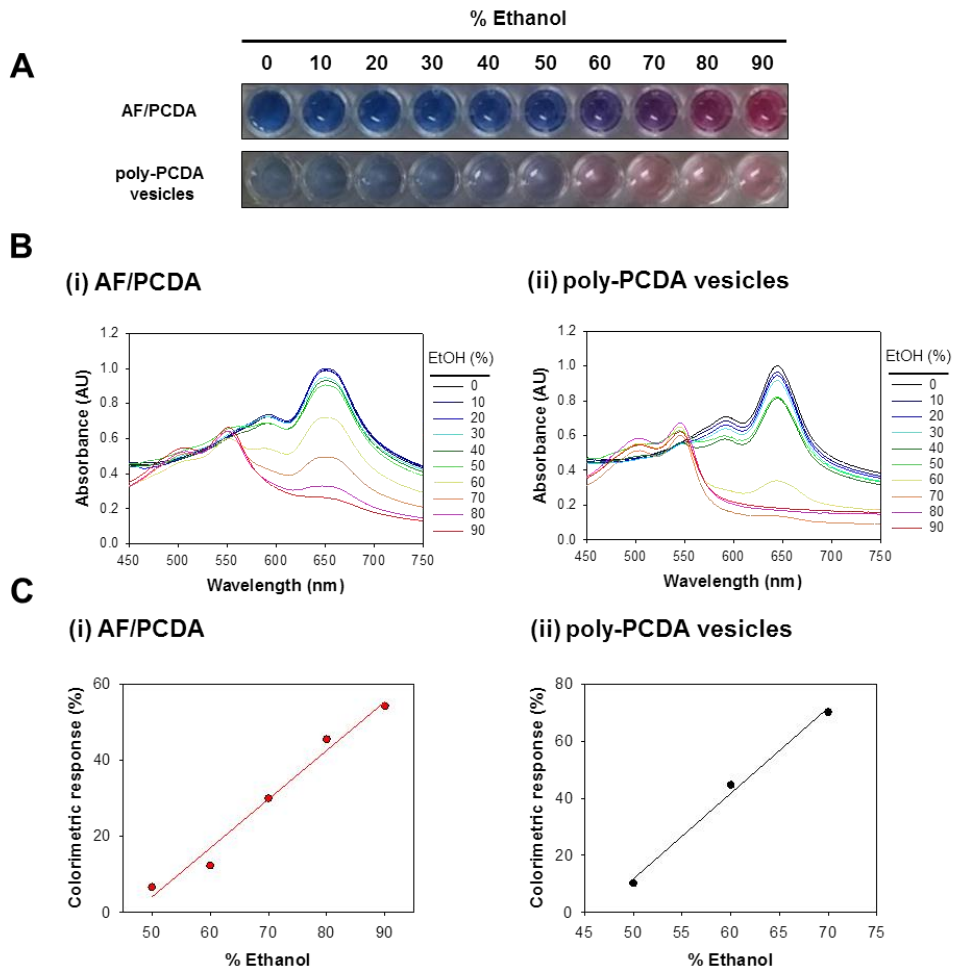

Figure 44. Colorimetric response of AF/PCDA to ethanol. (A) The color transition to red from initial blue was visualized for AF/PCDA and poly-PCDA vesicles with variations in ethanol concentration. (B) Absorption spectra of AF/PCDA and poly-PCDA vesicles with changes of ethanol concentration. (C) The colorimetric responses of AF-PCDA and poly-PCDA vesicles obtained in % CR were plotted as a function of ethanol concentration.

vesicles showed abrupt color change from blue to red at 65℃ (Figure 42A). To quantify the blue-to-red color transition of AF/PCDA and poly-PCDA vesicles, the % colorimetric response (% CR) was calculated by comparing the two maximum peaks at 650 nm and 550 nm of the absorption spectra representing the blue and red phases, respectively (Figure 42B). The plot of % CR as a function of temperature (Figure 42C) showed that % CR of AF/PCDA slowly increased from 55℃ to 80℃ while poly-PCDA vesicles underwent a steep change at 60℃ and reached plateau above 70℃. The blue-to-red color transition has been known to be caused by the increased segmental dynamics of PCDA molecules with heat and thus relieving the strain in the conjugated backbone of PDA [184, 185]. Therefore, the fact that AF/PCDA were capable of detecting temperature change in a wider range than poly-PCDA vesicles would be caused by the restricted molecular freedom of PCDA assembled on the amyloid fibrils.

The pH-responsive color changes of AF/PCDA and poly-PCDA vesicles were examined by adding either HCl or NaOH to the initial blue phase (Figure 43). While both AF/PCDA and poly-PCDA vesicles did not respond to the acidification, the apparent blue-to-red color transition occurred at basic pH around 11 for both species (Figure 43A). The pH-% CR plots obtained from their absorption spectra (Figure 43B) indicated that both AF/PCDA and poly-PCDA vesicles responded similarly (Figure 43C). Therefore, AF/PCDA system could be employed to detect pH variation on the basic range like poly-PCDA vesicles. AF/PCDA also exhibited the color transition with ethanol (Figure 44). In the case of AF/PCDA, the blue-to-red

color transition did not appear until 50% ethanol and started to occur slowly from 60% to 80% ethanol. The blue poly-PCDA vesicles, however, abruptly changed their color to red at 60% ethanol (Figure 44A). The ethanol-% CR plots indicated that AF/PCDA increased % CR linearly from 60% to 90% ethanol while poly-PCDA vesicles raised % CR rather quickly between 60% and 70% (Figure 44C). AF/PCDA could be considered to be adequate to monitor the solvent in a wider range. Taken together, AF/PCDA have been demonstrated to be more effective sensing agent exhibiting the colorimetric responses toward temperature, pH, and ethanol than poly-PCDA vesicles by widening the detection range which may result from structural restriction of the PCDA molecules polymerized on the amyloid fibrils.

1-4. Enhanced stability of AF/PCDA against mechanical stress

Owing to structural instability of poly-PCDA vesicles, their use as environment sensing agent could have been limited. In contrast, AF/PCDA could be versatile for their use as a sensing material because not only the PCDA molecules have been shown to be well-maintained upon exposure to the external stimuli but also amyloid fibrils are recognized to be one of the mechanically strongest biological materials available in nature [164]. In addition, the specific incorporation of PCDA molecules into amyloid fibrils and their topochemical photopolymerization into PDA on the fibrils would further fortify the resulting AF/PCDA. Therefore, mechanical stability of AF-PCDA was tested with sonication and compared with that of poly-PCDA vesicles and AF alone (Figure 45). The structural disruption and color

transitions of AF/PCDA and poly-PCDA vesicles were monitored after they were repeatedly treated with increasing number of the on/off cycle of sonication (10 sec/10 sec) (Figure 45A). As expected, AF/PCDA were demonstrated to be mechanically stable because not only their initial blue and red colors remained undisrupted even after 80 cycles of sonication (Figure 45A-a), but also the blue-to-red colorimetric transition was not affected even for the blue AF/PCDA pre-treated with 80 cycles of sonication (Figure 45A-c). For the poly-PCDA vesicles, however, their initial blue and red colors disappeared instantly right after 20 cycles of sonication, indicating structural vulnerability of the vesicles (Figure 45A-b). As a result, therefore, their colorimetric response was lost as the vesicular intactness was affected by sonication. The absorption spectra of AF/PCDA and poly-PCDA vesicles also indicated that the absorbance maxima of AF/PCDA were not affected by sonication (Figure 45B-a) while those of poly-PCDA vesicles drastically decreased only with 20 cycles of sonication (Figure 45B-b). The results obviously illustrated that poly-PCDA produced on the amyloid fibrils was mechanically tolerant toward the mechanical stress compared to poly-PCDA of the vesicles. Additionally, the fortifying effect of poly-PCDA to the fibrils was evaluated with TEM analyses of AF/PCDA and AF without PCDA incorporated following the sonication (Figure 46). AF alone were readily fragmented into short pieces with an average length of 200 nm after 20 cycles of sonication and completely broken down to the smaller pieces of 30 nm in average after 80 cycles. AF/PCDA, however, did not fragment into separate small pieces, which was distinctive from the AF fragmentation. Instead, those

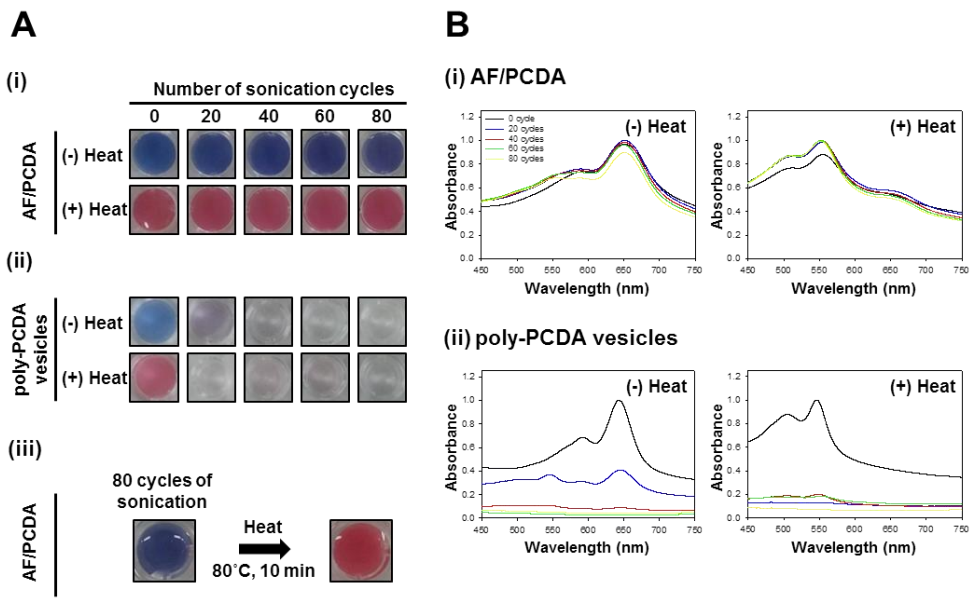

Figure 45. Enhanced stability of PCDA assembly in AF/PCDA against sonication-mediated mechanical stress. (A) The blue and red colors of AF/PCDA (i) and poly-PCDA vesicles (ii) obtained in the absence or presence of heat-treatment (80°C for 10 min) were subjected to the numbers of sonication indicated. The blue-to-red color transition of the blue AF/PCDA obtained after 80 cycles of sonication was observed with heat-treatment at 80°C for 10 min (iii). (B) Absorption spectra of AF/PCDA (i) and poly-PCDA vesicles (ii) obtained with and without the heat-treatment were shown after being subjected to the numbers of sonication indicated (black for 0 cycle, blue for 20 cycles, red for 40 cycles, green for 60 cycle, and yellow for 80 cycles).

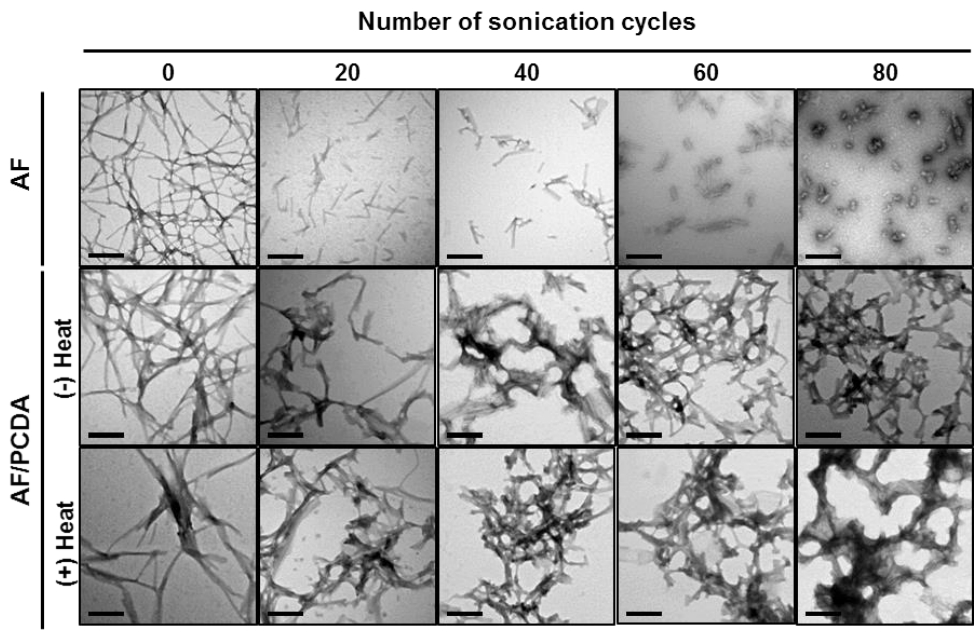

Figure 46. Enhanced stability of amyloid fibrils by interacting with PCDA. TEM images of AF and AF/PCDA obtained with and without the heat-treatment are shown after those fibrils were subjected to sonication with the number of cycles indicated. Scale bars represent 200 nm.

initial fibrils of AF/PCDA turned into the fibrillar networks with either thicker fibrils or rather smaller version of the fibrils as the sonication was repeated. Therefore, the incorporation of PCDA into AF and subsequent PDA formation yielded a colorimetric sensing material with mechanical strength far beyond that of conventional poly-PCDA vesicles by fortifying the fibrils with the on-site photopolymerization into PDA.

Herein, novel functional amyloid fibrils with chromic and fluorescent properties have been shown to be successfully produced by introducing PCDA into the self-assembly process of α-synuclein (Scheme 6). By taking advantage of the structural regularity of amyloid fibrils and the specific molecular interaction of a fatty acid analog of PCDA with α-synuclein as assessed with the crosslinking experiment with EEDQ and the accelerated fibrillation, the robust and effective PDA-based sensing material has been developed on the AF of α-synuclein. The resulting AF/PCDA exhibited the colorimetric response of blue-to-red transition toward the changes of temperature, pH, and ethanol concentrations in wider ranges than those observed with poly-PCDA vesicles, which could be due to restricted molecular freedom of PCDA polymerized on AF. In addition, AF/PCDA were more mechanically stable than either AF alone or poly-PCDA vesicles as evaluated with their structural tolerance against the mechanical stress provided by sonication. Therefore, simplicity of AF/PCDA production, improved sensing capability, and the mechanical stability could allow this novel amyloid-based colorimetric sensing material to be employed in diverse

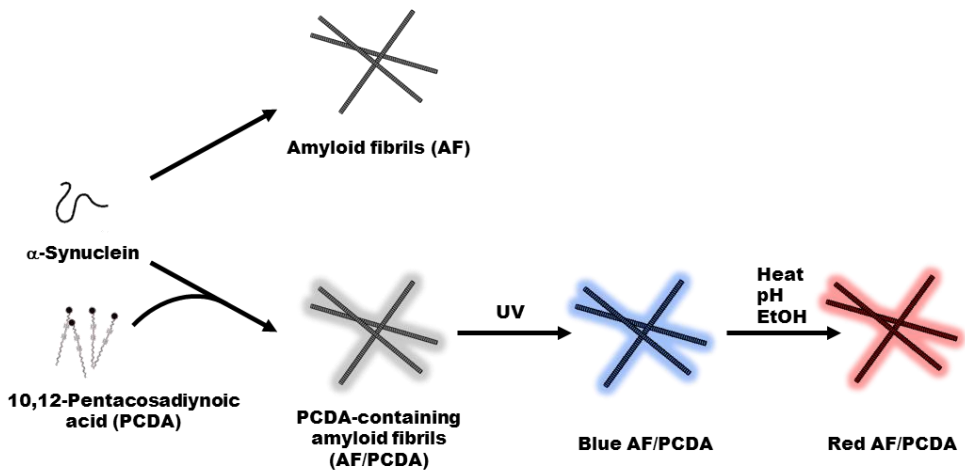

Scheme 6. Fabrication of PCDA-containing amyloid fibrils (AF/PCDA).

areas of sensor development by replacing the current vesicular type active material or fabricating the fibril-based two- or three-dimensional suprastructures such as films or hydrogels.

2. Litmus-type biosensor based on the PCDA-containing amyloid fibrils

2-1. Colorimetric transition of the PCDA-containing amyloid fibrils of α-synuclein layered on paper

The amyloid fibril and PCDA composites (AF/PCDA) prepared via co-incubation between α-synuclein and PCDA for 70 hours at 37℃ were spotted onto Whatman cellulose filter paper, air-dried for 2 hours, and exposed to UV light at 254 nm for 1 min. As confirmed in solution, the AF/PCDA spotted on paper turned to blue color upon UV exposure and subsequently converted to red with heat-treatment at 80℃ (Figure 47A). The PCDA monomers on paper did not respond to UV light, indicating that PCDA molecules could not align to form the color developing polymers by themselves on the paper. In the case of the PCDA vesicles, they became aggregated on paper, which left a few blue dots within the spot following UV exposure. Even in the presence of α-synuclein monomers, the PCDA molecules still did not turn to blue with UV, which suggests that amyloid fibrils are crucial to accommodate PCDA into an ordered alignment for the photopolymerization.

To prove whether amyloid fibrils could serve an optimal template for the PCDA alignment as well as to develop a handy procedure for a PCDA-

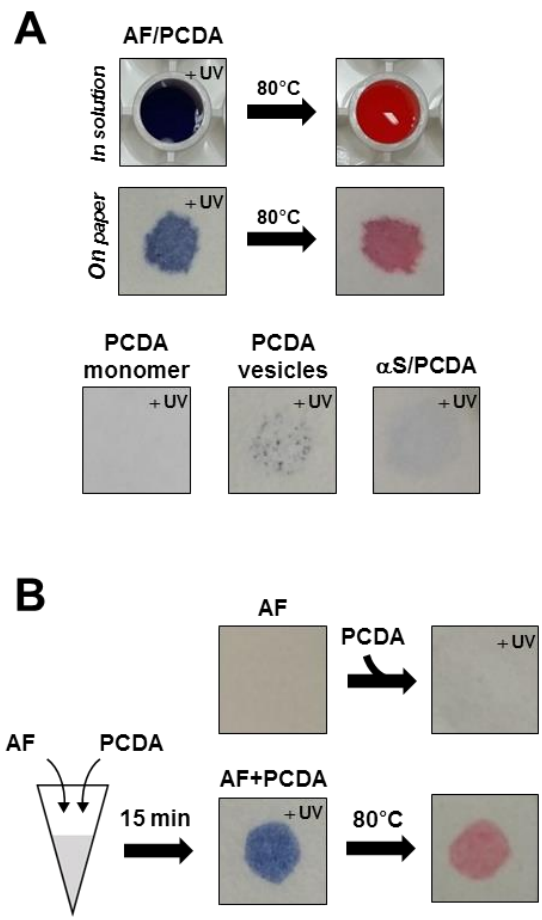
A
AF/PCDA
In solution
+UV
80°C
On paper
+UV
80°C
PCDA monomer
+UV
PCDA vesicles
+UV
αS/PCDA
+UV
B
AF
PCDA
+UV
AF
PCDA
15 min
AF+PCDA
+UV
80°C

Figure 47. Colorimetric litmus-type sensor developed with α-synuclein amyloid fibrils and PCDA. (A) Colorimetric responses of the amyloid fibril and PCDA composites (AF/PCDA) in solution and on paper to UV exposure and heat treatment. AF/PCDA were prepared via coincubation of α-synuclein (1 mg/ml) and PCDA (1 mM) for 70 hours at 37°C. PCDA monomers, PCDA vesicles, and PCDA monomers with monomeric α-synuclein (αSyn/PCDA) were spotted on paper for negative controls. (B) Colorimetric responses of the mixture of pre-made amyloids fibrils (AF) and PCDA (AF+PCDA) on paper. AF and PCDA were either separately spotted on paper in succession (upper row) or in the form of AF+PCDA obtained after 15 min of incubation between AF and PCDA (lower row). Both papers were subjected to UV exposure followed by heating.

based litmus-type sensor, the pre-made amyloid fibrils (AFs) of α-synuclein were employed to examine their colorimetric response on paper in the presence of PCDA (Figure 47B). Whereas two successive spotting of the pre-made AFs and PCDA with air-dry for 2 hours after each spotting did not exhibit blue color upon the UV exposure, a mixture of the pre-made AFs and PCDA (AF+PCDA) incubated for 15 min under dark prior to spotting onto Whatman paper gave rise to blue color with UV and transition to red with the heat-treatment at 80℃ for 5 min. These data indicate that the PCDA molecules may prefer the cellulose paper surface to the AFs pre-spotted on the paper. In solution, however, the PDA monomers apparently require AFs to be aligned on the templates. After all, two types of PCDA-based litmus-type sensing materials have been prepared with AFs of α-synuclein - AF/PCDA and AF+PCDA - .

2-2. Paper-based colorimetric thermal responses of AF/PCDA and AF+PCDA and their applications

To evaluate temperature sensing property of AF/PCDA and AF+PCDA spotted on paper with UV exposure, the blue-to-red color transition was examined for the spots after 5 min of incubation at various temperatures from 25℃ to 90℃ (Figure 48A). For the AF/PCDA, the color transition along with the fluorescence enhancement gradually occurred at the higher temperature range between 60℃ and 90℃ where the red color became apparent from 80℃. The AF+PCDA, on the other hand, exhibited their response at the lower range between 25℃ and 60℃, in which the discernable

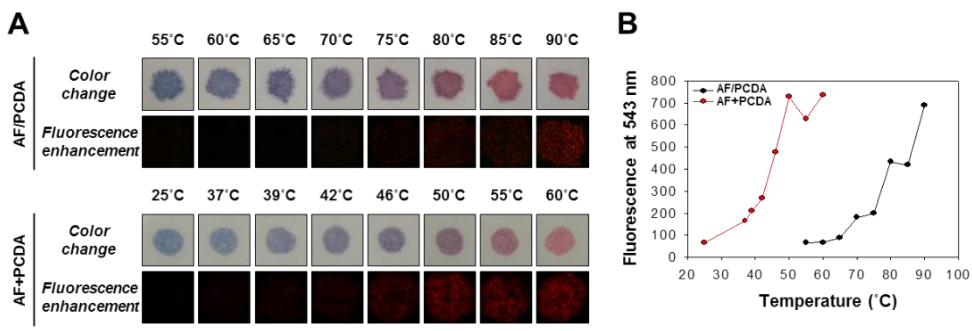

Figure 48. Thermal response of the litmus-type sensors. (A) Colorimetric transition and fluorescence enhancement of AF/PCDA and AF+PCDA on paper at various temperatures. (B) The fluorescence intensities of the heat-treated paper sensors were plotted with the temperatures by analyzing their fluorescence images shown in (a).

red appeared from 55℃. Difference in their color transition temperatures of AF/PCDA and AF+PCDA was clearly demonstrated with a plot of the fluorescence intensities of the spots obtained via digital image analysis following 5 min incubation at various temperatures (Figure 48B). Since AF/PCDA and AF+PCDA have mutually exclusive temperature ranges for the colorimetric response, the litmus-type thermal sensors employing either material could cover a wide range of temperature and act complementary to each other.

In order to confirm whether the litmus-type sensor is capable of following temperature change in real-time, the paper sensor prepared with AF+PCDA was continuously heated on a hot plate. The blue spot gradually changed its color to red as the temperature increased from 25℃ to 60℃ (Figure 49A). The red color did not convert back to blue when the temperature decreased to room temperature. This irreversible thermal sensing property detecting only ascending temperature change would be useful for the paper sensor to monitor thermal history of materials by assessing a maximum temperature the materials have experienced. Another use of the litmus-type thermal sensor is to locate an exact heated spot adjacent to unaffected areas as demonstrated with the blue AF+PCDA-containing paper which converted to red in a shape of musical sharp sign after a local heating provided to the copper tapes attached underneath the blue paper in the same shape (Figure 49B). Intriguingly, the entire paper sensor turned to dark brown upon additional UV exposure with complete disappearance of the red sharp sign which then reappeared as the copper tapes were heated over. This reversibility

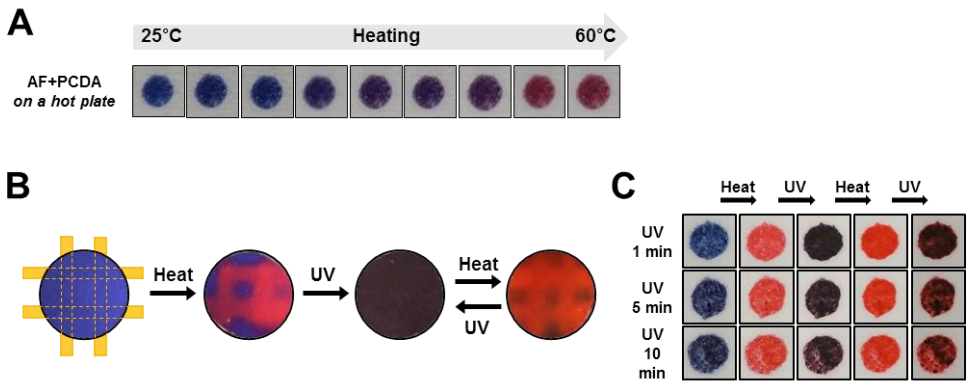

Figure 49. Applications of the AF+PCDA litmus-type sensors in temperature detection. (A) Monitoring temperature change of a hot plate in real-time with the litmus-type sensor of AF+PCDA. (B) Monitoring the local heating of the AF+PCDA litmus type sensor with the copper tapes aligned and heated in a shape of musical sharp sign; and reversible thermal sensing property of the paper sensor observed with additional UV and heat treatments. (C) Reversibility of the thermochromic sensing property of AF+PCDA on paper assessed with variations in the duration of initial UV exposure.

lasted at least three to four times. In order to clarify whether this reversibility was due to either the excess PCDA monomers on AFs not photopolymerized with a prior UV exposure or a large-scale conformational change of the activated poly-PCDA network, the duration of initial UV exposure was varied for the AF+PCDA paper sensor (Figure 49C). The red spot derived from the blue AF+PCDA obtained with 1 min of the initial UV exposure turned to dark brown upon an additional UV exposure for 20 min, which again showed the color transition to red with heating for 1 min at 80℃. Upon another subsequent UV exposure, the red became blueish. The first red-to-purple transition, however, became less apparent as the duration of initial UV exposure increased to obtain the blue spot for AF+PCDA. This result suggests that the reversible heat sensing property of AF+PCDA on paper could be caused by the presence of unreacted excess PCDA monomers yet to be aligned within the templates. Taken together, the litmus-type sensors developed with amyloid fibrils of α-synuclein in the presence of PCDA have been demonstrated to detect not only thermal history of materials in general but also their heated local spots in a reversible manner.

2-3. Interaction between PCDA and amyloid fibrils within AF/PCDA and AF+PCDA

Since the simple mixture between pre-made AFs and PCDA was demonstrated to detect the lower temperatures, the molecular interaction of PCDA for amyloid fibrils would be distinctive in between AF/PCDA and AF+PCDA. Sonication was employed to test tightness of PCDA binding to

the fibrils. Following repetitive sonications up to 3 times with 2 sec of sonication for each, both AF/PCDA and AF+PCDA were separately precipitated to remove unbound or unleashed PCDA. After resuspending the precipitates, they were spotted onto the paper and subjected to UV exposure at 254 nm for 1 min (Figure 50A). The resulting blue color development indicated that AF+PCDA had lost most of its ability to be photopolymerized right after the first sonication. Two consecutive sonications deprived AF+PCDA of the blue color development on paper. AF/PCDA, on the other hand, turned to blue even after three times of sonication. These data suggest that PCDA molecules have bound to AF less tightly within AF+PCDA than AF/PCDA, which could be responsible for the difference in their colorimetric response toward temperatures. In other words, the paper sensor prepared with AF/PCDA has required the higher temperatures to exhibit the blue-to-red transition since the PCDA molecules appear to exist in a more tightly bound and, thereby, restricted state within AF which would hamper the conformational mobility of poly-PCDA for the red color transition.

Distinctive mode of interaction between PCDA and AF in AF/PCDA and AF+PCDA was investigated with Raman spectroscopy (Figure 50B). For vesicular poly-PCDA, three primary peaks were observed at 1442 cm^{-1}, 1794 cm^{-1}, and 2092 cm^{-1} in the spectrum, which correspond to alkene, C=O, and alkyne stretching mode of poly-PCDA, respectively. Two of the primary peaks of poly-PCDA shifted to 1458 cm^{-1} and 2081 cm^{-1} in AF/PCDA with a new small peak emerged at 1520 cm^{-1}. The peak of poly-PCDA at 1794 cm^{-1} was not found in either AF/PCDA or AF+PCDA. In the case of AF+PCDA,

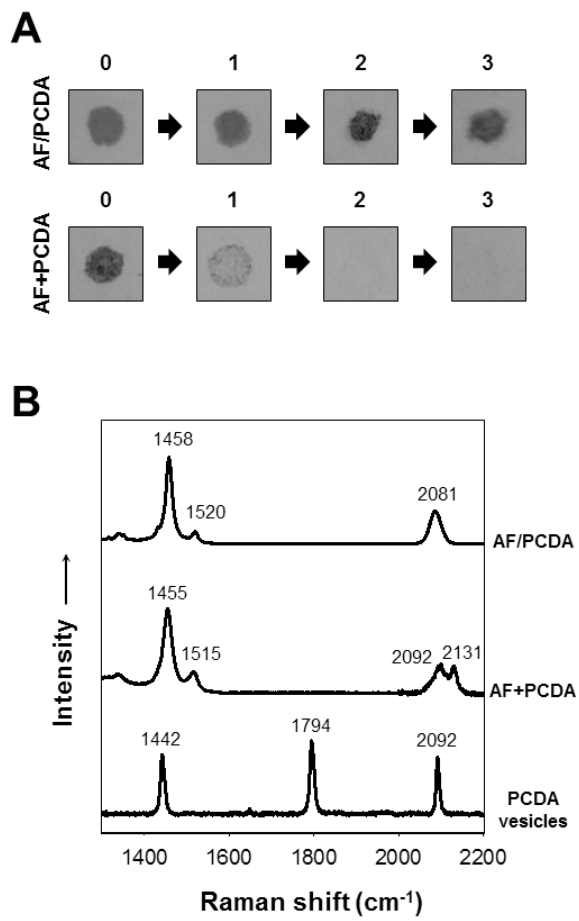

Figure 50. Distinctive interactions of PCDA molecules with the amyloid fibrils in either AF/PCDA or AF+PCDA. (A) Analysis of the tightness of PCDA binding to amyloid fibrils by observing the blue color development with UV exposure following a number of repetitive sonications for 2 sec each as indicated on the top of panels. (B) Raman spectra of AF/PCDA, AF+PCDA, and PCDA vesicles obtained after UV exposure.

the alkene peak appeared at 1455 cm^{-1} with an additional peak at 1515 cm^{-1}. In the high frequency Raman shift range, the alkyne peak appeared split into two at 2092 cm^{-1} and 2131 cm^{-1}. Although those peaks are not designated with specific chemical bonds, variations in the Raman scattering peaks of PCDA in the complexes clearly indicate unique environment and special molecular arrangement of PCDA in AF/PCDA and AF+PCDA. Taken together, it is pertinent to consider that the difference in thermal sensing property between AF/PCDA and AF+PCDA could be attributed to distinctive molecular alignment of PCDA and its molecular freedom in the complexes.

2-4. Colorimetric response of the litmus-type sensor to organic solvents

Difference in their sensing ability of the litmus-type sensors prepared with either AF/PCDA or AF+PCDA was also examined with various volatile organic solvents (Figure 51). The AF/PCDA sensors instantly changed their colors from blue to purple when they were dipped in the solvents as shown in Figure 51A, but the color transitions were not observed with the solvent vapors even after 1 hour of exposure. The blue paper sensors made with AF+PCDA, on the other hand, exhibited various colors from purple to discrete red as they contacted the solvents directly. When they exhibited the color transition especially in chloroform, methylene chloride, benzene, toluene, and xylene, their resulting red colors became more vivid when compared with the purple colors of the AF/PCDA sensors. Intriguingly, the blue AF+PCDA sensors were demonstrated to be capable of detecting the

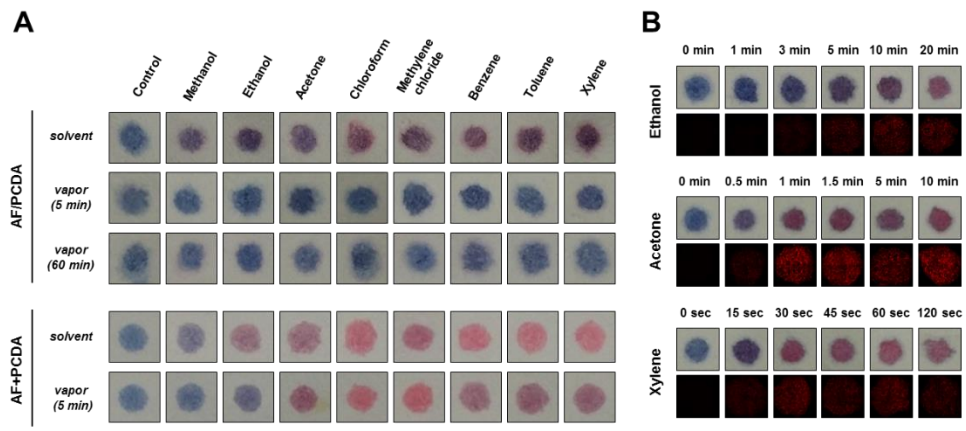

Figure 51. Colorimetric and fluorescent responses of the litmus-type sensors with AF/PCDA and AF+PCDA to various organic solvents. (A) Solvatochromic properties of the AF/PCDA and AF+PCDA on paper upon the exposure to solvents and their vapors. (B) Time-resolved colorimetric transition and fluorescence enhancement of the AF+PCDA paper sensors with the exposure to the solvent vapors of ethanol, acetone, and xylene.

vapors of solvents such as acetone, chloroform, methylene chloride, benzene, toluene, and xylene within 5 min of exposure (Figure 51A). The less tight binding and thus high mobility of poly-PCDA on AFs in AF+PCDA would be responsible for its improved sensitivity toward the solvent vapors from that of the AF/PCDA sensors as seen in the thermal sensing property of AF+PCDA detecting the lower temperatures. Furthermore, the vapor-induced color change of the AF+PCDA sensors exhibited a gradual shift in color from blue to red emitting fluorescence as the vapor exposure time increased especially for ethanol, acetone, and xylene (Figure 51B). This time-dependent vapor detection property could be used to monitor the duration of toxic vapor exposures.

In this study, the litmus-type sensors have been made with α-synuclein amyloid fibrils and 10, 12-pentacosadiynoic acid (PCDA). The PCDA molecules were fabricated into the amyloid fibrils via either coincubation with monomeric α-synuclein (AF/PCDA) or mixing with its pre-made fibrils (AF+PCDA). The PCDA molecules aligned on amyloid fibrils were photopolymerized to exhibit blue color with UV exposure and respond to external stimuli such as temperature and solvents by exhibiting the blue-to-red color transition on paper. The paper sensors prepared with AF/PCDA and AF+PCDA showed different sensing properties toward the stimuli possibly due to molecular freedom of the bound PCDA. The litmus-type sensor with AF+PCDA shown to contain the less tightly bound PCDA was able to detect the lower temperatures and the vapors of certain organic solvents within a

short period of exposure. Furthermore, the AF+PCDA sensor could monitor the temperature change of materials in real-time and locate the heated spots by exhibiting the blue-to-red color transition. Therefore, the litmus-type sensors conveniently manufactured by placing the nanocomposites of amyloid fibrils and polydiacetylene onto a filter paper can be employed to monitor thermal history of materials in general and organic compounds prevalent in polluted areas.

IV. Conclusions

This study has shown that amyloid fibrils of α-synuclein can be utilized as promising biomaterials via playing a role as a powerful template for assembly of 10,12-pentacosadiynoic acid (PCDA).

(1) α-Synuclein specifically interacts with PCDA which has a carboxylic group with along aliphatic chain like fatty acids in nature.

(2) PCDA molecules can be aligned on amyloid fibrils (AF) via either coincubation with monomeric α-synuclein (AF/PCDA) or mixing with its pre-made fibrils (AF+PCDA).

(3) PCDA molecules aligned on AF were photopolymerized with UV and responded to external stimuli such as temperature, pH and solvents, exhibiting blue-to-red color transition.

(4) PCDA molecules assembled with AF template remained stable not only in solution, but also on paper unlike poly-PCDA vesicles.

References

[1] Goedert, M. α-Synuclein and neurodegenerative diseases. *Nat. Rev. Neurosci.* **2** (2001) 492-501.

[2] Adamcik, J.; Jung, J. -M.; Flakowski, J.; De Los Rios, P.; Dietler, G. et al. Understanding amyloid aggregation by statistical anlaysis of atomic force microscopy images. *Nature Nanotechnol.* **5** (2010) 423-428.

[3] Xue, W. -F.; Homans, S. W.; Radford, S. E. Amyloid fibril length distribution quantified by atomic force microscopy single-particle image analysis. Protein Eng. Des. Sel. 22 (2009) 489-496.

[4] Eanes, E. D. and Glenner, G. G. X-ray diffraction studies on amyloid filaments. *J. Histochem. Cytochem.* **16** (1968) 673–677.

[5] Serpell, L. Amyloid structure. *Essays Biochem.* **56** (2014) 1-10.

[6] Wille, H.; Bian, W.; McDonald, M.; Kendall, A.; Colby, D. W. et al. Natural and synthetic prion structure from X-ray fiber diffraction. *Proc. Natl. Acad. Sci.* **106** (2009) 16990–16995.

[7] Selkoe, D. J. Folding proteins in fatal ways. *Nature* **426** (2003) 900-904.

[8] Spillantini, M. G.; Schmidt, M. L.; Lee, V. M. -Y.; Trojanowski, J. Q.; Jakes, R. et al. α-Synuclein in Lewy bodies. *Nature* **388** (1997) 839-840.

[9] de Lau, L. M.; Breteler, M. M. Epidemiology of Parkinson's disease.

Lancet Neurol. **5** (2006) 525-535.

[10] Auluck, P. K.; Caraveo, G.; Lindquist, S. α-Synuclein: membrane interactions and toxicity in Parkinson's disease. *Annu. Rev. Cell. Dev. Biol.* **26** (2010) 211-233.

[11] Dick, F. D.; De Palma, G.; Ahmadi, A.; Scott, N. W.; Prescott, G. J. Environmental risk factors for Parkinson's disease and parkinsonism: the Geoparkinson study. *Occup. Environ. Med.* **64** (2007) 666–672.

[12] Betarbet, R.; Sherer, T. B.; MacKenzie, G.; Garcia-Osuna, M.; Panov, A. V. Chronic systemic pesticide exposure reproduces features of Parkinson's disease. *Nature Neurosci.* **3** (2000) 1301-1306.

[13] Fukushima, T.; Tan, X.; Luo, Y.; Kanda, H. Relationship between blood levels of heavy metals and parkinson's disease in China. *Neuroepidemiology* **34** (2010) 18–24.

[14] Montgomery, E. B. Heavy metals and the etiology of Parkinson's disease and other movement disorders. *Toxicology.* **97** (1995) 3-9.

[15] Uversky, V. N.; Li, J.; Fink, A. L. Pesticides directly accelerate the rate of α-synuclein fibril formation: a possible factor in Parkinson's disease. *FEBS Lett.* **500** (2001) 105-108.

[16] Uversky, V. N.; Li, J.; Fink, A. L. Metal-triggered structural transformations, aggregation, and fibrillation of human α-synuclein. A possible molecular NK between Parkinson's disease and heavy metal exposure. *J. Biol. Chem.* **276** (2001) 44284-44296.

[17] Marques, O.; Outeiro, T. F. α-Synuclein: from secretion to

dysfunction and death. *Cell Death Dis.* **3** (2012) e350.

[18] Polymerpoulos, M. H.; Lavedan, C.; Leroy, E.; Ide, S. E.; Dehejia, A. et al. Mutation in the α-synuclein gene identified in families with Parkinson's disease. Science 276 (1997) 2045-2047.

[19] Zarranz, J. J.; Alegre, J.; Gomez-Esteban, J. C.; Lezcano, E.; Ros, R. et al. The new mutation, E46K, of α-synuclein causes parkinson and Lewy body dementia. *Ann. Neurol.* **55** (2004) 164-173.

[20] Kurger, R.; Kuhn, W.; Muller, T.; Woitalla, D.; Graeber, M. et al. Ala30Pro mutation in the gene encoding α-synuclein in Parkinson's diseae. *Nat. Genet.* **18** (1998) 106-108.

[21] Singleton, A.; Gwinn-Hardy, K.; Sharabi, Y.; Li, S. T.; Holmes, C. et al. Association between cardiac denervation and parkinsonism caused by α-synuclein gene triplication. *Brain* **127** (2004) 768-772.

[22] Singleton, A. B.; Farrer, M.; Johnson, J.; Singleton, A.; Hageu, S. et al. α-Synuclein locus triplication causes Parkinson's disease. *Science* **302** (2003) 841.

[23] Goldsbury, C.; Frey, P.; Olivieri, V.; Aebi, U.; Müller S. A. Multiple assembly pathways underlie amyloid-β fibril polymorphisms. *J. Mol. Biol.* **352** (2005) 282-298.

[24] Wetzel, R.; Shivaprasad, S.; Williams, A. D. Plasticity of amyloid fibrils. *Biochemistry* **46** (2007) 1-10.

[25] Morozova-Roche, L. A.; Zamotin, V.; Malisauskas, M.; Ohman, A.; Chertkova, R. et al. Fibrillation of carrier protein albebetin and its biologically active constructs. Multiple oligomerix intermediates and

pathways. *Biochemistry* **43** (2004) 6910-6919.

[26] Gosal, W. S.; Morten, I. J.; Hewitt, E. W.; Smith, D. A,; Thomson, N. H. et al. Competing pathways determine fibril morphology in the self-assembly of β_2-microglobulin into amyloid. *J. Mol. Biol.* **351** (2005) 850-864.

[27] Bhak, G.; Choe, Y. -J.; Paik, S. P. Mechanism of Amyloidogenesis: Nucleation-dependent Fibrillation versus Double-concerted Fibrillation. *BMB Rep.* **42** (2009) 541-551.

[28] Kelly, J. W. Mechanisms of amyloidogenesis. *Nat. Struct. Mol. Biol.* **7** (2000) 824-826.

[29] Serio, T. R.; Cashikar, A. G.; Kowal, A. S.; Sawicki, G. J.; Moslehi, J. J. et al. Nucleated conformational conversion and the replication of conformational information by a prion determinant. *Science* **289** (2000) 1317-1321.

[30] Fabrizio, C; Dobson, C. M. Protein misfolding, functional amyloid, and human disease. *Annu. Rev. Biochem.* **75** (2006) 333-366.

[31] Wood, S. J.; Wypych, J.; Steavenson, S.; Louis, J. -C.; Citron, M. et al. α-Synuclein fibrillogenesis is nucleation-dependent. Implications for the pathogenesis of Parkinson's disease. *J. Biol. Chem.* **274** (1999) 19509-19512.

[32] Nguyen, P. H.; Li, M. S.; Stock, G.; Straub, J. E.; Thirumalai, D. Monomer adds to preformed structured oligomers of Aβ-peptides by a two-stage dock-lock mechanism. *Proc. Natl. Acad. Sci.* **104** (2007) 111–116.

[33] Park, J. -W.; Ahn, J. S.; Lee, J. -H.; Bhak, G.; Jung, S. et al. Amyloid fibrillar meshwork formation of ion-induced oligomeric species of Aβ40 with phthalocyanine tetrasulfonate and its toxic consequences. *Chem.Bio.Chem.* **9** (2008) 2602-2605.

[34] Dong, J.; Canfield, J. M.; Mehta, A. K.; Shokes, J. E.; Tian, B. et al. Engineering metal ion coordination to regulate amyloid fibril assembly and toxicity. *Proc. Natl. Acad. Sci. U.S.A.* **104** (2007) 13313-13318.

[35] Kim, Y. -S.; Lee, D.; Lee, E. -K.; Sung, J. Y.; Chung, K. C. et al. Multiple ligand interaction of α-synuclein produced various forms of protein aggregates in the presence of Aβ25-35, copper, and eosin. *Brain Res.* **908** (2001) 93-98.

[36] Bhak, G.; Lee, J. -H.; Hahn, J. -S.; Paik. S. R. Granular assembly of α-synuclein leading to the accelerated amyloid fibril formation with shear stress. *PLoS ONE* **4** (2009) e4177.

[37] Lee, J. -H.; Bhak, G.; Lee, S. -G.; Paik, S. R. Instantaneous amyloid fibril formation of α-Synuclein from the oligomeric granular structures in the presence of hexane. *Biophys. J.* **95** (2008) L16-L18.

[38] Vamvaca, K.; Volles, M. J.; Lansbury, P. T. The first N-terminal amino acids of α-synuclein area essential for α-helical structure formation in vitro and membrane binding in yeat. *J. Mol. Biol.* **389** (2009) 413-424.

[39] Lorenzen, N.; Lemminger, L.; Pedersen, J. N.; Nielsen, S. B.; Otzen, D. E. The N-terminus of α-synuclein is essential for both monomeric

and oligomeric interactions with membranes. *FEBS Lett.* **588** (2014) 497-502.

[40] Li, H. T.; Du, H. N.; Tang, L.; Hu, J.; Hu, H. Y. Structural transformation and aggregation of human α-synuclein in trifluoroethanol: non-amyloid component sequence is essential and beta-sheet formation is prerequisite to aggregation. *Biopolymers* **64** (2002) 221–226.

[41] Herrera, F. E.; Chesi, A.; Paleologou, K. E.; Schmid, A.; Munoz, A. et al. Inhibition of α-synuclein fibrillization by dopamine is mediated by interactions with five C-terminal residues and with E83 in the NAC region. *Plos One* **3** (2008) e3394.

[42] Nielsen, M. S.; Vorum, H.; Lindersson, E.; Jensen, P. H. Ca^{2+} binding to α-synuclein regulates ligand binding and oligomerization. *J. Biol. Chem.* **276** (2001) 22680-22684.

[43] Paik, S. R.; Shin, H. J.; Lee, J. H. Metal-catalyzed oxidation of α-synuclein in the presence of copper(II) and hydrogen peroxide. *Arch. Biochem. Biophys.* **378** (2000) 269-277.

[44] Paik, S. R.; Shin, H. J.; Lee, J. H.; Chang, C. S.; Kim, J. Copper(II)-induced self-oligomerization of α-synuclein. *Biochem. J.* **340** (1999) 821-828.

[45] Dunker, A. K.; Brown, C. J.; Lawson, J. D.; Iakoucheva, L. M.; Obradovic, Z. Intrinsic disorder and protein function. *Biochemistry* **41** (2002) 6573–6582.

[46] Dyson, H. J.; Wright, P. E. Intrinsically unstructured proteins and their functions. *Nat. Rev. Mol. Cell. Biol.* **6** (2005) 197-208.

[47] Wright, P. E.; Dyson, H. J. Intrinsically unstructured proteins: re-assessing the protein structure-function paradigm. *J. Mol. Biol.* **293** (1999) 321-331.

[48] Vucetic, S.; Obradovic, Z.; Vacic, V.; Radivojac, P.; Peng, K. et al. DisProt: a database of protein disorder. *Bioinformatics* **21** (2005) 137-140.

[49] Fukuchi, S.; Sakamoto, S.; Nobe, Y.; Murakami, S. D. Amemiya, T. et al. IDEAL: Intrinsically disordered proteins with extensive annotations and literature. *Nucleic Acids Res.* **40** (2012) D507–D511.

[50] Das, S.; Pal, U.; Das, S.; Bagga, K.; Roy, A. et al. Sequence complexity of amyloidogenic regions in intrinsically disordered human proteins. *PLoS One* **9** (2014) e89781.

[51] Weinreb, P. H.; Zhen, W.; Poon, A. W.; Conway, K.A.; Lansbury, P. T. NACP, a protein implicated in Alzheimer's disease and learning, is natively unfolded. *Biochemistry* **35** (1996) 13709-13715.

[52] Nielsen, M. S; Vorum, H.; Lindersson, E.; Jensen, P. H. Ca^{2+} binding to α-synuclein regulates ligand binding and oligomerization. *J. Biol Chem.* **276** (2001) 22680-22684.

[53] Lee, D.; Lee, E. K.; Lee, J. H.; Chang, C. S.; Paik, S. R. Self-oligomerization and protein aggregation of α-synuclein in the presence of Coomassie Brilliant Blue. *Eur. J. Biochem.* **268** (2001)

295-301.

[54] Paik, S. R.; Lee, D.; Cho, H. J.; Lee, E. N.; Chang, C. S. Oxidized glutathione stimulated the amyloid formation of α-synuclein. *FEBS Lett.* **573** (2003) 63-67.

[55] Lee, E. N.; Lee, S. Y.; Lee, D.; Kim, J.; Paik, S. R. Lipid interaction of α-synuclein during the metal-catalyzed oxidation in the presence of Cu^{2+} and H_2O_2. *J. Neurochem.* **84** (2003) 1128-1142.

[56] Lee, E. N.; Cho, H. J.; Lee, C. H.; Lee, D.; Chung, K. C. et al. Phthalocyanine tetrasulfonates affect the amyloid formation and cytotoxicity of α-synuclein. *Biochemistry* **43** (2004) 3704-3715.

[57] Lee, C. H.; Kim, H. J.; Lee, J. H.; Cho, H. J.; Kim, J. et al. Dequalinium-induced protofibril formation of α-synuclein. *J. Biol. Chem.* **281** (2006) 3463-3472.

[58] Shin, H. J.; Lee, E. K.; Lee, J. H.; Lee, D.; Chang, C. S. et al. Eosin interaction of α-synuclein leading to protein self-oligomerization. *Biochim. Biophys. Acta.* **1481** (2000) 139-146.

[59] Kim, J.; Moon, C. H.; Jung, S.; Paik, S. R. α-Synuclein enhances bioluminescent activity of firefly luciferase by facilitating luciferin localization. *Biochim. Biophys. Acta.* **1794** (2009) 309-314.

[60] Yang, J. E.; Hong, J. W.; Kim, J.; Paik, S. R. Amyloid polymorphism of α-synuclein induced by active firefly luciferase. B. *Korean Chem. Soc.* **35** (2014) 425-430.

[61] Koo, H. J.; Yang, J. E.; Park, J. H.; Lee, D.; Paik, S. R. α-Synuclein-mediated defense against oxidative stress via modulation of

glutathione peroxidase. *Biochim. Biophys. Acta.* **1834** (2013) 972-976.

[62] Chiti, F.; Dobson, C. M. Protein misfolding, functional amyloid, and human disease. Annu. Rev. Biochem. 75 (2006) 333-66.

[63] Brown, D. R. Oligomeric α-synuclein and its role in neuronal death. *IUMBM Life.* **62** (2010) 334-339.

[64] Volles, M. J.; Lee, S. J.; Rochet, J. C.; Shtilerman, M. D.; Ding, T. T. et al. Vesicle permeabilization by protofibrillar α-synuclein: implications for the pathogenesis and treatment of Parkinson's disease. *Biochemistry* **40** (2001) 7812-7819.

[65] van Rooijen, B. D.; Claessens, M. M.; Subramaniam, V. Membrane permeabilization by oligomeric α-synuclein: in search of the mechanism. *PLoS ONE* **5** (2010) e14292.

[66] Kayed, R.; Head, E.; Thompson, J. L.; McIntire, T. M.; Milton, S. C. et al. Common structure of soluble amyloid oligomers implies common mechanism of pathogenesis. *Science* **300** (2003) 486-489.

[67] Xin, W.; Emadi, S.; Williams, S.; Liu, Q.; Schulz, P. et al. Toxic oligomeric α-synuclein variants present in human Parkinson's disease brains are differentially generated in mammalian cell models. *Biomolecules* **22** 2015 1634-1651.

[68] Karpinar, D. P.; Balija, M. B.; Kügler, S.; Opazo, F.; Rezaei-Ghaleh, N. et al. Pre-fibrillar α-synuclein variants with impaired β-structure increase neurotoxicity in Parkinson's disease models. *EMBO J.* **21** (2009) 3256-3268.

[69] Winner, B.; Jappelli, R.; Maji, S. K.; Desplats, P. A.; Boyer, L. et al. In vivo demonstration that α-synuclein oligomers are toxic. *Proc. Natl. Acad. Sci. USA.* **8** (2011) 4194-4199.

[70] Goldberg, M. S.; Lansbury, P. T. Is there a cause-and-effect relationship between α-synuclein fibrillization and Parkinson's disease? *Nat. Cell. Biol.* **2** (2000) E115-E119.

[71] Ding, T. T.; Lee, S. J.; Rochet, J. C.; Lansbury, P. T. Annular α-synuclein protofibrils are produced when spherical protofibrils are incubated in solution or bound to brain-derived membranes. *Biochemistry* **41** (2002) 10209-10217.

[72] Zakharov, S. D.; Hulleman, J. D.; Dutseva, E. A.; Antonenko, Y. N.; Rochet, J. C. et al. Helical α-synuclein forms highly conductive ion channels. *Biochemistry* **46** (2007) 14369-14379.

[73] Kayed, R.; Sokolov, Y.; Edmonds, B.; McIntire, T.M.; Milton, S. C. et al. Permeabilization of lipid bilayers is a common conformation-dependent activity of soluble amyloid oligomers in protein misfolding diseases. *J. Biol. Chem.* **279** (2004) 46363-46366.

[74] Celej, M. S.; Sarroukh, R.; Goormaghtigh, E.; Fidelio, G. D.; Ruysschaert, J. -M. et al. Toxic prefibrillar α-synuclein amyloid oligomers adopt a distinctive antiparallel β-sheet structure. *Biochem. J.* **443** (2012) 719-726.

[75] Apetri, M. M.; Maiti, N. C.; Zagorski, M.G.; Carey, P. R.; Anderson, V. E. Secondary structure of α-synuclein oligomers: characterization by raman and atomic force microscopy. *J. Mol. Biol.* **355** (2006) 63-

71.

[76] Hong, D. P.; Han, S.; Fink, A. L.; Uversky, V. N. Characterization of the non-fibrillar α-synuclein oligomers. *Protein. Pept. Lett.* **18** (2011) 230-240.

[77] Bhak, G.; Lee, J.; Kim, T. H.; Lee, S.; Lee, D.et al. Molecular inscription of environmental information into protein suprastructures: temperature effects on unit assembly of α-synuclein oligomers into polymorphic amyloid fibrils. *Biochem. J.* **464** (2014) 259-269.

[78] Lee, J. H.; Bhak, G.; Lee, S. G.; Paik, S. R. Instantaneous amyloid fibril formation of α-synuclein from the oligomeric granular structures in the presence of hexane. *Biophys. J.* **95** (2008) L16-L18.

[79] Bronstein, I.; Fortin, J.; Stanley, P. E.; Stewart, G. S.; Kricka, L. J. Chemiluminescent and bioluminescent reporter gene assays. *Anal. Biochem.* **219** (1994) 169–181.

[80] Greer, L. F. III; Szalay, A. A. Imaging of light emission from the expression of luciferases in living cells and organisms: a review. *Luminescence* **17** (2002) 43–73.

[81] Muller, F. L.; Lustgarten, M. S.; Jang, Y.; Richardson, A.; Van Remmen, H. Trends in oxidative aging theories. *Free Radic. Biol. Med.* **43** (2007) 477−503.

[82] Jenner, P. Oxidative stress in Parkinson's disease. *Ann. Neurol*. **53** (2003) S26–S38.

[83] Lubos, E.; Loscalzo, J.; Handy, D. E. Glutathione peroxidase-1 in

health and disease: from molecular mechanisms to therapeutic opportunities. *Antioxid. Redox. Signal.* **15** (2011) 1957–1997.

[84] Power, J. H.; Blumbergs, P. C. Cellular glutathione peroxidase in human brain: cellular distribution, and its potential role in the degradation of Lewy bodies in Parkinson's disease and dementia with Lewy bodies. *Acta. Neuropathol.* **117** (2009) 63–73.

[85] Ramos, S. Effects of dietary flavonoids on apoptotic pathways related to cancer chemoprevention. *J. Nutr. Biochem.* **18** (2007) 427-442.

[86] Balasundram, N.; Sundram, K.; Samman, S. Phenolic compounds in plants and agri-industrial by-products: antioxidant activity, occurrence, and petential uses. *Food Chem.* **99** (2006) 191-203.

[87] Arnous, A.; Makris, D. P.; Kefalas, P. Effect of principal polyphenolic components in relation to antioxidant characteristics of aged red wines. *J. Agr. Food Chem.* **49** (2001) 5736–5742.

[88] Puupponen-Pimiä, R.; Nohynek, L; Meier, C.; Kähkönen, M.; Heinonen, M. et al. Antimicrobial properties of phenolic compounds from berries. *J. Appl. Microbiol.* **90** (2001) 494–507.

[89] Middleton, E.; Kandaswami, C.; Theoharides, T. C. The effects of plant flavonoids on mammalian cells: implications for inflammation, heart disease and cancer. *Pharmacol. Rev.* **52** (2000) 673–751.

[90] Manach, C.; Mazur, A.; Scalbert, A. Polyphenols and prevention of cardiovascular diseases. *Curr. Opin. Lipidol.* **16** (2005) 77–84.

[91] Kay, C. D. The future of flavonoid research. *Br. J. Nutr.* **104** (2010) S91-950.

[92] Koh, S. H.; Lee, S. M.; Kim, H. Y.; Lee, K. Y.; Lee, Y. J. et al. The effect of epigallocatechin gallate on suppressing disease progression of ALS model mice. *Neurosci. Lett.* **6** (2006) 103-07.

[93] Ortega-Arellano, H. F.; Jimenez-Del-Rio, M.; Velez-Pardo, C. Life span and locomotor activity modification by glucose and polyphenols in Drosophila melanogaster chronically exposed to oxidative stress-stimuli: implications in Parkinson's disease. *Neurochem. Res.* **36** (2011) 1073-1086.

[94] Halliwell, B. Role of free radicals in the neurodegenerative diseases: therapeutic implications for antioxidnat treatment. *Drugs Aging.* **18** (2001) 658-716.

[95] Zhang, F.; Shi, J. S.; Zhou, H.; Wilson, B. Hong, J. S. et al. Resveratrol attenuates early pyramidal neuron excitability impairment and death in acute rat hippocampal slices caused by oxygen-glucose deprivation. *Epx. Neurol.* **212** (2010) 44-52.

[96] Sakata, Y.; Zhuang, H.; Kwansa, H.; Koehler, R. C.; Doré, S. Resveratrol protects against experimental stroke: putative neuroprotective role of heme oxygenase 1. *Exp. Neurol.* **224** (2010) 325-329.

[97] Okawara, M.; Katsuki, H.; Kurimoto, E.; Shibata, H. Kume, T. et al. Resveratrol protects dopaminergic neurons in midbrain slice culture from multiple insults. *Biochem. Pharmacol.* **73** (2007) 550-560.

[98] Ataie, A.; Sabetkasaei, M.; Haghparast, A.; Moghaddam, A. H.; Kazeminejad. B. Neuroprotective effects of the polyphenolic antioxidant agent, curcumin, against homocysteine-induced cognitive impairment and oxidative stress in the rat. *Pharmacol. Biochem. Behav.* **96** (2010) 378-385.

[99] Harish, G.; Venkateshappa, C.; Mythri, R. B.; Dubey, S. K.; Mishra, K. et al. Bioconjugates of curcumin display improved protection against glutathione depletion mediated oxidative stress in a dopaminergic neuronal cell line: Implications for Parkinson's disease. *Bioorg. Med. Chem.* **18** (2007) 2631-2638.

[100] Guo, Q.; Zhao, B.; Shen, S.; Hou, J. Hu, J. et al. ESR study on the structure-antioxidant activity relationship of tea catechins and their epimers. *Biochim. Biophys. Acta.* **1427** (1999) 13-23.

[101] Nanjo, F.; Mori, M.; Goto, K.; Hara, Y. Radical scavenging activity of tea catechins and their related compounds. *Biosci. Biotechnol. Biochem.* **63** (1999) 1621-1623.

[102] Ebrahimi, A.; Schluesener, H. Natural polyphenols against neurodegenerative disorders: potentials and pitfalls. *Ageing. Res. Rev.* **11** (2012) 329-345.

[103] Paik, S. R.; Lee, J. H.; Kim, D. H.; Chang, C. S.; Kim, J. Aluminum-induced structural alterations of the precursor of the non-Aβ component of Alzheimer's disease amyloid. *Arch. Biochem. Biophys.* **344** (1997) 325−334.

[104] Barltrop, J. A.; Owen, T. C.; Cory, A. H.; Cory, J. G. 5-(3-

carboxymethoxyphenyl)-2-(4,5-dimethylthiazolyl)-3-(4-sulfophenyl) tetrazolium, inner salt (MTS) and related analogs of 3-(4,5-dimethylthiazolyl)-2,5-diphenyltetrazolium bromide (MTT) reducing to purple water-soluble formazans as cell-viability indicators. *Bioorg. Med. Chem. Lett.* **1** (1991) 611–614.

[105] Golovko, M. Y.; Rosenberger, T. A.; Faergeman, N. J.; Feddersen, S.; Cole, N. B. et al. Acyl-CoA synthetase activity links wild-type but not mutant α-synuclein to brain arachidonate metabolism. *Biochemistry* **45** (2006) 6956-6966.

[106] Golovko, M. Y.; Barceló-Coblijn, G.; Castagnet, P. I.; Austin, S.; Combs, C. K. et al. The role of α-synuclein in brain lipid metabolism: a downstream impact on brain inflammatory response. *Mol. Cell. Biochem.* **326** (2009) 55-66.

[107] Oba, Y.; Ojika, M.; Inouye, S. Firefly luciferase is a bifunctional enzyme: ATP-dependent monooxygenase and a long chain fatty acyl-CoA synthetase. *FEBS Lett.* **540** (2003) 251-254.

[108] Oba, Y.; Sato, M.; Ojika, M.; Inouye, S. Enzymatic and genetic characterization of firefly luciferase and Drosophila *CG6178* as a fatty acyl-CoA synthetase. *Biosci. Biotechnol. Biochem.* **69** (2005) 819-828.

[109] Lee, J. -H.; Lee, In. -H.; Choe, Y. -J.; Kang, S.; Kim, H. Y. et al. Real-time analysis of amyloid fibril formation of α-synuclein using a fibrillation-state-specific fluorescent probe of JC-1. *Biochem. J.*

418 (2009) 311-323.

[110] Cerf, E.; Sarroukh, R.; Tamamizu-Kato, S.; Breydo, L.; Derclaye, S. et al. Antiparallel β-sheet: a signature structure of the oligomeric amyloid β-peptide. *Biochem. J.* **421** (2009) 415-423.

[111] Cerf, E.; Ruysschaert, J. -M.; Goormaghtigh, E.; Raussens, V. ATR-FTIR, a new tool to analyze the oligomeric content of Aβ samples in the presence of apolipoprotein E isoforms. *Spectroscopy* **24** (2010) 245-249.

[112] Carmona, P.; Rodríguez-Casado, A.; Alvarez, I.; de Miguel, E.; Toledano, A. FTIR microspectroscopic analysis of the effects of certain drugs on oxidative stress and brain protein structure. *Biopolymers* **89** (2008) 548-554.

[113] Byler, D. M.; Susi, H. Examination of the secondary structure of proteins by deconvolved FTIR spectra. *Biopolymers* **25** (1986) 469-487.

[114] Dong, A.; Huang, P.; Caughey, W. S. Protein secondary structures in water from second-derivative amide I infrared spectra. *Biochemistry* **29** (1990) 3303-3308.

[115] Barth, A. Infrared spectroscopy of proteins. *Biochim. Biophys. Acta* **1767** (2007) 1073-1101.

[116] Horowitz, P. M.; Criscimagna, N. L. Differential binding of the fluorescent probe 8-anilinonaphthalene-2-sulfonic acid to rhodanese catalytic intermediates. *Biochemistry* **24** (1985) 2587-2593.

[117] Bhak, G.; Lee, S.; Park, J. W.; Cho, S.; Paik, S. R. Amyloid hydrogel

derived from curly protein fibrils of α-synuclein. *Biomaterials* **31** (2010) 5986-5995.

[118] Goto, Y.; Yagi, H.; Yamaguchi, K.; Chtani, E.; Ban, T. Structure, formation and propagation of amyloid fibrils. *Curr. Pharm. Des.* **14** (2008) 3205-3218.

[119] Yamaguchi, K.; Takahashi, S.; Kawai, T.; Naiki, H.; Goto, Y. Seeding-dependent propagation and maturation of amyloid fibril conformation. *J. Mol. Biol.* **352** (2005) 952-960.

[120] Kodali, R.; Williams, A. D.; Chemuru, S.; Wetzel, R. Aβ(1-40) forms five distinct amyloid structures whose beta-sheet contents and fibril stabilities are correlated. *J. Mol. Biol.* **401** (2010) 503-517.

[121] Ursini, F.; Maiorino, M.; Gregolin, C. The selenoenzyme phospholipid hydroperoxide glutathione peroxidase. *Biochim. Biophys. Acta.* **839** (1985) 62-70.

[122] Lansbury, P. T.; Lashuel, H. A.; A century-old debate on protein aggregation and neurodegeneration enters the clinic. *Nature* **443** (2006) 774–779.

[123] Lin, M. T.; Beal, M. F. Mitochondrial dysfunction and oxidative stress in neurodegenerative diseases. *Nature* **443** (2006) 787–795.

[124] Barnham, K. J.; Masters, C. L.; Bush, A. I. Neurodegenerative diseases and oxidative stress. *Nat. Rev. Drug Discov.* **3** (2004) 205–214.

[125] Tabner, B. J.; Turnbull, S.; El-Agnaf, O. M.; Allsop, D. Formation of hydrogen peroxide and hydroxyl radicals from Aβ and α-synuclein as a possible mechanism of cell death in Alzheimer's disease and Parkinson's disease. *Free Radic. Biol. Med.* **32** (2002) 1076–1083.

[126] Lindenau, J.; Noack, H.; Asayama, K.; Wolf, G. Enhanced cellular glutathione peroxidase immunoreactivity in activated astrocytes and in microglia during excitotoxin induced neurodegeneration. *Glia* **24** (1998) 252–256.

[127] Fukuhara, R.; Kageyama, T. Tissue distribution, molecular cloning, and gene expression of cytosolic glutathione peroxidase in Japanese monkey. *Zoolog. Sci.* **20** (2003) 861–868.

[128] Sian, J.; Dexter, D. T.; Lees, A. J.; Daniel, S.; Agid, Y. et al. Alterations in glutathione levels in Parkinson's disease and other neurodegenerative disorders affecting basal ganglia. *Ann. Neurol.* **36** (1994) 348–355.

[129] Hudson, S. A.; Ecroyd, H.; Kee, T. W.; Carver, J. A. The thioflavin-T fluorescence assay for amyloid fibril detection can be biased by the presence of exogenous compounds. *FEBS J.* **276** (2009) 5960-5972.

[130] Caruana, M.; Högen, T.; Levin, J.; Hillmer, A.; Giese, A. et al. Inhibition and disaggregation of α-synuclein oligomers by natural polyphenolic compounds. *FEBS Lett.* **585** (2011) 1113-1120.

[131] Porat, Y.; Abramowitz, A.; Gazit, E. Inhibition of amyloid fibril

formation by polyphenols: structural similarity and aromaticinteractions as a common inhibition mechanism. *Chem. Biol. Drug Des.* **67** (2006) 27-37.

[132] Ehrnhoefer, D. E.; Bieschke, J.; Boeddrich, A.; Herbst, M.; Masino, L. et al. EGCG redirects amyloidogenic polypeptides into unstructured, off-pathway oligomers. *Nat. Struct. Mol. Biol.* **15** (2008) 558-566.

[133] Fantini, J.; Carlus, D.; Yahi, N. The fusogenic tilted peptide (67-78) of α-synuclein is a cholesterol binding domain. *Biochim. Biophys. Acta.* **1808** (2011) 2343-2351.

[134] Mauch, D. H.; Nägler, K,. Schumacher, S.; Göritz, C.; Müller, E. C. et al. CNS synaptogenesis promoted by glia-derived cholesterol. *Science* **294** (2001) 1354-1357.

[135] Saher, G.; Brügger, B.; Lappe-Siefke, C.; Möbius, W.; Tozawa, R. et al. High cholesterol level is essential for myelin membrane growth. *Nat Neurosci.* **8** (2005) 468-475

[136] Martins, I. J.; Berger, T.; Sharman, M. J.; Verdile, G.; Fuller, S. J. et al. Cholesterol metabolism and transport in the pathogenesis of Alzheimer's disease. *J. Neurochem.* **111** (2009) 1275-1308.

[137] Hu, G.; Antikainen, R.; Jousilahti, P.; Kivipelto, M.; Tuomilehto, J. Total cholesterol and the risk of Parkinson disease. *Neurology* **70** (2008) 1972-1979.

[138] Liu, J. P.; Tang, Y.; Zhou, S. Toh, B. H.; McLean, C. et al. Cholesterol involvement in the pathogenesis of neurodegenerative

disease. *Mol. Cell. Neurosci.* **43** (2010) 33-42.

[139] Bar-On, P.; Rockenstein, E.; Adame, A.; Ho, G.; Hashimoto, M. et al. Effects of the cholesterol-lowering compound methyl-beta-cyclodextrin in models of α-synucleinopathy. *J. Neurochem.* **98** (2006) 1032-1045.

[140] Koob, A. O.; Ubhi, K.; Paulsson, J. F.; Kelly, J.; Rockenstein, E. et al. Lovastatin ameliorates α-synuclein accumulation and oxidation in transgenic mouse models of alpha-synucleinopathies. *Exp. Neurol.* **221** (2010) 267-274.

[141] Scoville, S. P.; Shirley, W. M. Investigations of chromatic transformations of polydiacetylene with aromatic compounds. *J. Appl. Polym. Sci.* **120** (2011) 2809-2820.

[142] Charoenthai, N.; Pattanatornchai, T.; Wacharasindhu, S.; Sukwattanasinitt, M.; Traiphol, R. Roles of head group architecture and side chain length on colorimetric response of polydiacetylene vesicles to temperature, ethanol and pH. *J. Colloid. Interf. Sci.* **360** (2011) 565-573.

[143] Reppy, M. A.; Pindzola, B. A. Biosensing with polydiacetylene materials: structures, optical properties and applications. *Chem. Commun.* (2007) 4317-4338.

[144] Ogawa, K. Study on polymerization mechanism of pentacosadiynoic acid langmuir-blodgett films using high energy beam irradiations. *J. Phys. Chem.* **93** (1989) 5305-5310.

[145] Charych, D. H.; Nagy, J. O.; Spevak, W.; Bednarski, M. D. Direct

colorimetric detection of a receptor-ligand interaction by a polymerized bilayer assembly. *Science* **261** (1993) 585-588.

[146] Carpick, R. W.; Sasaki, D. Y.; Burns, A. R. First observation of mechanochromism at the nanometer scale. *Langmuir* **16** (2000) 1270-1278.

[147] Oliveira, T. V.; Soares, N. F. F.; Silva, D. J.; Andrade, N. J.; Medeiros, E. A. A. et al. Development of PDA/Phospholipids/Lysine vesicles to detect pathogenic bacteria. *Sensor Actuat. B-Chem.* **188** (2013) 385-392.

[148] Sokolovski, M.; Sheynis, T.; Kolusheva, S.; Jelinek, R. Membrane interactions and lipid binding of casein oligomers and early aggregates. *BBA-biomembranes* **1778** (2008) 2341-2349.

[149] Jeon, H.; Lee, J.; Kim, M. H.; Yoon, J. Polydiacetylene-based electrospun fibers for detection of HCl Gas. Macromol. Rapid Commun. 2012, 33, 972-976.

[150] Wu, J.; Lu, X.; Shan, F.; Guan, J.; Lu. Q. Polydiacetylene-embedded supramolecular electrospun fibres for a colourimetric sensor of organic amine vapour. *RSC Adv.* **3** (2013) 22841-22844.

[151] Zhou, G.; Wang, F.; Wang, H.; Kambam, S.; Chen, X. Colorimetric and fluorometric detection of neomycin based on conjugated polydiacetylene supramolecules. *Macromol. Rapid. Comm.* **34** (2013) 944-948.

[152] Park, H. K.; Gokarna, A.; Hulme, J. P.; Park, H. G.; Chung, B. H. Fluorescent nanoscale detection of biotin-streptavidin interaction

using near-field scanning optical microscopy. *Nanotechnology* **19** (2008) 235103.

[153] Palladino, P.; Castelletto, V.; Dehsorkhi, A.; Stetsenko, D.; Hamley, I. W. Reversible thermal transition of polydiacetylene based on KTTKS collagen sequence. *Chem. Commun.* **48** (2012) 9774-9776.

[154] Meyuhas, D.; Nir, S.; Lichtenberg, D. Aggregation of phospholipid vesicles by water-soluble polymers. *Biophys. J.* **71** (1996) 2602-2612.

[155] Tarahovsky, Y. S.; Yagolnik, E. A.; Muzafarov, E. N.; Abdrasilov, B. S.; Kim, Y. A. Calcium-dependent aggregation and fusion of phosphatidylcholine liposomes induced by complexes of flavonoids with divalent iron. *BBA-biomembranes* **1818** (2012) 695-702.

[156] Eklund, K. K.; Takkunen, J. E.; Kinnunen, P. K. J. Cation-induced aggregation of acidic phospholipid vesicles: the role of fatty acid unsaturation and cholesterol. *Chem. Phys. Lipids* **57** (1991) 59-66.

[157] Bordi, F.; Cametti, C. Salt-induced aggregation in cationic liposome aqueous suspensions resulting in multi-step self-assembling complexes. *Colloid Surface B* **26** (2002) 341-350.

[158] Rambaran, R. N.; Serpell, L. C. Amyloid fibrils: abnormal protein assembly. *Prion* **2** (2008) 112-117.

[159] Gazit, E. A. Possible role for pi-stacking in the self-assembly of amyloid fibrils. *FASEB J.* **16** (2002) 77-83.

[160] Marshall, K. E.; Serpell, L. C. Insights into the structure of amyloid fibrils. *Open Biol. J.* **2** (2009) 185-192.

[161] Vilar, M.; Chou, H.-T.; Lührs, T.; Maji, S. K.; -Loher, D. R. et al.

The fold of α-synuclein fibrils. *P. Natl. Acad. Sci. USA* **105** (2008) 8637-8642.

[162] Fändrich, M.; Meinhardt, J.; Grigorieff, N. Structural polymorphism of Alzheimer Aβ and other amyloid fibrils. *Prion* **3** (2009) 89-93.

[163] Bousset, L.; Pieri, L.; -Arlandis, G. R.; Gath, J.; Jensen, P. H. et al. Structural and functional characterization of two α-synuclein strains. *Nat. Commun.* **4** (2013) 2575.

[164] Knowles, T. P. J.; Buehler, M. J. Nanomechanics of functional and pathological amyloid materials. *Nat. Nanotechnol*. **6** (2011) 469-479.

[165] Carny, O.; Shalev, D. E.; Gazit, E. Fabrication of coaxial metal nanocables using a self-assembled peptide nanotube scaffold. *Nano Lett*. **6** (2006) 1594-1597.

[166] Knowles, T. P. J.; Oppenheim, T.; Buell, A. K.; Chirgadze, D. Y.; Welland, M. E. Nanostructured films from hierarchical self-assembly of amyloidogenic proteins. *Nat. Nanotechnol.* **5** (2010) 204-207.

[167] Channon, K. J.; Devlin, G. L.; MacPhee, C. E. Efficient energy transfer within self-assembling peptide fibers: a route to light-harvesting nanomaterials. *J. Am. Chem. Soc.* **131** (2009) 12520-12521.

[168] Lee, D.; Choe, Y. –J.; Choi, T. S.; Bhak, G.; Lee, J. et al. Photoconductivity of pea-pod-type chains of gold nanoparticles encapsulated within dielectric amyloid protein nanofibrils of α-synuclein. *Angew. Chem. Int. Edit.* **50** (2011) 1332-1337.

[169] Hamedi, M.; Herland, A.; Karlsson, R. H.; Inganäs, O. Electrochemical devices made from conducting nanowire networks self-assembled from amyloid fibrils and alkoxysulfonate PEDOT. *Nano Lett.* **8** (2008) 1736-1740.

[170] Li, C.; Alam, M. M.; Bolisetty, S.; Adamcik, J.; Mezzenga, R. New biocompatible thermo-reversible hydrogels from PNiPAM-decorated amyloid fibrils. *Chem. Commun.* **47** (2011) 2913-2915.

[171] Guglielmi, F.; Monti, D. M.; Arciello, A.; Torrassa, S.; Cozzolino, F. et al. Enzymatically active fibrils generated by the self-assembly of the ApoA-I fibrillogenic domain functionalized with a catalytic moiety. *Biomaterials* **30** (2009) 829-835.

[172] Smith, P. K.; Krohn, R. I.; Hermanson, G. T.; Mallia, A. K.; Gartner, F. H. et al. Measurement of protein using bicinchoninic acid. *Anal. Biochem.* **150** (1985) 76－85.

[173] Klusheva, S.; Boyer, L.; Jelinek, R. A. Colorimetric assay for rapid screening of antimicrobial peptides. *Nat. Biotechnol.* **18** (2000) 225－227.

[174] Lee, J.-H.; Shin, H.-J.; Chang, C.-S.; Paik, S. R. Comparisons of the NACP self-oligomerizations induced by Aβ25-35 in the presence of dicyclohexylcarbodiimide and N-(ethoxycarbonyl)-2-ethoxy–1,2-dihydroquinoline. *Neurochem. Res.* **23** (1998) 1427−1434.

[175] Broersen, K.; Brink, D.; Fraser, G.; Goedert, M.; Davletov, B. α-Synuclein adopts an α-helical conformation in the presence of

polyunsaturated fatty acids to hinder micelle formation. *Biochemistry* **45** (2006) 15610−15616.

[176] An, J. J.; Rhee, Y.; Kim, S. H.; Kim, D. M.; Han, D.-H. et al. Effect of 4-hydroxy-2-nonenal modification on α-synuclein aggregation. *J. Biol. Chem.* **282** (2007) 5862−5870.

[177] Necula, M.; Chirita, C. N.; Kuret, J. Rapid anionic micelle-mediated α-synuclein fibrillization in vitro. *J. Biol. Chem.* **278** (2003) 46674−46680.

[178] de Franceschi, G.; Frare, E.; Pivato, M.; Relini, A.; Penco, A. et al. Structural and morphological characterization of aggregated species of α-synuclein induced by docosahexaenoic acid. *J. Biol. Chem.* **286** (2011) 22262−22274.

[179] Okawa, Y.; Takajo, D.; Tsukamoto, S.; Hasegawa, T.; Aono, M. Atomic force microscopy and theoretical investigation of the lifted-up conformation of polydiacetylene on a graphite substrate. *Soft Matter*, **4** (2008) 1041−1047.

[180] Miller, T. M.; Kwock, E. W.; Baird, T., Jr.; Hale, A. Properties and photodefinition of poly(aromatic diacetylenes). *Chem. Mater.* **6** (1994) 1569−1574.

[181] Su, Y.-L.; Li, J.-R.; Jiang, L. Effect of amphiphilic molecules upon chromatic transitions of polydiacetylene vesicles in aqueous solutions. *Colloids Surf. B* **39** (2004) 113−118.

[182] Kim, J.-M.; Lee, Y. B.; Yang, D. H.; Lee, J.-S.; Lee, G. S. et al. A polydiacetylene-based fluorescent sensor chip. *J. Am. Chem. Soc.*

127 (2005) 17580−17581.

[183] Hwang, H.; Song, S.; Kim, J. M. Reversible modulation of fluorescence signals of conjugated polydiacetylene supramolecules in a microfluidic sensor chip. *Bull. Korean Chem. Soc.* **31** (2010) 273−274.

[184] Yan, X.; An, X. Thermal and photic stimuli-responsive polydiacetylene liposomes with reversible fluorescence. *Nanoscale* **5** (2013) 6280−6283.

[185] Lifshitz, Y.; Golan, Y.; Konovalov, O.; Berman, A. Structural Transitions in Polydiacetylene Langmuir Films. *Langmuir* **25** (2009) 4469−4477.

국문 초록

아밀로이드성 단백질인 알파-시뉴클린(α-Synuclein, αS)은 파킨슨씨병 환자에게서 공통적으로 관찰되는 루이소체(Lewy Bodies)의 주요 구성성분이다. αS이 아밀로이드로 조립화되는 과정에는 올리고머(Oligomer)가 중간체로 관찰되며 이들은 단위조립(Unit Assembly) 과정을 통해 다양한 물리화학적 특성을 나타내는 섬유상 구조체로 조립화되어 아밀로이드 다형성(Polymorphism)을 나타낸다. 더 나아가 αS 올리고머는 지질막 표면상에서 단위조립화를 나타냄으로써 방사성 아밀로이드 구조체를 형성하고, 그 결과 지질막 구조를 붕괴시킴이 확인되었다. 따라서, αS 올리고머의 지질막상 단위조립화 특성은 αS에 의한 세포퇴화의 분자적 원인으로 간주되고 있다.

이에 본 연구에서는 αS 상호작용성 분자들을 탐색하여 올리고머에 의한 세포독성을 제어하고자 하였다. 먼저 αS과 효소간 상호작용을 통해 효소의 활성이 향상되고 아밀로이드 형성이 촉진됨을 확인할 수 있었다. 반딧불 루시페라아제(LUC)과 글루타티온 과산화효소(GPX-1)은 αS과 결합하여 각각 8.1 μM, 17.3 nM의 Kd 값을 나타낸다. 이들은 새로운 지지체(Template)를 제공함으로써 αS 섬유화를 촉진시키고 섬유 다형성을 유도한다. 형광염료결합 분석법, 투과전자현미경, 푸리에 변환 적외선분광법을 이용하여 효소에 의해 유도된 아밀로이드 섬유의 형태적 차이를 관찰하였다. LUC에

의해 유도된 아밀로이드 섬유의 형태적 특징은 핵 의존성 섬유화 과정(Nucleation-Dependent Fibrillation)을 통해 다음 세대로전달되었다. 따라서 씨앗(Seed) 제어는 아밀로이드 섬유의 생화학적 특성변화를 유도하기 위한 효과적인 방법이라 할 수 있다. 또한, LUC에 의한 아밀로이드 섬유의 다형성 결과로부터 세포 내 다양한 분자들 또한 아밀로이드 섬유를 다양하게 만들고 이는 세포 내에서 다양한 활성을 갖도록 자가증식(Self-Propagation)할 것이라 예상할 수 있다. S과 GPX-1간 상호작용의 결과물인 섬유 구조체를 금 나노입자가 결합된 항체로 GPX-1을 표시하고 전자현미경으로 관찰하면, 섬유 구조체 안에 갇혀 있는 GPX-1을 확인할 수 있다. 흥미롭게도 이 GPX-1는 섬유 구조체 안에 잠복상태(Latent Form)로 갇혀 있다가 그물에서 빠져나오며 활성이 완전히 회복되었다. 따라서 S과 그 아밀로이드 섬유는 GPX-1 자극제(Activator)와 활성효소 저장소의 역할을 함으로써 산화적 스트레스로부터 세포를 보호하는 새로운 기능을 보여준다.

몇몇 폴리페놀은 αS 올리고머가 세포막과 세포생존율에 끼치는 영향을 제어하는 것으로 관찰되었다. 우선, β-Sheet 구조가 없고, 반복적인 막 투과 과정을 통해 Curly Amyloid Fibril (CAF)로 조립되며 라이포솜 표면에서 즉각적으로 Radiating Amyloid Fibril (RAF)를 형성하는 특정 올리고머를 활성 올리고머(Active Oligomer)라 정의하였다. S의 타이로신 내재 형광(Tyrosine Intrinsic Fluorescence) 변화를 측정함으로써 단백질과 페놀화합물인 레스베라트롤

(Resveratrol, RSV), 커큐민(Curcumin, CUR), 녹차 카테킨((-)-Epigallocatechin Gallate, EGCG)이 결합하는 것을 확인하였다. CBB로 염색한 SDS-PAGE와 CD 분광법을 통해 이들 페놀화합물이 αS 섬유화에 영향을 주어 다른 특성을 갖는 올리고머(Compact Oligomer) 형성을 유도하거나 β-Sheet을 다량 함유하는 아밀로이드 섬유 형성을 촉진시키는 것을 관찰하였다. 특히 녹차 폴리페놀인 EGCG의 경우, 올리고머를 빠르게 아밀로이드로 조립시켜 올리고머가 더 이상 지질막 및 세포에 영향을 주지 못하도록 했다. 따라서 EGCG를 포함한 αS 상호작용성 분자들은 올리고머에 의한 세포독성을 제어할 수 있으며, 이는 파킨슨씨병의 치료물질로 활용될 수 있음을 보여준다.

규칙적인 구조와 높은 물리적 강도가 특성인 아밀로이드 섬유는 재료과학 측면에서 응용 가능성이 높은 생물재료라 평가된다. 이에 본 연구에서는 αS 아밀로이드 섬유를 지지체로 하여 Diacetylene의 일종인 10,12-Pentacosadiynoic Acid (PCDA) 기반 비색성 센서를 개발하였다. PCDA는 αS의 올리고머 형성을 촉진 시킬 뿐만 아니라 섬유화 과정에도 영향을 주어 섬유화를 촉진시키고 그 결과 두께가 증가한 섬유 구조체를 형성한다. UV를 조사하면, PCDA를 포함하는 아밀로이드 섬유(AF/PCDA)는 파란색을 띠고 열을 가하면 빨간색으로 변한다. 이와 같은 파랑-빨강 색 전이는 pH와 에탄올에 노출되었을 때에도 관찰된다. 구조가 안정한 AF/PCDA는 PCDA Vesicle과 달리 반복적인 음파처리(Sonication)에

도 색을 잘 유지하였다. 따라서 AF/PCDA는 강도가 향상된 PDA 기반의 새로운 비색성 센서이며, 다양한 분야에서 활용 가능할 것이다. 더 나아가 아밀로이드 섬유과 PCDA를 이용하여 온도와 유기용매를 감지할 수 있는 리트머스 형태의 센서도 개발하였다. PCDA 분자들은 αS 모노머와 함께 반응하여 섬유구조체를 형성하거나(AF/PCDA), 이미 만들어진 아밀로이드 섬유와 반응하여 (AF+PCDA) 아밀로이드 섬유에 결합되고, 이들은 종이 위에서 UV에 의해 고분자화 되어 파란색을 띤다. AF/PCDA와 AF+PCDA로 제작된 종이 센서는 온도와 유기용매 감지에 대해 서로 다른 민감도를 보인다. 아밀로이드 섬유에 약하게 결합된 PCDA는 분자 자유도가 높아 감지 능력에 영향을 준다. 또한, AF+PCDA 센서는 온도 변화를 성공적으로 감지할 수 있어 물질의 열 이력(Thermal History)를 추적하는데 활용될 수 있다. 이와 같은 결과로부터 αS 아밀로이드 섬유는 PCDA의 지지체로 적합하여 온도와 유기용매를 감지할 수 있는 리트머스 형태의 센서로 개발될 수 있다.

주요어

알파-시뉴클린; 활성 올리고머; 단위 조립; 알파-시뉴클린 상호작용성 분자; 폴리다이아세틸렌; 아밀로이드 기반 센서